الجمهورية الجزائرية الديمقراطية الشعبية People's Democratic Republic of Algeria وزارة التعليم العالي والبحث العلمي

Ministry of Higher Education and Scientific Research

University Center Abdelhafid Boussouf – Mila

s I I I I

المركـز الجامعي عبد الحفيظ بوالصوف ميلـة

Institute: Mathematics and Computer Sciences

Order N°:.....

Registration number: M136/2022

www.centre-univ-mila.dz

Department: Mathematics

Field: Mathematics **Specialty:** Dynamical Systems

Thesis

Submitted for the degree of Doctorate LMD

Developing and investigating mathematical models for simulation and control of some infectious diseases

Presented by: Chennaf Bouchra

Board of Examiners

Boularouk Yakoub	MCA	Abdelhafid Boussouf Univ-Center of Mila	Chairman
Abdelouahab	Pr	Abdelhafid Boussouf	Supervisor
Mohammed-Salah		Univ-Center of Mila	
Kaouache Smail	MCA	Abdelhafid Boussouf Univ-Center of Mila	Examiner
Bououden Rabah	MCA	Abdelhafid Boussouf Univ-Center of Mila	Examiner
Houmor Tarek	MCA	Constantine 1 University	Examiner
Basti Bilal	MCA	Mohamed Boudiaf M'sila University	Examiner

University year: 2024/2025

Abstract

This thesis constructs and analyzes mathematical models to simulate and control specific infectious diseases, with a primary emphasis on tuberculosis (TB). Both continuous and discrete dynamical systems are utilized to study disease spread and evaluate the effectiveness of public health measures. Some compartmental models are formulated to represent different stages of infection, key risk factors, and control measures such as vaccination, chemoprophylaxis, and public health policies. Real-world data from Algeria, Ukraine, India, and Russia are used to evaluate the effectiveness of these strategies in various demographic and healthcare contexts. In addition, game theory is applied to study vaccination behavior, using Nash equilibrium concepts to account for factors such as perceived risk, cost, and disease prevalence. By integrating mathematical modeling with strategic decision-making approaches, this study enhances disease control strategies and promotes better public health outcomes.

Keywords: Epidemiologic model, parameter estimation, stability, simulation, control

Résumé

Cette thèse propose et analyse des modèles mathématiques pour simuler et contrôler certaines maladies infectieuses, en mettant un accent particulier sur la tuberculose (TB). Elle s'appuie sur des systèmes dynamiques continus et discrets afin d'examiner la transmission de la maladie et d'évaluer l'effet des interventions de santé publique. Quelques modèles compartimentaux sont élaborés pour représenter les différents stades de l'infection, les principaux facteurs de risque ainsi que les stratégies de contrôle telles que la vaccination, la chimioprophylaxie et les politiques sanitaires. Des données empiriques issues de l'Algérie, de l'Ukraine, de l'Inde et de la Russie ont été utilisées afin d'analyser l'efficacité de ces stratégies dans divers contextes démographiques et sanitaires. Par ailleurs, la théorie des jeux est mobilisée pour étudier les comportements liés à la vaccination, en intégrant les concepts d'équilibre de Nash pour prendre en compte des éléments tels que le risque perçu, le coût et la prévalence de la maladie. En combinant la modélisation mathématique et les approches stratégiques de prise de décision, cette recherche vise à optimiser les mesures de contrôle des maladies et à améliorer la santé publique.

Mots-clés : Modèle épidémiologique, estimation des paramètres, stabilité, simulation, contrôle

ملخص

تتناول هذه الأطروحة بناء وتحليل نماذج رياضية لمحاكاة والتحكم في بعض الأمراض المعدية، مع التركيز الأساسي على مرض السل (TB). يتم استخدام كل من الأنظمة الديناميكية المستمرة والمتقطعة لدراسة انتشار المرض وتقييم فعالية التدابير الصحية العامة. يتم صياغة نموذج مقسم لتمثيل المراحل المختلفة للعدوى، وعوامل الخطر الرئيسية، وإجراءات المكافحة مثل التطعيم، والوقاية الكيميائية، والسياسات الصحية العامة. تُستخدم بيانات حقيقية من الجزائر وأوكرانيا و الهند و روسيا لتقييم فعالية هذه الاستراتيجيات في سياقات ديموغرافية ورعاية صحية متنوعة. بالإضافة إلى ذلك، يتم تطبيق نظرية الألعاب لدراسة سلوك التطعيم، باستخدام مفاهيم توازن ناش لأخذ عوامل مثل المخاطر المتصورة، والتكلفة، وانتشار المرض في الاعتبار. من خلال دمج النمذجة الرياضية مع أساليب اتخاذ القرار الاستراتيجية، تعزز هذه الدراسة استراتيجيات مكافحة الأمراض وتعزز نتائج الصحة العامة.

الكلمات المفتاحية:

نموذج وبائي، تقدير المعاملات، الاستقرار، المحاكاة، التحكم.

		•	. •	
1		ica [·]	tic	n
	CU	ıLa	LIL	/ I

I wholeheartedly dedicate this work to those who have guided, inspired, and supported me—my family, friends, and advisors. Your encouragement and wisdom have been invaluable in shaping both my academic and personal growth. Thank you for always believing in me.

Bouchra Chennaf

Acknowledgements

All praise and gratitude are due to Allah, who has blessed me with faith, resilience, and perseverance to complete this work.

I sincerely appreciate my supervisor, Professor **Mohammed Salah Abdelouahab** from the University Center Abdelhafid Boussouf of Mila, for his continuous support, valuable guidance, and expertise. His encouragement and insightful feedback greatly contributed to the completion of this research.

I would like to extend my deep gratitude to the esteemed members of my thesis jury for their time, insightful feedback, and constructive evaluation of my work. My sincere thanks go to:

- Dr. Yakoub Boularouk (President of the Jury, University Center Abdelhafid Boussouf, Mila).
- Dr. Smail Kaouache (Examiner, University Center Abdelhafid Boussouf, Mila).
- Dr. Rabah Bououden (Examiner, University Center Abdelhafid Boussouf, Mila).
- **Dr. Houmor Tarek** (Examiner, Constantine 1 University).
- **Dr. Bilal Basti** (Examiner, Mohamed Boudiaf M'sila University).

I am also sincerely grateful to Dr. **Bilal Basti** from Mohamed Boudiaf M'sila University for his unwavering support, availability, and valuable advice during the course of this research. His guidance has been truly invaluable.

Additionally, I would like to express my heartfelt gratitude to my esteemed teachers, **Abdelmajid Kouachi** and **Aïdi Nabil**, who believed in my potential and inspired me to pursue my academic journey. I am deeply grateful for their encouragement and guidance. Furthermore, I extend my sincere thanks to all my teachers from middle school, high school, and university, each of whom has played a significant role in shaping my education.

My heartfelt thanks extend to everyone who contributed to improving this work, whether through suggestions, constructive criticism, or encouragement. Every piece of feedback has been instrumental in refining this manuscript.

A special note of appreciation goes to my parents, **Ammar Chennaf** and **Zouina Bouleklaoui**, as well as my brothers, **Djalal, Ilyasse, Mohammed Cherif, Akram, and Youcef**. Their unwavering support, motivation, and prayers have been a source of strength, and I am profoundly grateful for their belief in me.

Lastly, I extend my sincere gratitude to all those who, in any way, have helped in the completion of this work.

May Allah send His blessings upon His noble messenger, his family, and his companions, and may He grant us success in all aspects of life.

My scientific contributions

- Chennaf, B., Abdelouahab, M. S., and Lozi, R. (2023). Analysis of the dynamics of tuberculosis in Algeria using a compartmental VSEIT model with evaluation of the vaccination and treatment effects. Computation, 11(7), 146.
- Chennaf, B., Abdelouahab, M. S., and Lozi, R. (2024). A Novel Compartmental VS-LIT Model Used to Analyze the Dynamics of Tuberculosis in Algeria and Ukraine and the Assessment of Vaccination and Treatment Effects. Ukrainian Mathematical Journal, 75(12), 1932-1947.
- Chennaf, B., and Abdelouahab, M. S. (2024). A Discrete-Time Epidemic Model to Analyze and Control Multidrug-Resistant and Extensively Drug-Resistant Tuberculosis in Russia and India. Journal of innovative applied mathematics and computational sciences, 4(1), 63-85.
- Basti, B., Chennaf, B., Boubekeur, M. A., and Bounouiga, S. Fractional Mathematical Model for Exploring the Influence of Infectious Diseases on Population with Chronic Conditions. Advanced Theory and Simulations, 2301285.

Contents

1	Gen	General introduction			
	1.1	Overv	riew	1	
	1.2	Resea	rch goals	4	
	1.3	Thesis	soutline	5	
2	Basi	ics of d	ynamical systems	6	
	2.1	What	is a dynamical system?	6	
	2.2	Conti	nuous dynamical systems	7	
		2.2.1	Principles of continuous dynamical systems	8	
		2.2.2	Analysis of equilibrium points, linearization, and stability	11	
		2.2.3	Poincaré map	19	
		2.2.4	Periodic solutions in planar systems	21	
		2.2.5	Bifurcation theory	22	
	2.3	Discre	ete dynamical systems	28	
		2.3.1	Principles of discrete dynamical systems	29	
		2.3.2	Stability analysis	34	
		2.3.3	Bifurcation theory	36	
	Con	clusion	1	40	
3	Mat	hemati	ical modeling of		
	infe	ctious	diseases	41	
	3.1	A Brie	ef history of epidemics	42	
	3.2	Termi	nology	43	
	3.3	Mathe	ematical modeling in epidemiological research	44	
		3.3.1	The dynamic infection process	45	

Contents

		3.3.2	What are the goals of epidemic modeling?	45
	3.4	The fu	undamental reproductive ratio \mathcal{R}_0	46
	3.5	Introd	luction to simple epidemic models	48
		3.5.1	\mathcal{SI} model	48
		3.5.2	<i>SIS</i> model	50
		3.5.3	\mathcal{SIR} model	53
		3.5.4	\mathcal{SIRS} model	61
		3.5.5	\mathcal{SEIR} Model	65
	3.6	Case s	studies and applications of infectious disease modeling	66
		3.6.1	Dengue Fever and the $\mathcal{SIR} - \mathcal{SI}$ model	67
		3.6.2	Ebola and the \mathcal{SEIR} control model	68
	Con	clusion	1	69
4	Son	ne meth	nods of	
	para	ameter	estimation	70
	4.1	Maxin	mum likelihood estimation	71
		4.1.1	Likelihood function	71
		4.1.2	Optimization	72
		4.1.3	Bias and mean squared error (MSE)	72
	4.2	Nonli	near least squares method	73
		4.2.1	Model fitting	73
		4.2.2	Nonlinear least squares procedure	74
		4.2.3	Distinction from linear least squares	74
	4.3	Metho	ods for solving nonlinear least squares problems	74
		4.3.1	Gauss-Newton method	75
		4.3.2	Levenberg-Marquardt algorithm	
		4.3.3	TNC algorithm	
		4.3.4	Trust Region Constrained method	77
		4.3.5	Trust Region Reflective method	78
	Con	clusion	L	78
5			mpartmental	
	VSI	\mathcal{CIT} mo		79
	5.1	_	round on tuberculosis	79
	5.2		mic modeling and analysis	80
		5.2.1	Formulating of the $VSLIT$ model	80
		5.2.2	Preservation of the feasible set	83

Contents xi

		5.2.3 Existence of equilibrium points and global stability	84
	5.3	Simulating numerically and estimating parameters	90
	5.4	Sensitivity analysis	94
	5.5	Discussion and results of numerical simulations	94
	Con	clusion	96
6	Dis	crete-Time modeling of tuberculosis epidemics: chemoprophylaxis strate-	
	gies	for combating MDR and XDR TB in Russia and India	98
	6.1	Formulation of discrete TB model	99
	6.2	The feasible region	102
	6.3	Disease-free equilibrium	103
		6.3.1 Existence of the DFE	103
		6.3.2 Basic reproduction number \mathcal{R}_0	103
		6.3.3 Global stability investigation of the DFE	
	6.4	Endemic equilibrium	107
		6.4.1 Existence of EE	107
		6.4.2 Global stability investigation of the EE	108
	6.5	Data fitting for discrete model	109
	6.6	Analyzing the sensitivity of \mathcal{R}_0	113
	6.7	Numerical results	115
	Con	clusion	121
7	Gan	ne theory in tuberculosis vaccination: analyzing Nash equilibria for op-	
	tima	al strategies in Algeria	122
	7.1	Material and methods	123
	7.2	Equilibrium points	125
	7.3	Basic reproduction number	125
	7.4	Herd immunity threshold vaccination rate	125
	7.5	Nash equilibrium vaccination strategy	126
	7.6	Uncertainty and sensitivity analysis	130
	Con	clusion	134
Co	onclu	sions and Outlook	135
Re	eferei	nces	136

List of Figures

2.1	Flow representation	8
2.2	Regular attractors	10
2.3	Chua Attractor	11
2.4	Lorenz Attractor	11
2.5	Lyapunov stability	12
2.6	Asymptotic stability	13
2.7	Poincaré section	21
2.8	The buckling of the beam under a heavy load (77)	23
2.9	Representation of a saddle-node bifurcation.	24
2.10	Illustration of a transcritical bifurcation	25
2.11	Supercritical pitchfork bifurcation	26
2.12	Subcritical pitchfork bifurcation	27
2.13	Illustration of a supercritical Hopf bifurcation	28
2.14	Fixed points of $g(x) = 4x(1-x)$	29
2.15	Visualization of a 2-periodic cycle, where the intersections of $f^2(x)$ with $y =$	
	<i>x</i> indicate periodic points	31
2.16	Cobweb plot for $f(x) = 2.9x(1-x)$ showing convergence to a stable fixed	
	point	33
2.17	Cobweb plot for $f(x) = 3.4x(1-x)$ illustrating convergence to a 2-periodic	
	orbit	33
2.18	Cobweb plot for $f(x) = 3.4495x(1-x)$ showing convergence to a 4-periodic	
	orbit	34
2.19	Cobweb plot for $f(x) = 4x(1-x)$ illustrating chaotic dynamics	34
2.20	Bifurcation diagram illustrating the Fold bifurcation	38
2.21	Bifurcation diagram illustrating the period-doubling bifurcation	39

List of Figures xiii

2.22	Bifurcation diagram illustrating the transcritical bifurcation	40
3.1	The dynamic infection process	45
3.2	Diagram illustrating the dynamics of an \mathcal{SI} model	49
3.3	Simulation results of the \mathcal{SI} model with a transmission rate of $\beta=0.5$ and	
	initial values given by $S_0 = 999$ and $I_0 = 1$	50
3.4	Flow diagram representing the dynamics of an \mathcal{SIS} model	51
3.5	Numerical results from the SIS model with parameters $\beta = 0.5$ and $\gamma = 0.2$,	
	initialized with $S(0)=990$ susceptible individuals and $\mathcal{I}(0)=10$ infected	
	individuals	52
3.6	Schematic representation of the \mathcal{SIR} model	54
3.7	Phase plane trajectories of system (3.7) for $\gamma = 0.333333$ and $\beta = 1. \dots$	55
3.8	Numerical simulation of the \mathcal{SIR} model without vital dynamics, illustrating	
	the spread and decline of an epidemic with $\beta=0.5$ and $\gamma=0.2.$	56
3.9	Schematic representation of the \mathcal{SIR} model incorporating vital dynamics	57
3.10	Numerical simulation of the \mathcal{SIR} model with birth and death dynamics us-	
	ing: $\beta = 0.5$, $\gamma = 0.2$, $\mu_1 = 0.01$, $\mu_2 = 0.02$, $\mu_3 = 0.015$, and initial conditions	
	$S(0) = 990, I(0) = 10, R(0) = 0. \dots$	61
3.11	Flow diagram representing the \mathcal{SIRS} model	62
3.12	Numerical simulation of the \mathcal{SIRS} model without vital dynamics, using	
	parameter values $\beta=0.5,\ \gamma=0.2,$ and $\nu=0.1,$ with initial conditions	
	$S(0) = 990, I(0) = 10, \text{ and } R(0) = 0. \dots \dots \dots \dots \dots \dots$	63
3.13	Flowchart representing the \mathcal{SIRS} model with vital dynamics	64
3.14	Numerical simulation of the \mathcal{SIRS} model with vital dynamics, illustrating	
	the evolution of the compartments over time	65
3.15	Diagram illustrating the transitions in the \mathcal{SEIR} model	66
3.16	Numerical simulation of the \mathcal{SEIR} model without vital dynamics, using	
	parameters $\beta=0.5$, $\gamma=0.1$, $\delta=0.2$, and initial values $\mathcal{N}=1000$, $\mathcal{S}(0)=$	
	985, $\mathcal{E}(0) = 10$, $\mathcal{I}(0) = 5$, $\mathcal{R}(0) = 0$	66
3.17	Diagram illustrating the transitions in the $\mathcal{SIR}-\mathcal{SI}$ Dengue model	67
3.18	Diagram illustrating the transitions in the \mathcal{SEIR} Ebola model with control	
	strategies	68
5.1	Flowchart of the proposed $VSLIT$ model	81
5.2	Proportion of one-year-old children in Algeria who received the BCG vaccine	
	from 1990 to 2020	91

5.3	Proportion of one-year-old children in Ukraine who received the BCG vaccine from 1990 to 2020
5.4	
5.4	Fitting the data for tuberculosis cases in Algeria
5.6	
3.0	Effect of the parameters α , β , γ , μ , ϵ , and p on the fundamental reproduction rate \mathcal{R}_0
6.1	Flow diagram of the discrete model (6.2) depicting the transitions between
	various compartments in the system
6.2	TB incidence data and model fit for Russia. The data points are shown in green, while the fitted model is depicted in red. The basic reproduction num-
	ber, $\mathcal{R}_0 = 0.22 < 1.$
6.3	TB incidence data and model fit for India. The data points are shown in green, while the fitted model is depicted in red. The basic reproduction num-
	ber, $\mathcal{R}_0 = 6.42 > 1.$
6.4	Representation of \mathcal{R}_0 versus β , τ , γ , ϵ and α
6.5	Representation of \mathcal{R}_0 versus $\beta, \nu, \omega, \sigma$, and μ
6.6	Effect of the chemoprophylaxis treatment rate on the compartments of the
C 7	discrete model (6.2)
6.76.8	Effect of the vaccination rate on the compartments of the discrete model (6.2). 119 Comparision of the discrete model and continuous model vs Russia's Data 120
7.1	Model diagram showing the interactions between compartments in the \mathcal{VSLIT}
	tuberculosis model
7.2	The fundamental reproduction rate varsus the vaccination rate p . The critical
	vaccination rate for achieving herd immunity is denoted by $p_{\rm HI}$ 126
7.3	Optimal vaccination rate p_{NE} varsus the relative vaccination cost C for different values of β
7.4	Basic reproduction number \mathcal{R}_0 Varsus the relative vaccination cost C , assum-
	ing the population follows the Nash equilibrium vaccination strategy 129
7.5	Distribution of the fundamental reproduction rate \mathcal{R}_{0} across parameter sets 133
7.6	Partial Rank Correlation Coefficients (PRCCs) for \mathcal{R}_0 , showing the sensitivity
	to model parameters
7.7	Distribution of the optimal vaccination rate $p_{\rm NE}$ across parameter sets 133
7.8	Partial Rank Correlation Coefficients (PRCCs) for p_{NE} , showing the sensitiv-
	ity to model parameters

List of Figures xv

7.9	Distribution of the relative disparity between the Nash equilibrium vaccina-
	tion rate and the herd immunity vaccination rate
7.10	Partial Rank Correlation Coefficients (PRCCs) for the relative difference, show-
	ing the sensitivity to model parameters

List of Tables

5.1	Model parameters and initial data for equation (5.2)	92
5.2	Sensitivity index for the model (5.2) in Algeria and Ukraine	95
6.1	Initial conditions and model parameters for Russia and India	111
6.2	Sensitivity Index for the Basic Reproduction Number \mathcal{R}_0	114
7.1	Model parameters for TB model (7.1).	131

General introduction

Contents

1.1	Overview	1
1.2	Research goals	4
1.3	Thesis outline	5

1.1 | Overview

Throughout history, mathematicians have sought to equip humanity with tools that improve the human experience. One such tool is mathematical modeling, a technique that allows for reasonably accurate predictions of future events. These forecasts assist in planning at both individual and societal levels. Individuals utilize mathematical models for financial decisions, including budgeting, insurance, loan management, and investments. On a broader scale, populations use them to address societal needs such as food supply, housing, and disease progression. Governments and other authorities depend on these models to strategize resource allocation, budgeting, infrastructure, and workforce planning for various concerns.

Over the past few hundred years, populations have suffered devastating losses due to infectious diseases. Once thought to occur randomly, these diseases were found to be transmitted through contact with infected individuals or hosts, such as mosquitoes. This discovery made it possible to track and predict the transmission. With this knowledge, mathematicians were tasked with developing methods to monitor this transmission and forecast future infections. Knowing how many people will become infected, where the infections will take place, how long infected people will remain infectious, and who

will need medical care is a key input for decision-makers, who are charged with providing the necessary facilities and care and with ensuring that necessary supplies are available and that means of infection prevention, such as vaccination and quarantine, are implemented.

There are many devastating diseases throughout history that have decimated populations. The first recorded epidemic was the Plague of Athens in about 430 B.C.E.; the historian Thucydides described it and its symptoms, progression, and mortality in his History of the Peloponnesian War. The plague that would become known as the Black Death swept through Europe from the Mediterranean. This disease is believed to have caused the deaths of approximately 50-100 million people in the following two years (1348-1350) (96).

In under a year, the Spanish Flu claimed the lives of 675,000 Americans - surpassing the total U.S. casualties from World War I, World War II, the Korean War, and the Vietnam War combined. On a global scale, the pandemic is estimated to have caused between 30 and 40 million deaths. According to the U.S. Centers for Disease Control, approximately 500 million people, or about one-third of the world's population at that time, were infected (14).

In 1520, smallpox devastated the Aztec population, killing nearly half—around 3.5 million people. The outbreak played a crucial role in the success of Cortez's conquest of Mexico, as the epidemic severely weakened the native population. Unable to mount an effective defense or chase the invaders, the Aztecs inadvertently gave the Spanish the opportunity to regroup, form alliances, and ultimately secure victory (16).

Daniel Defoe's account of the 1665 London plague vividly conveys the emotional toll of the epidemic (Defoe, 1722, as cited in Landa, 1991 (19)).

"At that time, mankind withered like grass, and life became but a fleeting shadow. The streets were overwhelmed by contagion, and its devastating effects left churchyards unable to accommodate the dead."

Epidemic diseases have undoubtedly inflicted significant harm on individuals and entire populations. Controlling these outbreaks remains a crucial objective for humanity, and mathematicians have long contributed to this vital endeavor.

The application of mathematics to the study of infectious diseases dates back to 1760, when Daniel Bernoulli (10) developed a method to assess the effectiveness of variolation, an early form of smallpox vaccination. In 1840, William Farr (28) used a normal curve to analyze quarterly smallpox mortality data. The early 20th century saw major advancements in mathematical modeling, notably with Sir Ronald Ross's research on malaria transmission between humans and mosquitoes. In 1911 (71), he published transmission models and introduced a threshold quantity that led to the concept of the

reproduction number, \mathcal{R}_0 . This groundwork, further developed by Kermack and McKendrick in the 1920s (42), provided a robust theoretical foundation for understanding infection dynamics and forecasting future outbreaks.

In recent decades, mathematical models have been essential for analyzing the transmission dynamics of tuberculosis (TB). As one of the world's deadliest infectious diseases, analyzing its dynamics is essential for effective control. Research such as that of (84), which introduced a mathematical model to estimate long-term trends in TB incidence and mortality, has significantly contributed to shaping public health strategies. Their work highlighted the importance of factors like the latent infection period and the efficiency of various intervention approaches, including vaccination and treatment efforts.

A study by (26) utilized a compartmental model to examine TB transmission across various populations, emphasizing the influence of HIV co-infection and drug resistance on TB dynamics. The findings of this study helped inform strategies for managing TB in high-risk populations and underscored the importance of addressing drug-resistant strains of TB. Such mathematical models are vital for forecasting the transmission dynamics of multidrug-resistant tuberculosis (MDR-TB) and extensively drug-resistant tuberculosis (XDR-TB), especially in settings like (17), where these strains are prevalent.

In addition to these classical epidemiological models, game theory has emerged as an important tool in understanding the decision-making processes related to TB control. The use of game theory allows researchers to model the interactions between individuals, healthcare providers, and governments, all of whom may have differing incentives and strategies when it comes to disease prevention and treatment. For instance, a game-theoretic model can examine how individuals make decisions about TB testing and treatment based on perceived risks, costs, and benefits, while also considering the actions of healthcare providers and policymakers. By finding Nash equilibria in these models, researchers can identify optimal strategies for maximizing public health outcomes, such as increasing vaccination rates or improving treatment adherence. Game theory has been utilized in designing intervention strategies that balance individual and collective interests, playing a crucial role in the effective management of TB transmission (1; 35; 58; 68; 86).

Public health authorities are much more effective and efficient when they can predict the features of an epidemic. According to Michael Y. Li (50)According to (2018, p. 2), authorities aim to address several crucial questions:

- 1. What is the projected severity of the epidemic? This can be evaluated by:
 - a) The total number of individuals who might require medical attention.

- b) The peak number of infections occurring simultaneously.
- 2. What will be the duration of the epidemic? When will the peak occur, and what will the overall timeline look like?
- 3. How effective are interventions such as quarantine or vaccination in controlling the spread?
- 4. What is the optimal quantity of vaccines or antiviral medications that should be stockpiled?
- 5. Which strategies are most effective in containing, managing, and ultimately eliminating an endemic disease?

Mathematical models play a vital role in addressing these questions. By accurately forecasting disease progression and evaluating the effectiveness of containment strategies, they help improve public response, minimize infections, and reduce the overall impact on the population.

1.2 | Research goals

This study focuses on examining the dynamics of tuberculosis (TB) transmission through both continuous and discrete dynamical systems. The main aims of this study are:

- Develop a robust compartmental model to describe TB transmission, considering various stages of the disease, population groups, and risk factors, in order to understand TB dynamics in different epidemiological contexts.
- Analyze the impact of intervention strategies, including vaccination, chemoprophylaxis, and public health measures, on TB transmission. This includes assessing the effectiveness, feasibility, and limitations of these strategies.
- Apply the model to real-world case studies in countries like Algeria and Ukraine to evaluate TB control strategies in different demographic and healthcare settings, factoring in local conditions such as healthcare infrastructure and socio-economic status.
- Use game theory to investigate decision-making in TB vaccination strategies, examining how factors like perceived risk, cost, herd immunity, and disease prevalence affect vaccination decisions. The study aims to identify optimal vaccination strategies for reducing TB transmission effectively.

1.3 | Thesis outline

The structure of this thesis is as follows:

- Chapter 1: Basics of dynamical systems This chapter introduces the fundamental concepts of dynamical systems, covering both continuous and discrete frameworks. Topics include stability analysis, bifurcation theory, and their relevance to understanding epidemic transitions.
- Chapter 2: Mathematical modeling of infectious diseases Here, we explore the historical development of mathematical epidemiology, key terminologies, and the goals of epidemic modeling. The chapter reviews classical models, such as SIR and SEIR, and their applications in predicting disease dynamics.
- Chapter 3: Some methods of parameter estimation. This chapter explores the techniques used to estimate parameters in epidemic models, including maximum likelihood estimation and nonlinear least squares.
- Chapter 4: A novel compartmental VSLIT model introduces a new model for tuberculosis, based on the VSLIT framework, and applies it to data from Algeria and Ukraine.
- Chapter 5: Discrete-time epidemic modeling with chemoprophylaxis for controlling multidrug-resistant and extensively drug-resistant Tuberculosis in Russia and India discusses a discrete-time model for controlling multidrug-resistant tuberculosis, focusing on chemoprophylaxis strategies.
- Chapter 6: Game theory in tuberculosis vaccination: analyzing nash equilibria for optimal strategies in Algeria applies game theory to examine optimal vaccination strategies, focusing on Nash equilibrium solutions for vaccination decisions.
- Conclusions and Outlook The thesis concludes by summarizing the key findings, discussing their public health implications, and providing recommendations for future research.

Basics of dynamical systems

Contents			
2.1	What i	is a dynamical system?	6
2.2	Contir	nuous dynamical systems	7
	2.2.1	Principles of continuous dynamical systems	8
	2.2.2	Analysis of equilibrium points, linearization, and stability	11
	2.2.3	Poincaré map	19
	2.2.4	Periodic solutions in planar systems	21
	2.2.5	Bifurcation theory	22
2.3	Discre	te dynamical systems	28
	2.3.1	Principles of discrete dynamical systems	29
	2.3.2	Stability analysis	34
	2.3.3	Bifurcation theory	36
Con	clusion		40

This chapter explores the fundamental principles of dynamical systems. We begin by exploring the meaning and significance of dynamical systems. The second section covers the definitions and key properties of continuous dynamical systems. The third section focuses on defining and exploring the characteristics of discrete dynamical systems. Additionally, both sections address the concepts of stability and bifurcation theory.

2.1 | What is a dynamical system?

Dynamical systems are mathematical models used to describe the evolution of a system over time. In essence, any system whose state changes with time can be regarded as a dynamical system.

More formally, a dynamical system consists of two main components: a **state vector** that defines the current condition of the system, and a **rule (or function)** that governs how this state changes over time (73).

A dynamical system of dimension n is typically described by a set of n first-order differential equations in the space \mathbb{R}^n , which determine the system's temporal behavior.

These systems are commonly classified according to the nature of time:

- Discrete-time systems are those in which time progresses in distinct steps ($t \in \mathbb{Z}$ or $t \in \mathbb{N}$). These systems are modeled using difference equations or iterative applications.
- Continuous-time systems are characterized by time being a continuous variable $(t \in \mathbb{R})$, and their behavior is governed by differential equations.

Some examples of dynamic systems are:

1. Exponential Growth Model:

This model describes population growth and is governed by the equation:

$$\frac{dP}{dt} = kP.$$

where *P* represents the population size and k > 0 is the growth rate constant.

2. Simple Pendulum Model:

The dynamics of a simple pendulum are captured by the equation:

$$\frac{d^2\theta}{dt^2} + \frac{g}{L}\sin(\theta) = 0.$$

where θ denotes the angular displacement, g is the gravitational acceleration, and L is the length of the pendulum.

2.2 | Continuous dynamical systems

A continuous-time dynamical system is mathematically expressed as (47):

$$\frac{dx}{dt} = \dot{x} = f(x, t),\tag{2.1}$$

where f(x,t) is a smooth function defined on a subset $\mathcal{U} \subset \mathbb{R}^n \times \mathbb{R}$. In this formulation, $x = x(t) \in \mathbb{R}^n$ denotes the state vector and $t \in I \subseteq \mathbb{R}$ generally represents time.

■ A system is considered **autonomous** if f(x,t) does not explicitly include t. In this case, the system's trajectories remain unchanged over time.

■ A system is considered **nonautonomous** if f(x,t) explicitly depends on t.

To convert an n-dimensional nonautonomous system into an autonomous one, an additional variable x_{n+1} is introduced, where $x_{n+1} = t$. Thus, autonomous systems are developed by introducing such variables to remove explicit time dependence.

2.2.1 | Principles of continuous dynamical systems

Definition 2.1 (47) (Flow) The flow of a vector field describes the time evolution of a system and is mathematically expressed as:

$$\phi_t(x): \mathcal{U} \to \mathbb{R}^n$$
,

where $\phi_t(x) = \phi(x, t)$ is a smooth vector function that depends on $x \in \mathcal{U} \subseteq \mathbb{R}^n$ and $t \in I \subseteq \mathbb{R}$. This function satisfies the following differential equation:

$$\frac{d}{dt}\phi_t(x) = f(\phi_t(x)). \tag{2.2}$$

An initial condition is given by:

$$x(0) = x_0 \in \mathcal{U}$$
,

which ensures that the solution $\phi(t, x_0)$ satisfies:

$$\phi(0, x_0) = x_0.$$

(The solution may also be represented as $x(t, x_0)$ or simply x(t).)



Figure 2.1: Flow representation

Property 2.1 The function $\phi_t(x)$, representing the system's flow, exhibits the following properties:

- 1. $\phi_0 = I_d$ (the identity map),
- 2. $\phi_{t+s} = \phi_t \circ \phi_s$ (composition property).

Definition 2.2 (31) (Orbits and Phase Portraits) The function $\phi(t, x_0)$ is known as the trajectory, which corresponds to a specific initial state x_0 . The orbit of $x_0 \in \mathbb{R}^n$ is the set $\{\phi(t, x_0) \mid t \in I \subseteq \mathbb{R}\}$. The phase portrait is the collection of all qualitative trajectories of the system.

Definition 2.3 (60) (Limit Sets (ω - and α -Limit Sets))

- 1. A point $p \in \mathbb{R}^n$ is classified as an ω -limit (or α -limit) point if there exists a sequence $\{s_k\}$ such that $s_k \to +\infty$ (or $s_k \to -\infty$) and satisfies $\phi(s_k, x) \to p$ as $k \to \infty$.
- 2. The collection of all ω -limit (or α -limit) points forms the ω -limit set (or α -limit set), represented as $L_{\omega}(x)$ (or $L_{\alpha}(x)$).
- 3. The union of these sets, $L_{\omega}(x) \cup L_{\alpha}(x)$, defines the overall limit set of $\phi(t, x_0)$.

Definition 2.4 (44) (Cycle) A cycle refers to a periodic orbit, particularly a non-equilibrium orbit, denoted by L_0 . For any point x_0 in L_0 , the system satisfies the condition $\phi(t + T_0, x_0) = \phi(t, x_0)$ for a certain period $T_0 > 0$ and for all $t \in I$.

Definition 2.5 (44) (*Limit Cycle*) A limit cycle is a closed trajectory γ that belongs to either $L_{\omega}(x)$ or $L_{\alpha}(x)$, where x is a point not on the cycle γ .

Definition 2.6 (25) (Attractors) Consider a compact, closed, and invariant set A in the phase space, meaning that $\phi(t, A) = A$ for all t. The set A is deemed stable for the flow of (2.1) if, for any neighborhood U surrounding A, there exists another neighborhood V of A such that every trajectory $\phi(t, x_0)$ remains inside U whenever $x_0 \in V$.

Additionally, if

$$\lim_{t\to\infty}\phi(t,V)=A,$$

then A is said to be attractive. If A also contains a dense orbit, it is classified as an attractor.

The basin of attraction of A, denoted as B, consists of all points whose trajectories eventually converge to A, expressed as $B = \{x_0 \mid \lim_{t \to \infty} \phi(t, x_0) = A\}$.

Attractors can be categorized into two types: regular attractors and strange (or chaotic) attractors.

- **Regular attractors**: regular attractors characterize the evolution of non-chaotic systems and can be of three types:
 - **Fixed point:** This is the most basic type of attractor, represented by a single point within the phase space.

- Limit cycle (periodic attractor): This is a closed trajectory that attracts all nearby trajectories.
- Quasi-periodic attractor (torus): This is a trajectory that wraps around a torus, densely filling its surface, and eventually closes on itself after an infinite amount of time.

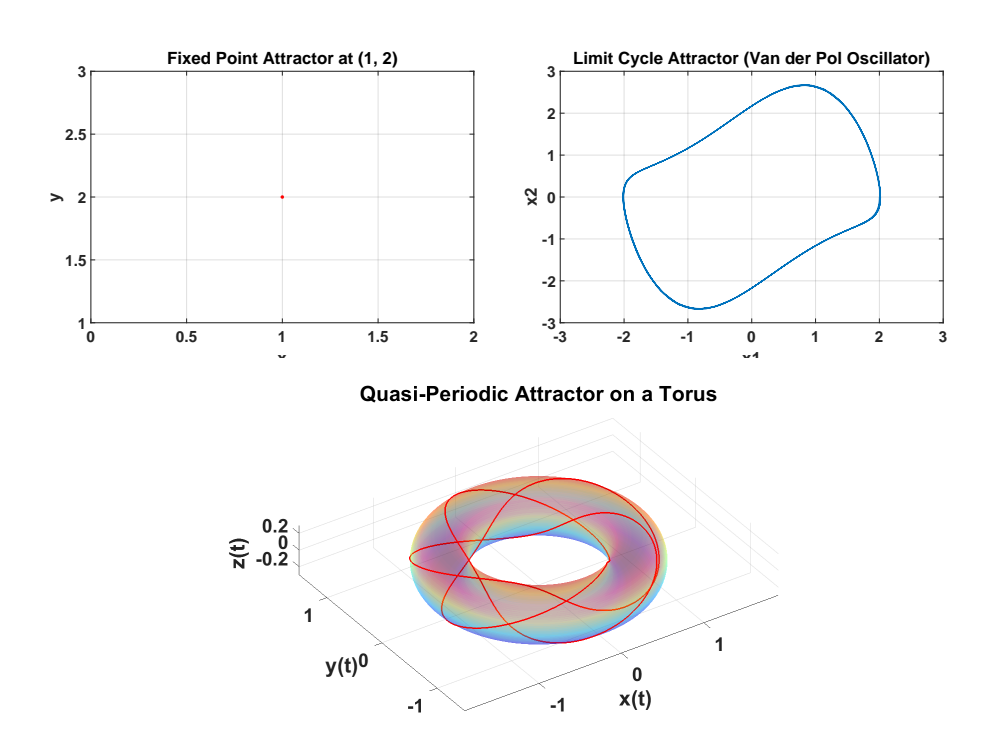
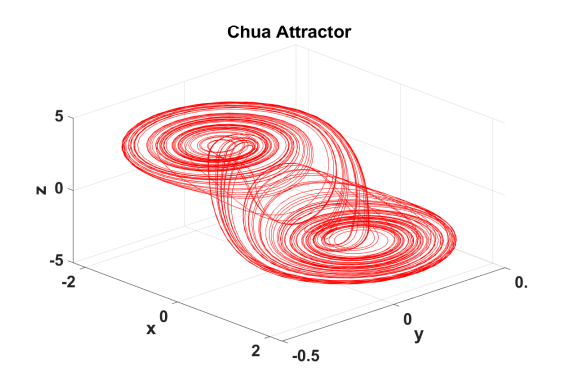


Figure 2.2: Regular attractors

■ **Strange attractors**: the strange attractor is a complex geometric form that characterizes the evolution of chaotic systems. It was introduced by Ruelle and Takens (18).

The features of a strange attractor are as follows:

- The attractor occupies zero volume within the phase space.
- The strange attractor possesses a fractal (non-integer) dimension. In a continuous autonomous system, this dimension satisfies 2 < d < n, where n denotes the phase space's dimension.
- It exhibits sensitivity to initial conditions (two trajectories that start close to each other will eventually diverge over time).



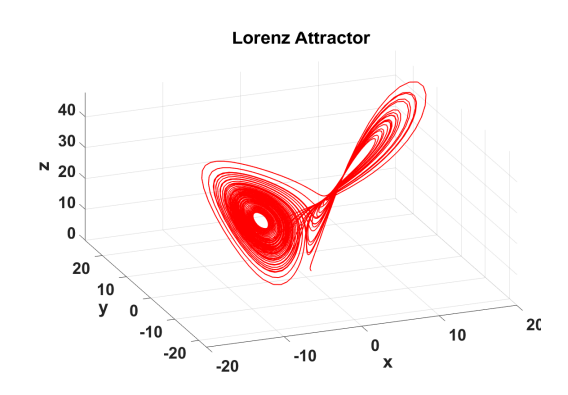


Figure 2.3: Chua Attractor

Figure 2.4: Lorenz Attractor

2.2.2 | Analysis of equilibrium points, linearization, and stability

2.2.2.1 | Equilibrium points and stability

Understanding equilibrium points is fundamental to analyzing a system's local behavior. These points, also known as critical, fixed, stationary, or steady-state points, play a crucial role in system dynamics.

Definition 2.7 (29) (*Equilibrium Point*) A point \bar{x} is considered an equilibrium of a continuous system if it satisfies

$$f(\bar{x}) = 0$$
 or $\phi(\bar{x}, t) = \bar{x}$, $\forall t \in I \subseteq \mathbb{R}$.

If this condition is not met, the point is classified as a regular point.

An equilibrium point corresponds to a constant solution $x(t) = \bar{x}$ of the system (2.1).

Geometrically, an equilibrium point represents the location where the function f(x) intersects the x-axis, indicating a state of balance in the system.

Let $\bar{x}(t)$ be a solution of (2.1). Generally, $\bar{x}(t)$ is considered stable if nearby solutions remain close over time. Furthermore, it is deemed asymptotically stable if these solutions not only stay near but also converge to $\bar{x}(t)$ as $t \to \infty$. The formal definition of stability is given below:

Definition 2.8 (94) (Lyapunov Stability) A solution $\bar{x}(t)$ is said to be stable (or Lyapunov stable) if, for every $\epsilon > 0$, there exists $\delta = \delta(\epsilon) > 0$ such that any solution y(t) of (2.1) satisfying

$$|\bar{x}(t_0) - y(t_0)| < \delta,$$

(where $|\cdot|$ denotes a norm in \mathbb{R}^n), also satisfies

$$|\bar{x}(t) - y(t)| < \epsilon$$
, $\forall t > t_0$, $t_0 \in \mathbb{R}$.

If this condition is not satisfied, the solution is considered unstable.

Lyapunov stability ensures that small perturbations in initial conditions do not cause significant deviations in system behavior over time.

Definition 2.9 (94) (Asymptotic Stability) A solution $\bar{x}(t)$ is considered asymptotically stable if it satisfies Lyapunov stability and, additionally, for every solution y(t) of (2.1), there exists a constant b > 0 such that if $|\bar{x}(t_0) - y(t_0)| < b$, then $\lim_{t \to \infty} |\bar{x}(t) - y(t)| = 0$.

Refer to Figures 2.5, 2.6 for a visual representation of these two definitions.

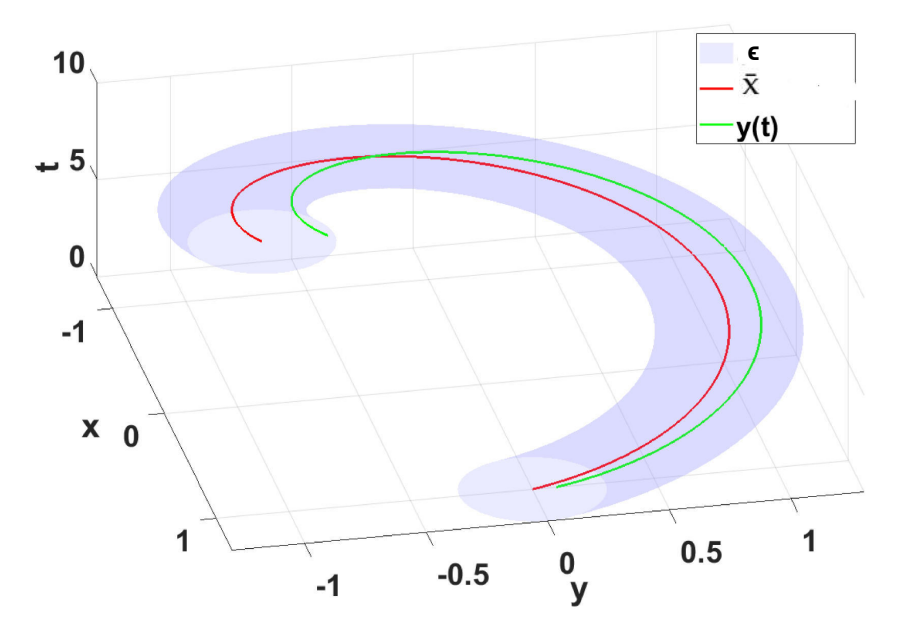


Figure 2.5: Lyapunov stability

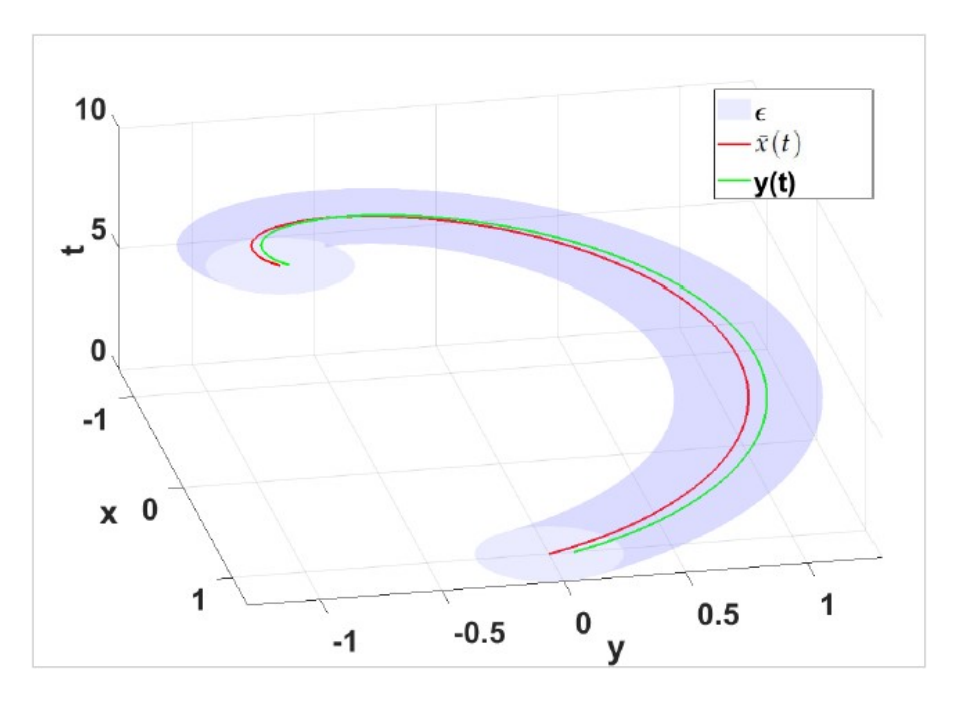


Figure 2.6: Asymptotic stability

2.2.2.2 | Linearization (Indirect method)

A common approach for analyzing nonlinear systems, such as the one given in equation (2.1), is to find their equilibrium points. A useful approach for examining solution behavior near a hyperbolic equilibrium is to linearize the system around that point. This technique, known as the second Lyapunov method or the indirect stability method, helps assess stability.

To assess the stability of the trajectory $\bar{x}(t)$, we analyze how solutions behave near it. We begin by introducing a small perturbation around the solution, denoted as z, ensuring that

$$x = \bar{x}(t) + z. \tag{2.3}$$

By substituting this into the system (2.1) and expanding using a Taylor series around $\bar{x}(t)$, yields:

$$\dot{x} = \dot{\bar{x}}(t) + \dot{z} = f(\bar{x}(t)) + J_f(\bar{x}(t))z + \mathcal{O}(|z|^2), \tag{2.4}$$

where J_f represents the Jacobian matrix of f, and $|\cdot|$ denotes a norm in \mathbb{R}^n . This approximation requires f to be at least twice continuously differentiable. Given that $\dot{\bar{x}}(t) = f(\bar{x}(t))$, the equation simplifies to:

$$\dot{z} = J_f(\bar{x}(t))z + \mathcal{O}(|z|^2). \tag{2.5}$$

This expression characterizes the local dynamics around $\bar{x}(t)$. To facilitate stability analysis, we focus on the linearized system by neglecting higher-order terms $\mathcal{O}(|z|^2)$:

$$\dot{z} = J_f(\bar{x}(t))z. \tag{2.6}$$

The stability of $\bar{x}(t)$ depends on the properties of this linear system. The analysis follows these steps:

- 1. Assess the stability of the trivial solution z = 0 in the linearized system (2.6).
- 2. Determine whether the stability (or instability) of the linearized system translates to the original nonlinear system at $\bar{x}(t)$.

In Step 1, solving the linear system can be complex, particularly if the system's coefficients vary with time. However, when $\bar{x}(t)$ corresponds to an equilibrium (i.e., $\bar{x}(t) = \bar{x}$, point), the Jacobian matrix simplifies to $J_f(\bar{x}(t)) = J_f(\bar{x}) = A$, which remains constant. In this case, the solution to (2.6) with initial condition z_0 at t = 0 is:

$$z(t) = e^{At}z_0. (2.7)$$

This solution is asymptotically stable if all eigenvalues of A have negative real parts. The next step in the analysis follows from the subsequent theorem.

Theorem 2.1 (Lyapunov's Stability Theorem via Linearization (7)) If all eigenvalues of the Jacobian matrix $A = J_f(\bar{x})$ have negative real parts, then the equilibrium point $x = \bar{x}$ in the nonlinear system (2.1) is asymptotically stable. On the other hand, if at least one eigenvalue has a positive real part, the equilibrium loses Lyapunov stability.

Definition 2.10 (Hyperbolic Equilibrium Point (60)) Consider a system $\dot{x} = f(x)$ with $x \in \mathbb{R}^n$ and let $x = \bar{x}$ be an equilibrium point. This equilibrium is classified as hyperbolic if none of the eigenvalues of the Jacobian matrix $J_f(\bar{x})$ have a real part equal to zero.

Definition 2.11 (60) Consider the system (2.1). An equilibrium point \bar{x} is called a **sink** if all eigenvalues of the Jacobian matrix $J_f(\bar{x})$ have negative real parts. In contrast, it is identified as a **source** when all eigenvalues have positive real parts. If the equilibrium is hyperbolic and $J_f(\bar{x})$ has at least one eigenvalue with a positive real part and another with a negative real part, the equilibrium is termed a **saddle point**.

Theorem 2.2 (Hartman-Grobman Theorem (31)) If the Jacobian matrix $J_f(\bar{x})$ at an equilibrium point \bar{x} has no eigenvalues with zero real parts or purely imaginary eigenvalues, then there exists a local homeomorphism h in a neighborhood U of $\bar{x} \in \mathbb{R}^n$. This homeomorphism maps the trajectories of the nonlinear system φ_t from equation (2.1) onto those of the linearized system $e^{tJ_f(\bar{x})}$, preserving their qualitative behavior and possibly their time parametrization.

The Hartman-Grobman theorem plays a crucial role in studying the local and qualitative dynamics of a system. It asserts that near a hyperbolic equilibrium point, the behavior of a nonlinear system closely resembles that of its linearized counterpart. Additionally, the theorem enables the identification of local solutions for the nonlinear system through homeomorphism.

Definition 2.12 (Stable and Unstable Manifolds (31)) Consider a hyperbolic equilibrium point \bar{x} within a neighborhood U. The local stable and unstable manifolds, denoted by $W^s_{loc}(\bar{x})$ and $W^u_{loc}(\bar{x})$, are defined as follows:

$$W^s_{loc}(\bar{x}) = \{x \in U \mid \varphi(t, x) \to \bar{x} \text{ as } t \to +\infty, \ \varphi(t, x) \in U \text{ for all } t \ge 0\},$$

$$W^u_{loc}(\bar{x}) = \{x \in U \mid \varphi(t, x) \to \bar{x} \text{ as } t \to -\infty, \ \varphi(t, x) \in U \text{ for all } t \le 0\}.$$

The corresponding global stable and unstable manifolds are given by:

$$W^{s}(\bar{x}) = \bigcup_{t \leq 0} \varphi(t, W^{s}_{loc}(\bar{x})),$$

$$W^{u}(\bar{x}) = \bigcup_{t \geq 0} \varphi(t, W^{u}_{loc}(\bar{x})).$$

Theorem 2.3 (Stable Manifold Theorem for an Equilibrium Point (31)) Consider \bar{x} as a hyperbolic equilibrium of system (2.1), where the stable and unstable subspaces of the linearized system (2.6) are denoted by E^s and E^u , respectively. In the original nonlinear system, the local stable and unstable manifolds, $W^s_{loc}(\bar{x})$ and $W^u_{loc}(\bar{x})$, exist and have dimensions matching those of E^s and E^u . Furthermore, these manifolds are tangent to E^s and E^u at \bar{x} and maintain the same degree of smoothness as the function f.

When studying the stability of equilibrium points through linearization, the stability properties are determined by the roots of the characteristic polynomial associated with the Jacobian matrix at the equilibrium. Below are fundamental properties and results concerning these roots.

A polynomial with real coefficients is given by:

$$q(\lambda) = b_0 \lambda^m + b_1 \lambda^{m-1} + \dots + b_{m-1} \lambda + b_m, \quad b_i \in \mathbb{R}, b_0 \neq 0.$$
 (2.8)

Theorem 2.4 (Fundamental Theorem of Algebra) (94) The Fundamental Theorem of Algebra states that the polynomial $q(\lambda)$ in (2.8) has exactly m roots, which may be real or complex. These roots, denoted as $\lambda_1, \ldots, \lambda_m$, can also have multiplicities.

For polynomials with real coefficients, if λ is a root of (2.8), then its complex conjugate $\overline{\lambda}$ must also be a root. This follows from substituting λ into (2.8), taking the

complex conjugate, and using the fact that all coefficients are real. As a result, complex roots always appear in conjugate pairs.

The next theorem provides a method for estimating the number of positive real roots based on the polynomial's coefficients.

Theorem 2.5 (*Descartes' Rule of Signs*) (94) Given the coefficient sequence of (2.8):

$$b_m, b_{m-1}, \ldots, b_1, b_0,$$

let v denote the number of sign changes between consecutive terms in this sequence. The number of positive real roots of the polynomial is either v or a smaller even integer. For example, if v=1, the polynomial has exactly one positive real root.

2.2.2.3 | Routh-Hurwitz criterion

To assess the asymptotic stability of an equilibrium point, one typically computes the n eigenvalues λ_i of the matrix A and verifies that each eigenvalue has a negative real part, meaning $\text{Re}(\lambda_i) < 0$ for all i. An algebraic method, developed by Routh and Hurwitz, simplifies this process by using specific determinants known as the Routh-Hurwitz determinants (94).

Consider the dynamical system:

$$\frac{dx}{dt} = \Phi(x),$$

where *x* represents the state variables. Linearizing around an equilibrium point gives the system:

$$\frac{dx}{dt} = Bx,$$

where *B* is the Jacobian matrix evaluated at the equilibrium.

The stability of the equilibrium depends on the eigenvalues of *B*, which are obtained by solving the characteristic equation:

$$q(\lambda) = \det(B - \lambda I) = 0 \iff \lambda^n + b_1 \lambda^{n-1} + b_2 \lambda^{n-2} + \dots + b_{n-1} \lambda + b_n = 0.$$

the Routh-Hurwitz determinants are defined as follows:

$$R_{1} = |b_{1}|,$$

$$R_{2} = \begin{vmatrix} b_{1} & 1 \\ b_{3} & b_{2} \end{vmatrix},$$

$$R_{3} = \begin{vmatrix} b_{1} & 1 & 0 \\ b_{3} & b_{2} & b_{1} \\ b_{5} & b_{4} & b_{3} \end{vmatrix},$$

$$R_k = \begin{vmatrix} b_1 & 1 & 0 & \cdots & 0 \\ b_3 & b_2 & b_1 & \cdots & 0 \\ b_5 & b_4 & b_3 & \cdots & 0 \\ \vdots & \vdots & \vdots & \ddots & \vdots \\ b_{2k-1} & b_{2k-2} & b_{2k-3} & \cdots & b_k \end{vmatrix}.$$

Proposition 2.1 For an n-dimensional system, the elements r_{jk} of the Routh-Hurwitz determinants satisfy:

*
$$r_{jk} = b_{2j-k}$$
 for $0 \le 2j - k \le n$,
* $r_{jk} = 1$ when $2j = k$,
* $r_{jk} = 0$ when $2j < k$ or $2j > n + k$.

Proposition 2.2 An equilibrium point is asymptotically stable if and only if:

$$\forall \operatorname{Re}(\lambda_i) < 0 \iff \forall \operatorname{Re}(R_i) > 0.$$

Theorem 2.6 (Routh-Hurwitz Stability Criterion) (5) For the polynomial $q(\lambda)$ with $b_0 > 0$, the system exhibits uniform asymptotic stability if and only if all leading principal minors of the corresponding Hurwitz matrix are strictly positive.

2.2.2.4 | Lyapunov function (Direct method)

To analyze the stability of a hyperbolic equilibrium point \bar{x} , one typically examines the real parts of the eigenvalues of $J_f(\bar{x})$. However, for non-hyperbolic equilibrium points, stability analysis is often more challenging. A common approach involves constructing a positive definite function $\mathcal{L}: U \to \mathbb{R}$, known as a Lyapunov function, as outlined in the following theorem (94):

Theorem 2.7 *Consider the system:*

$$\dot{x} = f(x), \quad x \in \mathbb{R}^n. \tag{2.9}$$

Let \bar{x} be an equilibrium point, and suppose there exists a continuously differentiable function $\mathcal{L}: U \to \mathbb{R}$ defined in a neighborhood U of \bar{x} such that:

- $\mathcal{L}(\bar{x}) = 0$ and $\mathcal{L}(x) > 0$ for all $x \neq \bar{x}$,
- \blacksquare $\dot{\mathcal{L}}(x) < 0$ in $U \setminus \{\bar{x}\}$.

Then, the equilibrium \bar{x} is stable. Additionally, if:

 \blacksquare $\dot{\mathcal{L}}(x) < 0$ in $U \setminus \{\bar{x}\}$,

then \bar{x} is asymptotically stable.

Example 2.1 *Consider the system:*

$$\begin{cases} \dot{u} = -u - uv^2, \\ \dot{v} = -v + 3u^2v. \end{cases}$$

The origin (0,0) is an equilibrium point of this system.

We define the Lyapunov function as $V(u,v) = c_1u^2 + c_2v^2$, where $c_1, c_2 > 0$. Clearly, V(0,0) = 0 and V(u,v) > 0 for $(u,v) \neq (0,0)$.

Computing the derivative along system trajectories:

$$\operatorname{grad}(\mathcal{V}(u,v)) \cdot g(u,v) = -2c_1u^2 - 2c_1u^2v^2 - 2c_2v^2 + 6c_2u^2v^2.$$

Choosing $c_1 = 3$ and $c_2 = 1$ simplifies this expression to:

$$\operatorname{grad}(\mathcal{V}(u,v)) \cdot g(u,v) = -6u^2 - 2v^2 < 0 \text{ for } (u,v) \neq (0,0).$$

Thus, the function $V(u, v) = 3u^2 + v^2$ serves as a strict Lyapunov function in \mathbb{R}^2 , proving that (0,0) is asymptotically stable.

2.2.2.5 | LaSalle's invariance principle

Theorem 2.8 (46) (LaSalle's invariance principle) Consider a subset \mathbb{R}^n of \mathbb{R}^n , and assume that $U \subset \mathbb{R}^n$ is a positively invariant set. Let $\mathcal{L}: \mathbb{R}^n \to \mathbb{R}$ be a continuously differentiable function satisfying the following conditions:

- 1. The time derivative $\dot{\mathcal{L}}(x)$ is non-positive throughout U, i.e., $\dot{\mathcal{L}}(x) \leq 0$ for all $x \in U$.
- 2. Define the set E as $E = \{x \in U \mid \dot{\mathcal{L}}(x) = 0\}$, and let L represent the largest invariant subset contained in E.

Then, any bounded trajectory that originates within U will asymptotically approach the set L as time progresses.

This theorem is a fundamental tool for analyzing dynamical systems. Unlike Lyapunov's direct method, LaSalle's principle does not require \mathcal{L} to be positive definite or $\dot{\mathcal{L}}$ to be strictly negative. However, it ensures only the attractivity of an equilibrium and does not guarantee convergence to a single equilibrium unless L is reduced to a single point. Moreover, it does not provide information about the stability of the equilibrium.

Corollary 2.1 Let \mathbb{R}^n be an open, connected set containing \bar{x} , and suppose there exists a continuously differentiable, positive definite function $\mathcal{L}:U\to\mathbb{R}$ that satisfies $\dot{\mathcal{L}}(x)\leq 0$ for all $x\in U$. Then:

- *If the only positively invariant subset of* E *is* \bar{x} , *then* \bar{x} *is asymptotically stable.*
- If $\mathcal{L}(x) \to +\infty$ as $||x|| \to \infty$, then all trajectories of the system remain bounded and \bar{x} is globally stable.

Corollary 2.2 *Under the same conditions, if* E *is reduced to* \bar{x} *, then* \bar{x} *is globally asymptotically stable.*

2.2.3 | Poincaré map

The Poincaré map serves as a key method for analyzing periodic orbits in dynamical systems. It simplifies the analysis of an n-dimensional continuous system by transforming it into an iteration of a lower-dimensional discrete map. Specifically, near a periodic orbit, the system can be represented by a map acting on a transverse section of dimension n-1, thereby reducing the complexity of the problem (62).

Consider a dynamical system governed by $\dot{x} = f(x)$, where x_0 represents a periodic orbit. Let Σ be a hyperplane transverse to the orbit at x_0 . For any point x in a small neighborhood of x_0 , the solution that passes through x at t=0 will eventually return to Σ at some later time. This leads to the definition of the Poincaré map, also known as the first return map:

$$x \mapsto P(x). \tag{2.10}$$

Theorem 2.9 Let U be an open subset of \mathbb{R}^n , and assume that f is a C^k function in U. Suppose $\varphi(t,x_0)$ is a periodic solution of the system $\dot{x}=f(x)$ with period T, and the corresponding closed trajectory

$$\gamma_{x_0} = \{ x \in \mathbb{R}^n \mid x = \varphi(t, x_0), 0 \le t \le T \}.$$

remains entirely within U. Let Σ be a hyperplane that intersects γ_{x_0} transversely at x_0 . Then, for a sufficiently small $\epsilon > 0$, there exists a unique function $\tau(x) \in C^k$, defined in a neighborhood $N_{\epsilon}(x_0) \cap \Sigma$, such that:

$$\tau(x_0) = T$$
, and $\varphi(\tau(x), x) \in \Sigma$ for all $x \in N_{\epsilon}(x_0) \cap \Sigma$.

Furthermore, $\tau(x)$ represents the first return time of x to Σ , defining the Poincaré map $P: N_{\epsilon}(x_0) \cap \Sigma \to \Sigma$ given by:

$$P(x) = \varphi(\tau(x), x).$$

Definition 2.13 *The function P defining the Poincaré map is given by:*

$$P: N_{\epsilon}(x_0) \cap \Sigma \to \Sigma$$
, $x \mapsto P(x) = \varphi(\tau(x), x)$.

It is a C^k smooth function and acts as a local diffeomorphism.

The stability of a periodic orbit depends on the derivative of the Poincaré map. If P(0) = 0 and P'(0) < 1, the orbit is stable, whereas if P'(0) > 1, the orbit is unstable.

Theorem 2.10 Consider a system defined in an open set $U \subset \mathbb{R}^2$, where f is continuously differentiable. Let $\varphi(t)$ be a periodic solution of $\dot{x} = f(x)$ with period T. The derivative of the Poincaré map P(s) along the transverse section Σ at x = 0 is expressed as:

$$P'(0) = \exp\left(\int_0^T \nabla f(\varphi(t)) dt\right).$$

This derivative determines the local stability of the periodic orbit.

Corollary 2.3 *Under the same conditions as Theorem 2.10, the periodic trajectory* $\varphi(t)$ *forms a stable limit cycle if:*

$$\int_0^T \nabla f(\varphi(t)) \, dt < 0.$$

Conversely, the cycle is unstable if:

$$\int_0^T \nabla f(\varphi(t)) dt > 0.$$

Definition 2.14 A periodic orbit is termed a limit cycle of multiplicity k if:

$$d(s) = P(s) - s$$
 and $d^{(k)}(0) \neq 0$.

The classification depends on k as follows:

- If k = 1, the limit cycle is said simple.
- \blacksquare *If* k *is even, the limit cycle exhibits semi-stable.*
- If k is odd, its stability is determined by the sign of $d^{(k)}(0)$:
 - Stable if $d^{(k)}(0) < 0$,
 - *Unstable if* $d^{(k)}(0) > 0$.

Theorem 2.11 A planar analytic system governed by $\dot{x} = f(x)$ cannot sustain an unbounded sequence of limit cycles converging to a single orbit.

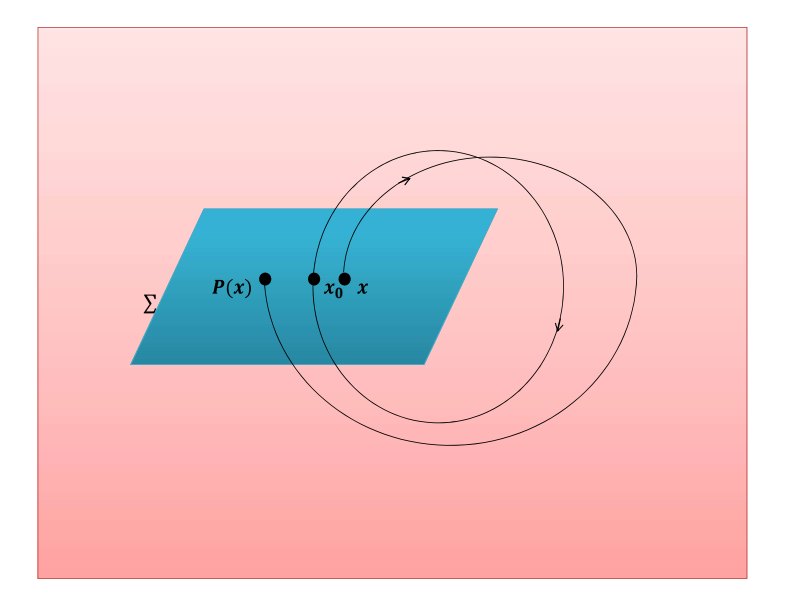


Figure 2.7: Poincaré section.

2.2.4 | Periodic solutions in planar systems

This subsection explores two-dimensional autonomous systems, represented as:

$$\begin{cases}
\dot{u} = F(u, v), \\
\dot{v} = G(u, v),
\end{cases}$$
(2.11)

where F and G are continuously differentiable functions. These conditions ensure the well-posedness of initial value problems, guaranteeing the existence and uniqueness of solutions. The following theorem provides fundamental insights into periodic solutions of system (2.11).

Theorem 2.12 (Poincaré-Bendixson (74)) If a compact and nonempty limit set of a planar dynamical system contains no equilibrium points, then it must correspond to a closed trajectory.

This result follows from the uniqueness of solutions, which prevents intersections of trajectories in the phase plane. Consequently, solutions must either be periodic or converge to an equilibrium.

Two well-known mathematical criteria establish conditions under which periodic orbits cannot exist: Bendixson's criterion and Dulac's criterion. These are presented below.

Theorem 2.13 (Bendixson's Criterion (3)) Let D be a simply connected open subset of \mathbb{R}^2 . If the divergence of the vector field, given by

$$\operatorname{div}(F,G) = \frac{\partial F}{\partial u} + \frac{\partial G}{\partial v},$$

is nonzero and maintains a constant sign throughout D, then system (2.11) does not admit periodic orbits in D.

Theorem 2.14 (Dulac's Criterion (3)) Consider a simply connected open region $D \subset \mathbb{R}^2$, and let B(u,v) be a continuously differentiable positive function in D. If the divergence of the weighted vector field

$$\operatorname{div}(BF,BG) = \frac{\partial(BF)}{\partial u} + \frac{\partial(BG)}{\partial v},$$

is nonzero and maintains a constant sign in D, then system (2.11) does not exhibit periodic orbits within D.

2.2.5 | Bifurcation theory

The dynamics of vector fields on a line are quite straightforward: solutions either stabilize at equilibrium points or move towards infinity. Although one-dimensional systems may appear simple, they are fascinating due to their dependence on parameters. As these parameters vary, the qualitative nature of the flow can change, potentially creating or eliminating fixed points or altering their stability. Such significant transformations in system dynamics are known as **bifurcations**, with the critical parameter values where these changes occur referred to as **bifurcation points**.

Bifurcations play a crucial role in scientific studies as they describe transitions and instabilities that arise when a control parameter varies. Consider a beam subjected to an increasing load: with a light weight, the beam remains upright and stable. However, beyond a critical threshold, the vertical position loses stability, causing the beam to buckle. In this case, the applied weight serves as the control parameter, while the beam's deviation from its vertical position represents the dynamic variable x (77).

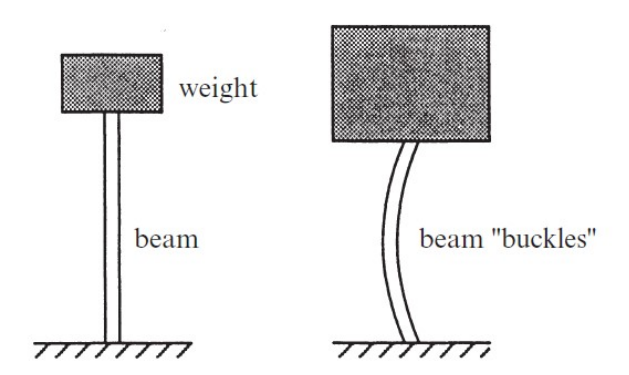


Figure 2.8: The buckling of the beam under a heavy load (77)

Let's explore the most fundamental types of bifurcation.

2.2.5.1 | Saddle-Node bifurcation

A saddle-node bifurcation arises in a first-order system given by:

$$\dot{x} = \mu + x^2,\tag{2.12}$$

where μ is a control parameter that influences the system's equilibrium states. The nature of equilibrium points varies based on μ :

- If μ < 0: Two equilibrium points exist at $\bar{x} = \pm \sqrt{-\mu}$, with one being stable and the other unstable.
- If $\mu = 0$: The two equilibrium points merge into a single semi-stable equilibrium at $\bar{x} = 0$.
- If μ > 0: No equilibrium points remain, eliminating steady-state solutions.

The critical value $\mu=0$ acts as the bifurcation point, signaling a fundamental shift in system behavior. This type of bifurcation is known as a **saddle-node bifurcation** since, for $\mu<0$, two equilibrium points emerge (one stable, one unstable), but they vanish when μ surpasses zero.

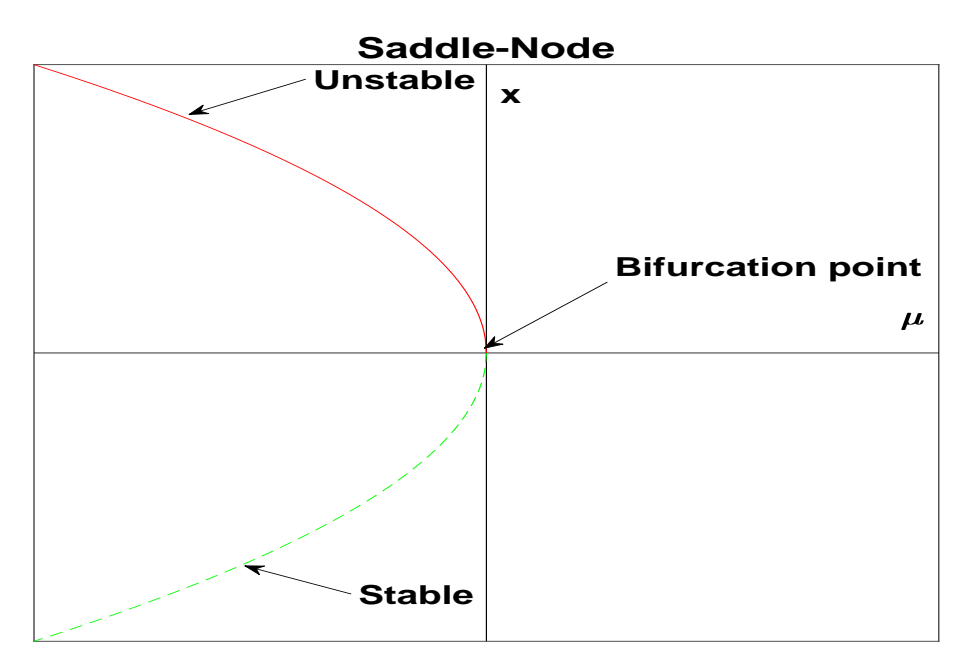


Figure 2.9: Representation of a saddle-node bifurcation.

2.2.5.2 | Transcritical bifurcation

A transcritical bifurcation occurs in the system:

$$\dot{x} = \mu x - x^2,\tag{2.13}$$

where μ is a parameter that governs the equilibrium states and their stability:

- If μ < 0: The system has two equilibrium points: x = 0 (stable) and $x = \mu$ (unstable).
- If $\mu = 0$: The equilibria coincide at x = 0, leading to a change in stability.
- If $\mu > 0$: The equilibrium points persist, but their stability reverses: x = 0 becomes unstable, while $x = \mu$ turns stable.

This phenomenon is known as a **transcritical bifurcation** because the equilibrium points exchange their stability characteristics as μ transitions through zero.

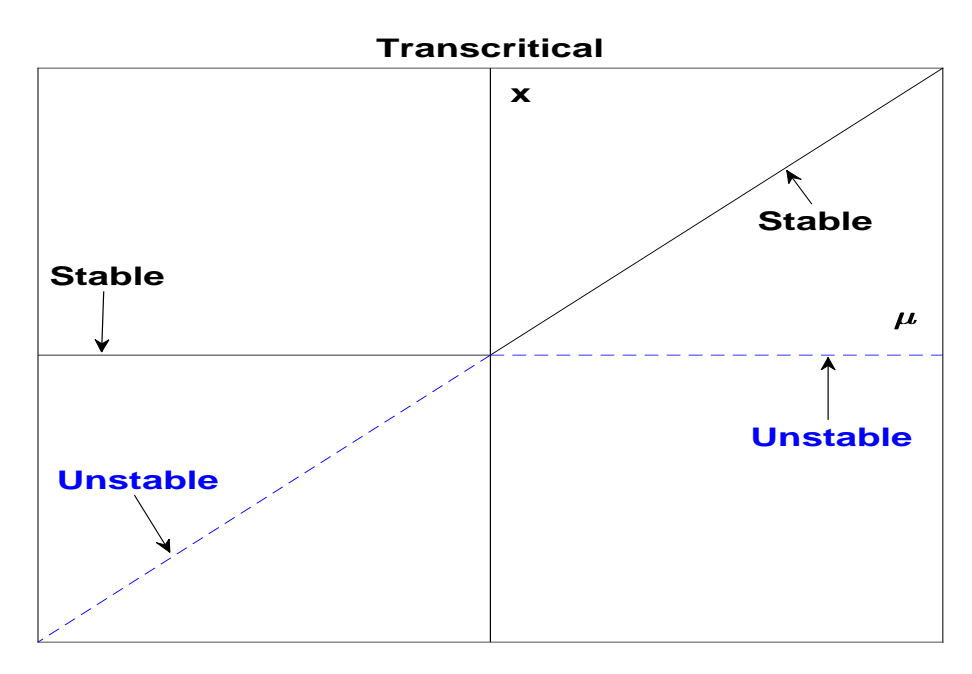


Figure 2.10: Illustration of a transcritical bifurcation.

2.2.5.3 | Pitchfork bifurcation

Supercritical Pitchfork bifurcation

The supercritical pitchfork bifurcation is described by the system:

$$\dot{x} = \mu x - x^3,\tag{2.14}$$

where μ is the bifurcation parameter. The stability and existence of equilibrium points are as follows:

- For μ < 0: A single stable equilibrium exists at x = 0.
- At $\mu = 0$: The equilibrium at x = 0 remains stable, and two additional equilibria begin to emerge.
- For $\mu > 0$: The equilibrium at x = 0 becomes unstable, while two new stable equilibria appear at $x = \pm \sqrt{\mu}$.

Stable Stable Unstable p Stable

Figure 2.11: Supercritical pitchfork bifurcation.

Subcritical Pitchfork bifurcation

The subcritical pitchfork bifurcation follows the system:

$$\dot{x} = \mu x + x^3,\tag{2.15}$$

where μ is the bifurcation parameter. The system behaves as follows:

- For μ < 0: There is a stable equilibrium at x = 0 and two unstable equilibria at $x = \pm \sqrt{-\mu}$.
- At $\mu = 0$: All three equilibria merge at x = 0.
- For $\mu > 0$: The equilibrium at x = 0 becomes unstable, while the two unstable equilibria disappear.

Subcritical Pitchfork Unstable Stable Unstable Unstable

Figure 2.12: Subcritical pitchfork bifurcation.

2.2.5.4 | Hopf bifurcation

Consider the system governed by the control parameter α :

$$\begin{cases} \dot{X} = \alpha X - Y - X(X^2 + Y^2), \\ \dot{Y} = X + \alpha Y - Y(X^2 + Y^2). \end{cases}$$

This system always has an equilibrium point at (X,Y) = (0,0) for any value of α . Expressing it in complex form:

$$\dot{z} = (\alpha + i)z - z|z|^2,$$

where z = X + iY, and rewriting it in polar coordinates $z = \rho e^{i\phi}$, yields:

$$\begin{cases} \dot{\rho} = \rho(\alpha - \rho^2), \\ \dot{\phi} = 1. \end{cases}$$
 (2.16)

The stability of ρ depends on α :

- For α < 0, the equilibrium ρ = 0 remains stable.
- At $\alpha = 0$, the system exhibits neutral stability.
- When $\alpha > 0$, $\rho = 0$ becomes unstable, giving rise to a stable limit cycle at $\rho_0(\alpha) = \sqrt{\alpha}$.

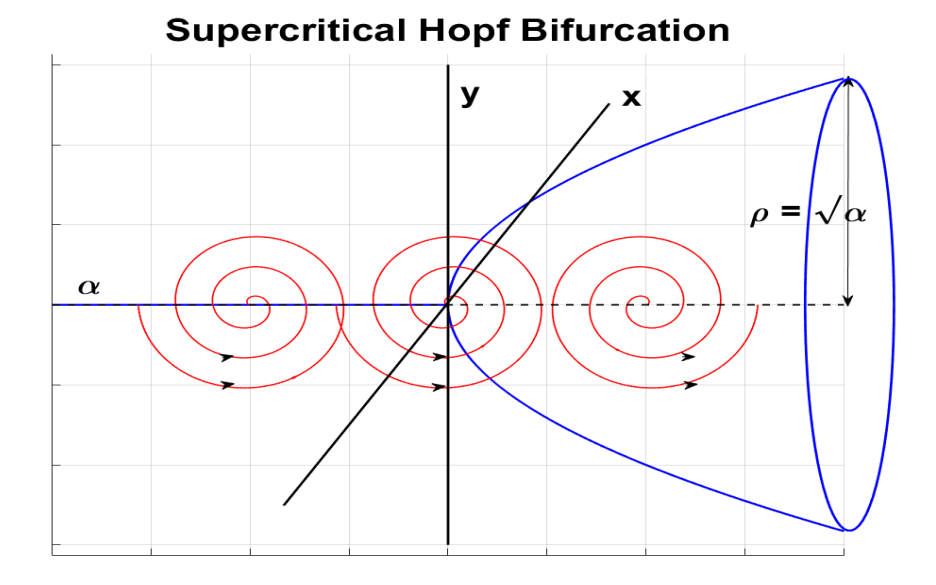


Figure 2.13: Illustration of a supercritical Hopf bifurcation.

This corresponds to a **supercritical Hopf bifurcation**, where a stable equilibrium transforms into a stable limit cycle as α moves past zero.

2.3 | Discrete dynamical systems

Definition 2.15 (Maps and Flows (47)) A map is generally a function $g: \mathcal{X} \to \mathcal{X}$, where the system evolves step by step, and the state at step n + 1, denoted as x_{n+1} , is given by:

$$x_{n+1} = g(x_n). (2.17)$$

Through iteration, this function follows:

$$g^{0}(x) = x$$
, $g^{1}(x) = g(x)$, $g^{k}(x) = g(g^{k-1}(x))$, $\forall k \ge 2$.

Similarly, the sequence of states progresses as:

$$x_0$$
, $x_1 = g(x_0)$, $x_2 = g^2(x_0)$, ..., $x_k = g^k(x_0)$.

For discrete dynamical systems, a flow $\phi_{\tau}(x)$ on \mathcal{X} provides an alternative representation, where $g(x) = \phi_{\tau}(x)$. Here, $x \in \mathcal{X}$ represents the state, and $\tau \in \mathbb{R}$ denotes the discrete time parameter.

2.3.1 | Principles of discrete dynamical systems

Definition 2.16 (*Orbits* (47)) *The forward orbit of an initial point* x_0 *is the sequence:*

$$O^+(x_0) = \{g^k(x_0)\}_{k=0}^{\infty} = \{x_0, g(x_0), g^2(x_0), \dots, g^n(x_0), \dots\}.$$

Similarly, the backward orbit of x_0 is given by:

$$O^{-}(x_0) = \{x_0, g^{-1}(x_0), g^{-2}(x_0), \dots, g^{-n}(x_0), \dots\}.$$

Definition 2.17 (Fixed Point (47)) A point \bar{x} is a fixed point of the function $g : \mathbb{R} \to \mathbb{R}$ if it satisfies:

$$g(\bar{x}) = \bar{x}$$
.

Example 2.2 Consider the function $g : \mathbb{R} \to \mathbb{R}$ given by g(x) = 4x(1-x). To identify its fixed points, we solve g(x) = x, leading to:

$$4x(1-x) = x.$$

Rearranging the terms, we find the solutions x = 0 and $x = \frac{3}{4}$.

A fixed point \bar{x} satisfies $g(\bar{x}) = \bar{x}$, applying g repeatedly gives:

$$g^2(\bar{x}) = g(g(\bar{x})) = g(\bar{x}) = \bar{x}.$$

Extending this further, we get $g^3(\bar{x}) = \bar{x}$ and, more generally, $g^k(\bar{x}) = \bar{x}$ for any $k \in \mathbb{N}$. Therefore, starting from $x_n = \bar{x}$, the sequence remains constant at \bar{x} , indicating that \bar{x} is an equilibrium point of the system.

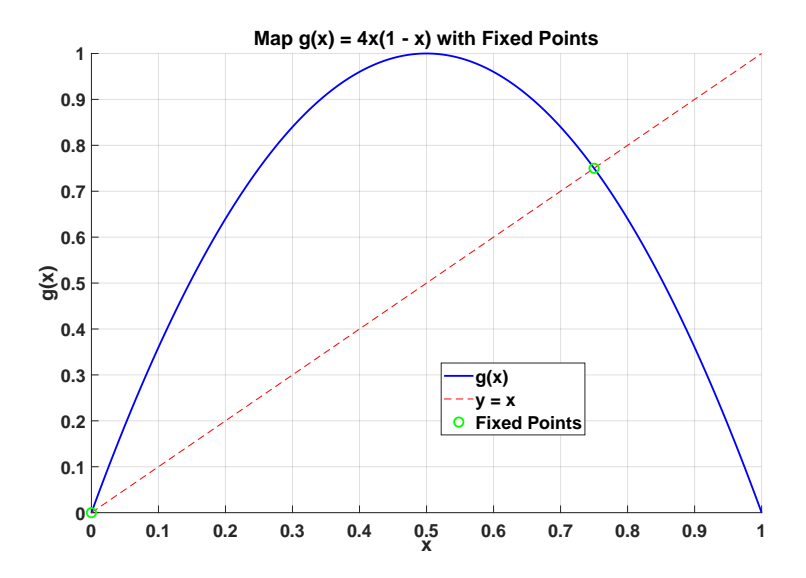


Figure 2.14: Fixed points of g(x) = 4x(1-x).

Definition 2.18 (Stable and Unstable Fixed Points (47)) A fixed point \bar{x} is considered stable if, for any $\epsilon > 0$, there exists $\delta > 0$ such that whenever $||x_0 - \bar{x}|| \leq \delta$, the sequence satisfies $||x_n - \bar{x}|| \leq \epsilon$ for all $n \geq 1$.

If a fixed point does not satisfy this stability condition, it is classified as unstable.

Definition 2.19 (Periodic Points (53)) A point x is called periodic with period k (or a k-periodic point) for a function $f : \mathbb{R} \to \mathbb{R}$ if:

$$f^k(x) = x$$
.

The smallest positive integer k that satisfies this equation is known as the fundamental period of x.

Example 2.3 Let us analyze the behavior of the logistic map:

$$f(x) = ax(1-x),$$

where $0 < a \le 4$. To find 2-periodic points, we solve the system:

$$\begin{cases} f^2(x) = x, \\ f(x) \neq x. \end{cases}$$

For $2 < a \le 4$, this system has two distinct solutions:

$$x_1 = \frac{a+1+\sqrt{a^2-2a-3}}{2a},$$

and

$$x_2 = \frac{a+1-\sqrt{a^2-2a-3}}{2a}.$$

These values correspond to the points in a periodic cycle of length 2. Graphically, they represent the intersections of the curve $f^2(x) = f(f(x))$ with the line y = x, while ensuring $f(x) \neq x$, as illustrated in Figure 2.15.

Definition 2.20 (Periodic Cycles (53)) For a one-dimensional function $g : \mathbb{R} \to \mathbb{R}$, suppose two distinct points p and q satisfy:

$$g(p) = q$$
, $g(q) = p$.

This implies:

$$g^2(p) = g(g(p)) = g(q) = p$$
, $g^2(q) = g(g(q)) = g(p) = q$.

This demonstrates that the set $\{p,q\}$ forms a cycle of period 2, also known as a 2-cycle or 2-orbit. Notably, the points within this cycle are fixed points of g^2 .

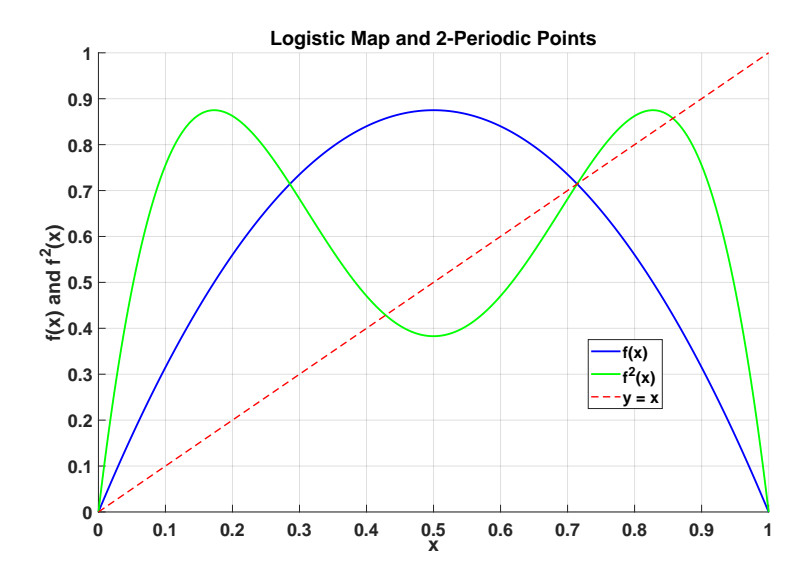


Figure 2.15: Visualization of a 2-periodic cycle, where the intersections of $f^2(x)$ with y = x indicate periodic points.

Definition 2.21 (Stability of a Periodic Point (53)) A periodic point with period k for a function $g: \mathbb{R} \to \mathbb{R}$ is classified based on its stability under g^k :

- It is termed stable if it functions as a stable fixed point of g^k .
- It is labeled unstable if it acts as an unstable fixed point of g^k .

Definition 2.22 (Stability of a Periodic Cycle (53)) A periodic orbit $(x_0, x_1, ..., x_{p-1})$ within a dynamical system defined by g is stable if each of its points x_i (for i = 0, 1, ..., p - 1) serves as a stable fixed point under the function g^p .

If a periodic orbit fails to meet this stability criterion, it is referred to as unstable.

Definition 2.23 (Eventually Fixed Points, Periodic Points, and Periodic Orbits (47))

- A point p is referred to as an eventually fixed point of a function g if it is not initially a fixed point but reaches one after a finite number of iterations. Specifically, p satisfies $g^n(p) = x$, where x is a fixed point of g, and for some positive integer n, it holds that $g^{n-1}(p) \neq x$. This ensures that applying g once more yields $g^{n+1}(p) = g(g^n(p)) = g(x) = x$, confirming that $g^n(p)$ remains unchanged under g.
- A point p is called an eventually periodic point if it does not start as periodic but becomes so after a finite number of iterations. More formally, p is eventually periodic with period k if there exists an integer N > 0 such that for all $n \ge N$, the condition $g^{n+k}(p) = g^n(p)$

holds. This implies that after a certain number of iterations, $g^n(p)$ behaves as a k-periodic point of g.

■ An orbit is referred to as an eventual periodic orbit if it initially follows a non-repeating path but eventually settles into a periodic cycle after a finite number of steps.

Cobweb method

The **cobweb method** is a visual technique for analyzing trajectories in dynamical systems. Fixed points of a function f(x) are located at the intersections of its graph with the line y = x. To depict the trajectory $O(x_0)$, the method follows these steps as described in (53):

- Draw a vertical segment from $(x_n, 0)$ to $(x_n, f(x_n))$.
- Connect it with a horizontal segment from $(x_n, f(x_n))$ to $(f(x_n), f(x_n))$ along the line y = x.
- Repeat the process to visualize the orbit's trajectory and its convergence or divergence.

Example 2.4 Examples with the logistic map f(x) = ax(1-x):

- 1. Convergence to a fixed point: For f(x) = 2.9x(1-x), the trajectory $O(x_0)$ spirals towards the fixed point $x^* = \frac{19}{29}$ (see Figure 2.16).
- 2. **Periodic orbits**: For f(x) = 3.4x(1-x), $O(x_0)$ converges to a 2-periodic orbit (see Figure 2.17).
- 3. *Higher-periodic orbits*: For f(x) = 3.4495x(1-x), $O(x_0)$ converges to a 4-periodic orbit (see Figure 2.18).
- 4. Chaotic behavior: For f(x) = 4x(1-x), $O(x_0)$ shows chaotic behavior (see Figure 2.19).

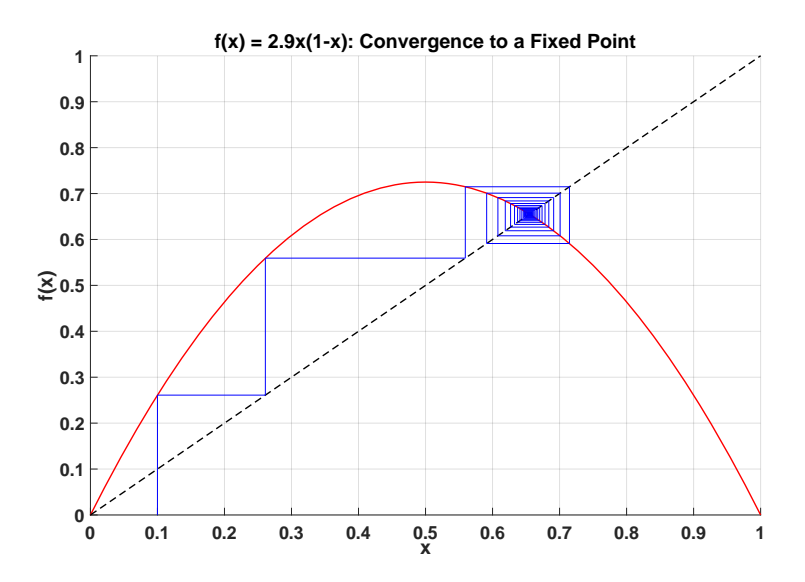


Figure 2.16: Cobweb plot for f(x) = 2.9x(1-x) showing convergence to a stable fixed point.

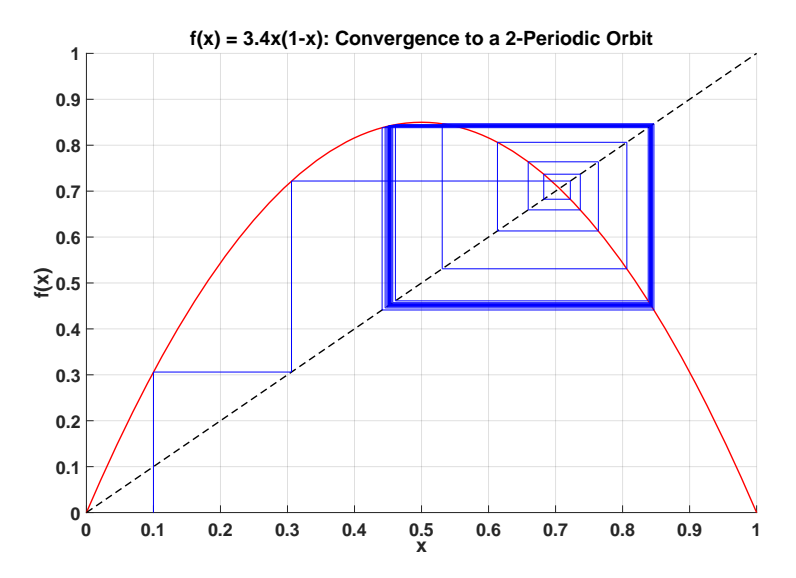


Figure 2.17: Cobweb plot for f(x) = 3.4x(1-x) illustrating convergence to a 2-periodic orbit.

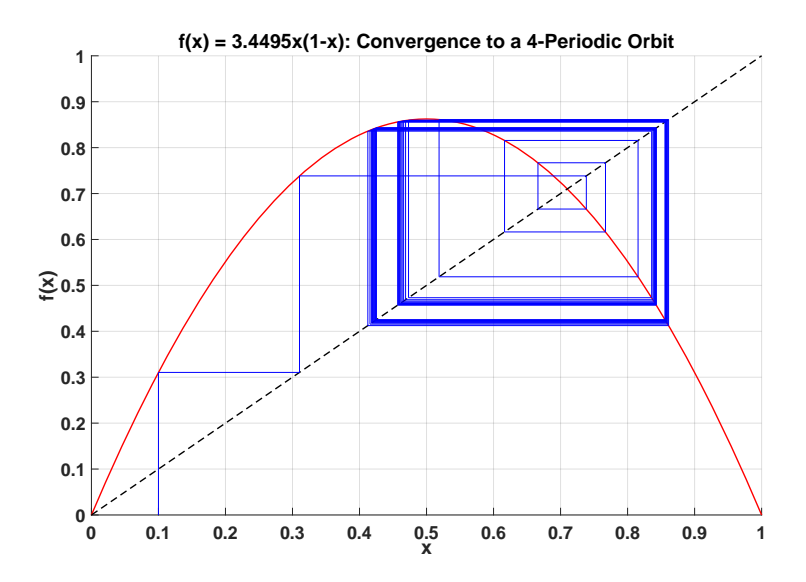


Figure 2.18: Cobweb plot for f(x) = 3.4495x(1-x) showing convergence to a 4-periodic orbit.

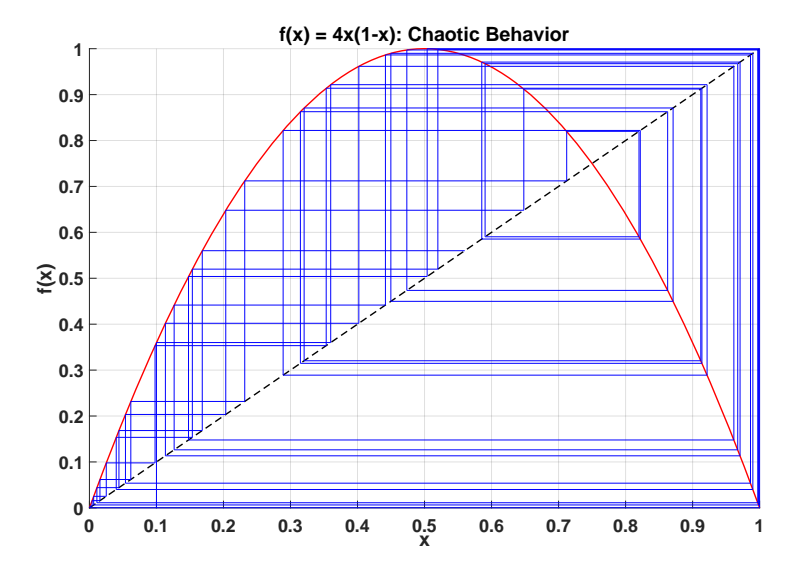


Figure 2.19: Cobweb plot for f(x) = 4x(1-x) illustrating chaotic dynamics.

2.3.2 | Stability analysis

Studying the behavior of a discrete dynamical system requires examining the stability of its fixed points. In this context, we focus primarily on fixed points. For periodic points with period p, it suffices to analyze the p-th iteration of the function (59).

Consider a discrete-time nonlinear system described by:

$$x(n+1) = F(x(n)),$$
 (2.18)

where the system's evolution follows:

$$x(n) = x(n, n_0, x(n_0)),$$
 (2.19)

subject to the initial condition:

$$x(n_0) = x(0). (2.20)$$

A fixed point \bar{x} of the system satisfies:

$$\bar{x} = F(\bar{x}). \tag{2.21}$$

Definition 2.24 A system is considered Lyapunov stable at a fixed point \bar{x} if any small perturbation from \bar{x} does not grow significantly over time, meaning the trajectory remains arbitrarily close to \bar{x} for all future steps. Formally, this means:

$$\forall \epsilon > 0, \exists \delta > 0 \text{ such that if } \|x(n_0) - \bar{x}\| < \delta, \text{ then } \|x(n, n_0, x(n_0)) - \bar{x}\| < \epsilon, \forall n \geq n_0.$$

Definition 2.25 A fixed point \bar{x} is said to be attractive if trajectories that begin close to \bar{x} tend to approach it as time progresses. Formally, this is expressed as:

$$\forall n_0 \in \mathbb{N}, \exists \delta_0(n_0) \text{ such that: } ||x(n_0) - \bar{x}|| < \delta_0(n_0) \Rightarrow \lim_{n \to \infty} x(n, n_0, x(n_0)) = \bar{x}.$$

If $\delta_0(n_0) = +\infty$, the fixed point is globally attractive.

Definition 2.26 A fixed point \bar{x} is considered asymptotically stable if it satisfies both Lyapunov stability and attractiveness.

2.3.2.1 | Linearization (Indirect method)

Consider a nonlinear system given by equation (2.18), which can be locally approximated near $\bar{x} = 0$ using a Taylor series expansion:

$$x(n+1) = Ax(n) + r(||x||).$$

where *A* is a constant matrix, and the remainder term r(||x||) satisfies:

$$\lim_{\|x\|\to 0} \frac{\|r(\|x\|)\|}{\|x\|} = 0.$$

By omitting the higher-order terms, we arrive at the linearized system:

$$x(n+1) = Ax(n)$$
.

This system represents a local approximation of equation (2.18) near $\bar{x} = 0$, enabling us to evaluate the stability of the nonlinear system at this equilibrium point.

Theorem 2.15 *Consider the eigenvalues of the matrix A:*

- 1. If all eigenvalues have absolute values strictly less than one, then \bar{x} is asymptotically stable.
- 2. If at least one eigenvalue has an absolute value greater than one, then \bar{x} is unstable.
- 3. If some eigenvalues lie on the unit circle while others are inside it, the stability of \bar{x} cannot be determined definitively.

2.3.2.2 | Lyapunov function (Direct method)

The Lyapunov direct method provides a stability analysis without requiring an explicit solution of the system's equations.

We introduce a function $\mathcal{L}(x(n)): \mathbb{R}^n \to \mathbb{R}^+$, known as the Lyapunov function, which satisfies the following condition:

■ The function $\mathcal{L}(x(n))$ is positive definite, meaning it satisfies $\mathcal{L}(x(n)) > 0$ for all $x(n) \neq 0$, and $\mathcal{L}(0) = 0$.

The key idea is to study the behavior of $\mathcal{L}(x(n))$ instead of directly analyzing $x(n, n_0, x(n_0))$. If the difference $\Delta \mathcal{L}(x(n))$ is negative definite for all n and for x(n) in a neighborhood of $\bar{x} = 0$, such that:

$$\forall x(n), \quad \Delta \mathcal{L}(x(n)) = \mathcal{L}(x(n+1)) - \mathcal{L}(x(n)) = \mathcal{L}(F(x(n))) - \mathcal{L}(x(n)) < 0,$$

then the equilibrium point $\bar{x} = 0$ is considered stable.

2.3.3 | Bifurcation theory

Consider the following nonlinear dynamical system:

$$x(n+1) = F(x(n), \alpha), \tag{2.22}$$

where $x(n) \in \mathbb{R}^n$, $\alpha \in \mathbb{R}^m$, $n \in \mathbb{N}$, and $F : \mathbb{R}^n \times \mathbb{R}^m \times \mathbb{N} \to \mathbb{R}^n$.

Definition 2.27 We define a bifurcation as a qualitative change in the solution \bar{x} of system (2.22) that arises from variations in the control parameter α . This change manifests as the emergence of new solutions, the disappearance of existing ones, or an alteration in their stability properties.

Definition 2.28 A bifurcation diagram is a graphical representation of the parameter space that maps all bifurcation points, illustrating how the system's qualitative behavior changes as a parameter varies.

Types of bifurcation

There are several types of bifurcation based on the properties of the second derivatives of the family of functions $F(x(n), \alpha)$. Each type of bifurcation is characterized by a normal form, which is the typical general equation for that type of bifurcation (31; 33). Among the different types of bifurcations for discrete dynamical systems, we find (59):

Fold bifurcation (Pli bifurcation)

The fold bifurcation is a catastrophic bifurcation. This means that when the control parameter varies, two cycles of order k with different stabilities appear. At the bifurcation point, the two cycles merge, and the multiplier $DF(x(k), \alpha)$ equals 1. To understand the mechanism of this bifurcation, let us now look at a specific example.

Example 2.5 Consider the dynamical system defined by the function:

$$f_c(x) = x^2 + x + c,$$

where c is the bifurcation parameter. The graphs of the function $f_c(x)$ for c > 0, c = 0, and c < 0 are shown in Figure 4.1.

The fixed points of the equation $x^2 + x + c = x$ are solutions of

$$x^2 + c = 0$$
.

For c>0, there are no real fixed points. For c=0, there is one fixed point at x=0. For c<0, there are two fixed points given by $x_1,x_2=\pm\sqrt{-c}$. The iteration $f_c(x)$ exhibits a fold bifurcation at c=0, with the fixed point x=0 having a multiplier f'(0)=1. For c<0, the multipliers of the points $x_1=\sqrt{-c}$ and $x_2=-\sqrt{-c}$ are:

$$f'(x_1) = 2\sqrt{-c} + 1 > 1$$
 (x₁ is repulsive),

$$f'(x_2) = -2\sqrt{-c} + 1 < 1$$
 (x₂ is attractive).

The bifurcation diagram in the (c, x) space is shown in Figure 2.20.

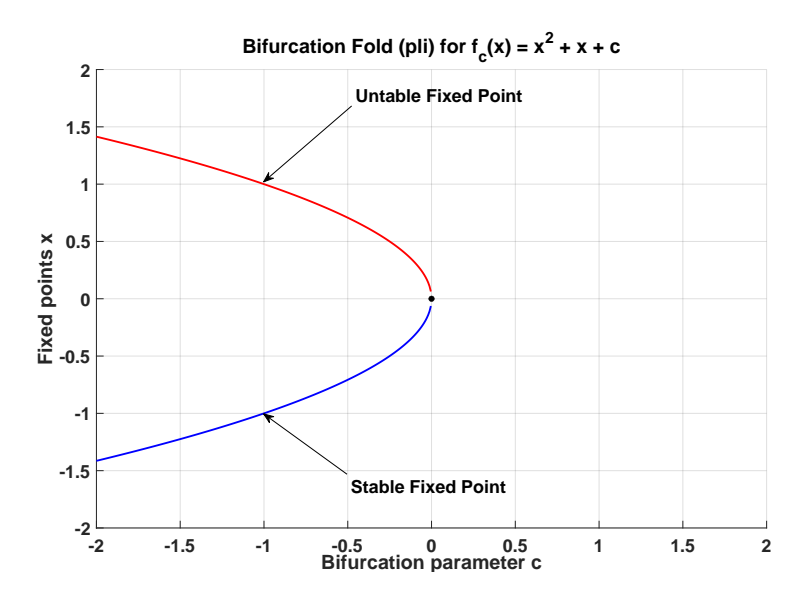


Figure 2.20: Bifurcation diagram illustrating the Fold bifurcation.

Period-doubling bifurcation (Flip bifurcation)

This bifurcation occurs when a stable cycle of order k has a multiplier that passes through $DF(x(k), \alpha) = -1$. The cycle then becomes unstable and gives rise to a stable cycle of order 2k.

Example 2.6 Consider the logistic function f defined by:

$$f_a(x) = ax(1-x).$$

where a is the bifurcation parameter. The logistic function $f_a(x)$ undergoes a period-doubling bifurcation at a=3 at the fixed point $x_1=\frac{a-1}{a}$ with a multiplier S=-1. The bifurcation diagram in the (a,x) space is shown in Figure 2.21.

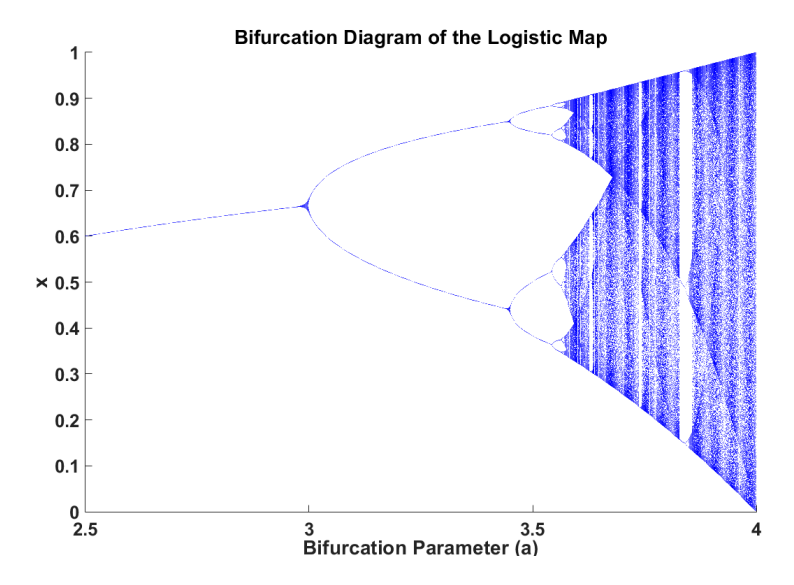


Figure 2.21: Bifurcation diagram illustrating the period-doubling bifurcation.

Neimark-sacker bifurcation

The Neimark-Sacker bifurcation can occur only in systems with dimensions greater than one. It is distinguished by the emergence of a closed invariant curve from a fixed point when the bifurcation parameter surpasses a critical threshold. This transition happens as the fixed point undergoes a stability change due to a pair of complex eigenvalues with a modulus of one.

Transcritical bifurcation

In a transcritical bifurcation, two fixed points of a dynamical system exchange their stability. The stability of one fixed point becomes unstable while the other becomes stable as the bifurcation parameter crosses a critical value.

Example 2.7 *Consider the system:*

$$f_{\alpha}(x) = \alpha x(1-x).$$

where α is the bifurcation parameter. For $\alpha < 0$, the system has one stable and one unstable fixed point. As α increases and passes through 0, the fixed points exchange stability, resulting in the transcritical bifurcation.

The associated bifurcation diagram, illustrated in Figure 2.22, depicts two fixed points intersecting at $\alpha = 0$, where the stability exchange occurs.

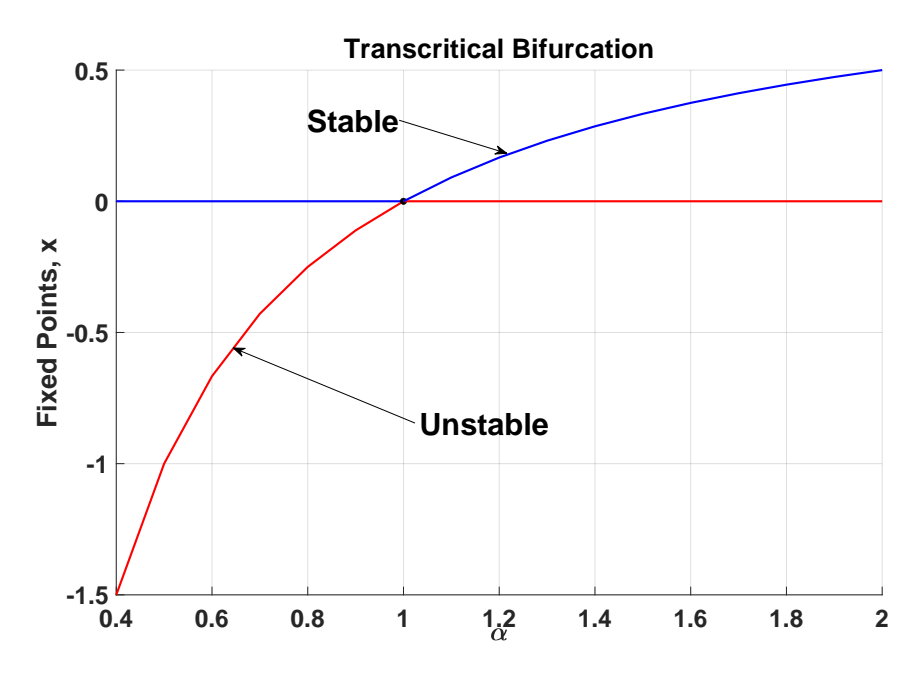


Figure 2.22: Bifurcation diagram illustrating the transcritical bifurcation.

Conclusion

In this chapter, we delved into the fundamental principles of dynamical systems, covering both continuous and discrete models. We began with a general overview, establishing the essential foundations for analyzing system behavior. The discussion on continuous dynamical systems focused on equilibrium points, stability analysis, and bifurcation theory, demonstrating their role in understanding qualitative system dynamics. Likewise, discrete dynamical systems were examined, highlighting their iterative nature, stability conditions, and bifurcation phenomena. These concepts collectively provide a comprehensive framework for studying complex systems and support more advanced investigations in the subsequent chapters.

Mathematical modeling of infectious diseases

Contents			
3.1	A Brief history of epidemics		42
3.2	Terminology		43
3.3	Mathematical modeling in epidemiological research		44
	3.3.1 The dyr	namic infection process	45
	3.3.2 What ar	re the goals of epidemic modeling?	45
3.4	The fundamental reproductive ratio \mathcal{R}_0 4		46
3.5	Introduction to simple epidemic models		48
	$3.5.1$ \mathcal{SI} mod	lel	48
	$3.5.2$ \mathcal{SIS} mo	odel	50
	$3.5.3$ \mathcal{SIR} m	odel	53
	3.5.4 $SIRS$ 1	model	61
	$3.5.5$ \mathcal{SEIR} 1	Model	65
3.6	Case studies and applications of infectious disease modeling		66
	3.6.1 Dengue	Fever and the $\mathcal{SIR} - \mathcal{SI}$ model	67
	3.6.2 Ebola ar	nd the \mathcal{SEIR} control model	68
Con	lusion		69

This chapter aims to explore the mechanisms behind the spread of contagious diseases by examining traditional epidemiological models, specifically the "SI, SIS, SIR, SIRS, SEIR" models.

In these models, the population is categorized into four distinct groups, known as 'compartments' in epidemiology:

- Susceptible or Healthy individuals (S): Those who have never contracted the disease and are at risk of infection.
- **Exposed individuals (E)**: People who have encountered an infected person and carry the pathogen without showing symptoms. They have minimal pathogen levels, which are not enough to transmit the infection to others.
- *Infected individuals* (*I*): Those who are currently ill and capable of spreading the disease (a key assumption in these models).
- **Recovered individuals (R)**: Individuals who have recovered and are immune. This category also includes deceased individuals, as they are no longer susceptible to the disease, which is considered for practical reasons.

3.1 | A Brief history of epidemics

The history of epidemics offers a compelling narrative that highlights humanity's struggle against disease. The "Black Death" in the 14th century is perhaps one of history's most notorious pandemics, and it swept across Europe. The population at the time, about 85 million, saw about a third of the population fall victim to the plague.

An early documented epidemic is the Plague of Athens, which struck Athens in the period between 430 and 426 BCE. The historian Thucydides chronicled the event, describing symptoms such as headaches, conjunctivitis, a rash, and fever, followed by severe stomach pain, vomiting, and "ineffective retching." Most victims perished within a week. The epidemic claimed tens of thousands of lives and spread swiftly across Athens. According to a study by Paul and Holladay (1979), the disease either disappeared or underwent significant changes over time, with subsequent studies proposing additional theories.

Epidemiological research, with its extensive history, has yielded numerous models and theories to explain the origins and spread of diseases. In earlier times, epidemics were frequently attributed to supernatural causes, such as divine punishment or malevolent spirits. For instance, AIDS, the dominant epidemic of the past few decades, was often interpreted in a religious context as retribution.

In the United States, the Yellow Fever outbreak in Philadelphia in 1793 marked the first major epidemic. Approximately 5,000 people out of a population of 50,000 died, while an estimated 20,000 fled the city. This epidemic left a lasting impact on the nation's political and social landscape.

In the 20th century, the Spanish flu pandemic of 1918–1920 emerged as one of the deadliest outbreaks, affecting an estimated 500 million people globally and resulting in up to 50 million deaths. The disease was caused by the H1N1 influenza virus, which also caused the swine flu pandemic nearly a century later. Many deaths were due to secondary bacterial lung infections, and complications included encephalitis lethargica, a condition explored in Oliver Sacks' book *Awakenings* and later dramatized in a 1990 film.

Following World War II, public health efforts emphasized eradicating disease-causing organisms. The development of antibiotics fostered optimism, and in 1978, the United Nations initiated the *Health for All*, 2000 initiative, aiming to eliminate diseases by the year 2000. This optimism, however, was tempered by the discovery of AIDS and the realization that microbes could evolve to resist treatments. The last case of smallpox had been recorded in 1977, fueling hopes of controlling infectious diseases (51).

In 2003, the SARS (Severe Acute Respiratory Syndrome) outbreak, caused by a coronavirus, emerged in China and Hong Kong. The virus was transmitted from bats to humans through civet cats. SARS, with symptoms resembling the flu, spread to countries including Singapore, the USA, and Canada but remained relatively contained, with fewer than 10,000 cases. No vaccine for SARS has been developed to date (38).

Another coronavirus-related outbreak, MERS (Middle Eastern Respiratory Syndrome), occurred in Saudi Arabia in 2012 and spread across various regions in the world, including Europe and the United States. It caused flu-like symptoms such as fever and cough but had a smaller global impact (24).

In late 2019, a COVID-19 pandemic in Wuhan, China, swept across the world at a quick velocity and produced widespread lockdown and far-reaching political and financial implications. This ongoing pandemic underscores the persistent challenges posed by emerging infectious diseases (23).

3.2 | Terminology

Epidemic: A rapid increase in the incidence of a pathology. Although often used in the context of infectious diseases, this term can be used for general biological phenomena (smallpox, avian flu, HIV, coronavirus, etc.).

Epidemic threshold: A theoretical threshold in mathematical models above which an epidemic will (or may) occur.

Pandemic: Caused by an emerging infectious disease that takes on continental or even global proportions.

Endemic: The usual and stable presence of a disease in a population.

Patient zero: The first recognized case of an infectious pathology that is the source of all other recorded cases.

Infectious agents (pathogens): Infectious agents are the pathogens responsible for infectious diseases. They can be of different types: bacteria, viruses, parasites, fungi, or prions.

Infectious diseases: Infectious diseases are transmissible diseases caused by a specific infectious agent or its toxins. They can spread directly from person to person, as seen with influenza, measles, or diphtheria; through vectors like mosquitoes for chikungunya or malaria; or via the environment, such as through contaminated food or water, as in salmonellosis or cholera.

Vertical transmission: The transmission of a disease is said to be vertical when it occurs from parents to offspring. This is the case, for example, with mother-to-child transmission.

Horizontal transmission: The transmission of a disease is said to be horizontal when it occurs after birth through contact with another person who is infected.

Incubation period: The time span from exposure to the onset of symptoms.

Latency period: The period between primary contact and when one is infectious.

3.3 | Mathematical modeling in epidemiological research

Mathematical models in epidemiology have been gaining momentum in the literature in recent years due to their numerous benefits. These models can address various challenges in epidemiology, such as predicting disease progression based on real data, analyzing epidemic dynamics to identify effective control strategies, monitoring and tracking the epidemic, and estimating disease-related parameters.

Epidemiological mathematical models are generally categorized into four main types: discrete or continuous models, ODE (Ordinary Differential Equation) models, PDE (Partial Differential Equation) models, and deterministic or stochastic models.

The transmission of an infectious disease occurs through several stages, commonly known as the infection or contagion process.

3.3.1 | The dynamic infection process

The spread of disease and surrounding environmental factors greatly influence its widescale transmission. A person becomes infected with an infectious disease when exposed to a source (also called a pathogen), which can take various forms (such as an infected person, a mosquito, or a contaminated water source). The contagion process refers to the event in which the infection is transferred from one pathogen to another.

The following diagram (Figure 3.1) visually represents this process:

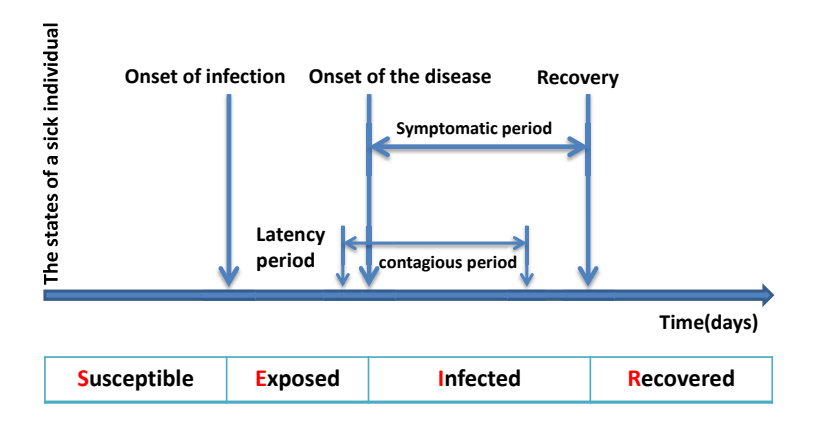


Figure 3.1: The dynamic infection process

This schematic shows the various phases or states of the disease. An individual becomes contagious only after infection. The infected person remains contagious for a certain time: they may either become susceptible to reinfection, develop resistance to new infections, or pass away.

3.3.2 | What are the goals of epidemic modeling?

Modeling in epidemiology is principally concerned with predicting the course or pattern of the disease in question. The investigation of an epidemic is commenced based on a sample, and depending upon findings thus obtained, a model is created in order to represent the population as a whole.

The objectives of epidemic modeling include:

- Enhancing the understanding of the processes through which diseases are transmitted.
- Highlighting the importance of a mathematical framework.

- Forecasting the future progression of the epidemic.
- Developing strategies to control epidemic spread, such as reducing the number of susceptible individuals through vaccination programs.
- Selecting optimal vaccine distribution strategies to eradicate certain diseases.
- Identifying relevant data to collect or record.
- Predicting the extent and size of epidemics.
- Forcing a clarification and specification of assumptions.

3.4 | The fundamental reproductive ratio \mathcal{R}_0

The fundamental reproductive ratio, \mathcal{R}_0 , is the expected number of cases caused by a single infectious person in a population in which each individual is susceptible for the period of infectiousness.

In actuality:

- If \mathcal{R}_0 < 1: The disease-free state is locally stable, and we can anticipate the infection to die out.
- If $\mathcal{R}_0 > 1$: The disease-free state is no longer stable, and the infection is able to persist and potentially spread widely in the population.

Calculation methods for \mathcal{R}_0

• The first method (Anderson and May (27))

The fundamental reproductive ratio is given by:

$$\mathcal{R}_0 = \beta * C * D$$

With: β : Probability of transmission per contact. C: Length of infection. D: Number of contacts in unit time.

Second method (Definition of Bockh 1886 (72))

Let F(a) denote the probability of a woman surviving to age a, and $\beta(a)$ denote the birth rate at age a. Then:

$$\mathcal{R}_0 = \int_0^\infty F(a)\beta(a)da$$

• Third method (Next generation matrix (72))

In this approach, \mathcal{R}_0 is determined as the spectral radius of the "next generation operator." This operator is derived by separating the population into two categories: the infected and the uninfected compartments.

In an n-compartment epidemiological model for n homogeneous compartments, the system state is represented by the vector y, in which y_j is the concentration or number in compartment j. The compartments are labeled in a way in which the latter are infectious (latent, infectious, etc.). The infection-free individuals are represented by the first k compartments (Susceptible, etc.).

We notice:

- $F_i(y)$: emergence velocity of new infection in compartment "i" (among different individuals) or in a vertical way (to baby from mother).
- $V_i^+(y)$: the speed of what comes from the other compartments by all causes (displacement, aging, healing).
- $V_i^-(y)$: the speed of leaving the compartment (movement, mortality, change of status...) in such a way:

We note Y_s the state without disease $Y_s = \{y/y_{v+1} = y_v = ... = y_n = 0\}$.

The following assumptions are made:

- 1. $y \ge 0$ et $F_i(y) \ge 0$, $V_i^+(y) \ge 0$, $V_i^-(y) \ge 0$.
- 2. if $y_i = 0$ so $V_i^+(y) = 0$, If there is nothing in a compartment, nothing can come out. This is the essential property of a compartmental model.
- 3. if $i \ge p$ so $F_i(y) = 0$. Compartments with an index lower than "p" are "uninfected". By definition, infected cannot appear in these compartments.
- 4. if $y \in Y_s$ or $\dot{y}_i = F_i(y) + V_i^+(y) V_i^-(y)$, so $F_i = 0$ and for $i \ge p$, we have $V_i^+(y) = 0$. If there are no carriers of germs in the population, there can be no new infected.

The linear system is rewritten:

$$\dot{y}(t) = F_i(y) + V_i^+(y) - V_i^-(y),$$

The Jacobian matrix around the point of equilibrium without disease y_0 of the linear system is written:

$$J(y_0) = DF(y_0) + D(V^+ - V^-)(y_0).$$

Or:
$$DF(y_0) = \begin{pmatrix} g & 0 \\ 0 & 0 \end{pmatrix} \text{ and } D(V^+ - V^-)(y_0) = \begin{pmatrix} v & 0 \\ J_1 & J_2 \end{pmatrix}.$$
 with: $v = \frac{dV_i}{dt} \int_{1 < i,j < m} dt dt$ and $g = \frac{dF_i}{dt} \int_{1 < i,j < m} dt dt$

Or: $g \ge 0$ is a positive matrix and v is an invertible Metzler matrix.

Definition 3.1

Metzler matrix or quasi-positive matrix or non-negative matrix, the matrix which has positive off-diagonal elements.

 $\mathcal{M}=(a_{ij}), a_{ij} \geqslant 0, i \neq j,$ if \mathcal{M} is a Metzler matrix so the following properties are equivalent:

- \blacksquare *M is asymptotically stable.*
- \mathcal{M} is invertible (det(\mathcal{M}) \neq 0) and \mathcal{M}^{-1} is positive definite.

Definition 3.2 The spectral radius of a matrix \mathcal{M} is the largest modulus among its eigenvalues. It is given by

$$\rho(\mathcal{M}) = \max_{\lambda \in \operatorname{sp}(\mathcal{M})} |\lambda|,$$

where $sp(\mathcal{M})$ denotes the spectrum of \mathcal{M} .

Definition 3.3

We have $\mathcal{R}_0 := \rho(-gv^{-1})$ in the following sense: ρ is the spectral radius of the matrix $-gv^{-1}$.

3.5 | Introduction to simple epidemic models

$3.5.1 \mid \mathcal{SI} \mod \mathsf{el}$

In 1906, **W. H. Hamer** introduced the SI model, which represents the earliest and simplest form of a dynamic infectious disease model (3).

The assumptions made in the SI model are:

- 1. The population size is \mathcal{N} , a fixed value, it means: $\mathcal{N}(t) = \mathcal{S}(t) + \mathcal{I}(t)$ so $\dot{\mathcal{N}} = \dot{\mathcal{S}} + \dot{\mathcal{I}} = 0$.
- 2. New individuals enter the population without any pre-existing immunity.
- 3. Once infected, the individuals stay infected (there's no cure or vaccine).

The Hamer model is represented using the following system of equations:

$$\begin{cases} \dot{S} = -\beta S \frac{\mathcal{I}}{\mathcal{N}}, \\ \dot{\mathcal{I}} = \beta S \frac{\mathcal{I}}{\mathcal{N}}. \end{cases}$$
(3.1)

With:

- \blacksquare \mathcal{N} : The total number of individuals in the population.
- \blacksquare \mathcal{S} : The number of individuals who are susceptible to the disease.
- \mathcal{I} : The number of individuals who are currently infected.
- **\blacksquare** β : The rate at which the disease is transmitted.



Figure 3.2: Diagram illustrating the dynamics of an SI model.

Since the population remains constant, S can be expressed as S = N - I. This implies that the dynamics of the susceptible population are directly influenced by the infected population I. The simplified system is given as:

$$\dot{\mathcal{I}} = \beta(\mathcal{N} - \mathcal{I}) \frac{\mathcal{I}}{\mathcal{N}}.$$
(3.2)

The equilibrium points of this system are:

- $\mathcal{I}_{DFE} = 0$: representing the disease-free equilibrium.
- $\mathcal{I}_{EE} = \mathcal{N}$: representing the endemic equilibrium.

To analyze stability, we define the function:

$$f(\mathcal{I}) = \beta(\mathcal{N} - \mathcal{I})\frac{\mathcal{I}}{\mathcal{N}}.$$

Taking its derivative:

$$f'(\mathcal{I}) = \beta - \frac{2\beta\mathcal{I}}{\mathcal{N}}.$$

Evaluating equilibrium stability:

- At $\mathcal{I}_{DFE} = 0$: $f'(0) = \beta > 0$, indicating instability.
- At $\mathcal{I}_{EE} = \mathcal{N}$: $f'(\mathcal{N}) = -\beta < 0$, indicating asymptotic stability.

Figure 3.3 depicts the results of a numerical simulation of the \mathcal{SI} model with a population of 1000 individuals, starting with 999 susceptible and 1 infected individual. Given a transmission rate of $\beta=0.5$, the simulation demonstrates the decline of the susceptible population as the number of infected individuals increases. Initially, infections rise rapidly before leveling off as the susceptible population diminishes. This model effectively captures disease transmission dynamics and stabilization as susceptible individuals are depleted.

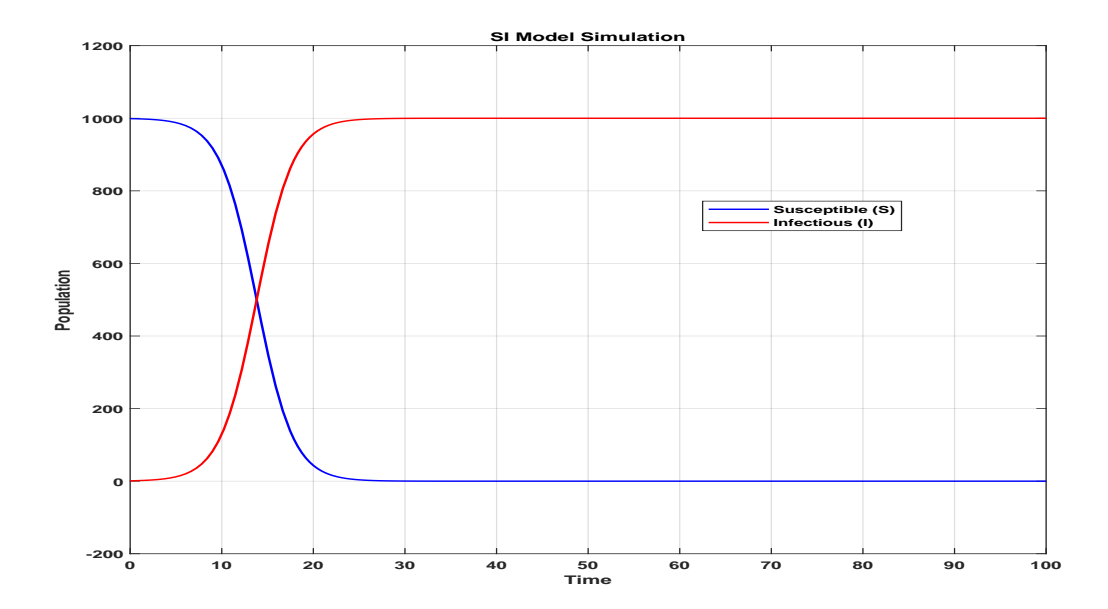


Figure 3.3: Simulation results of the SI model with a transmission rate of $\beta = 0.5$ and initial values given by $S_0 = 999$ and $I_0 = 1$.

$3.5.2 \mid \mathcal{SIS} \mod el$

This model is applicable to diseases such as tuberculosis, influenza, measles, and chickenpox, which do not provide immunity after recovery. To understand the transmission patterns of such diseases, Kermack and McKendrick (1932) introduced the \mathcal{SIS} model.

The model is governed by the following equations (51):

$$\begin{cases}
\dot{S} = -\beta S \frac{\mathcal{I}}{N} + \gamma \mathcal{I}, \\
\dot{\mathcal{I}} = \beta S \frac{\mathcal{I}}{N} - \gamma \mathcal{I}.
\end{cases} (3.3)$$

Where

- *S*: The number of individuals who are susceptible in the population.
- \mathcal{I} : The number of individuals who are infected in the population.
- *β*: The rate at which the disease spreads during contact between susceptible and infected individuals.
- γ : The rate at which infected individuals leave the population, either through recovery or death.

Since
$$\mathcal{N} = \mathcal{S} + \mathcal{I}$$
, then $\dot{\mathcal{N}} = \dot{\mathcal{S}} + \dot{\mathcal{I}} = 0$.

This suggests that the overall population size remains unchanged.

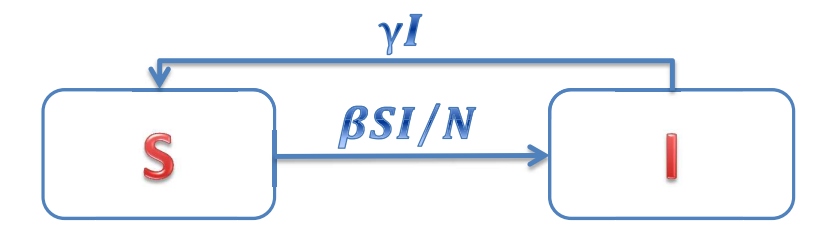


Figure 3.4: Flow diagram representing the dynamics of an SIS model.

The fundamental reproductive ratio, \mathcal{R}_0 , is given by:

$$\mathcal{R}_0 = \frac{\beta}{\gamma}.$$

By substituting S with (N - I), system (6.4) simplifies to:

$$\dot{\mathcal{I}} = \beta(\mathcal{N} - \mathcal{I})\frac{\mathcal{I}}{\mathcal{N}} - \gamma \mathcal{I}. \tag{3.4}$$

The equilibrium points, obtained from equation (6.5), are:

■ $\mathcal{I}_{DFE} = 0$: representing the disease-free equilibrium.

lacksquare $\mathcal{I}_{\it EE} = (eta - \gamma) rac{\mathcal{N}}{eta}$: representing the endemic equilibrium.

The *EE* exists when $\beta - \gamma > 0$, which implies $\mathcal{R}_0 > 1$.

- \mathcal{I}_{DFE} is asymptotically stable when $\mathcal{R}_0 < 1$ and unstable when $\mathcal{R}_0 > 1$.
- The EE is stable when it exists.

Figure 3.5 presents a numerical simulation of the Susceptible-Infected-Susceptible (SIS) model using predefined parameter values. The simulation runs with a transmission rate of $\beta=0.5$ and a recovery rate of $\gamma=0.2$, governing the spread of infection. The initial conditions assume 990 susceptible and 10 infected individuals, cycling between susceptibility and infection. These oscillations illustrate the ongoing transmission and recovery within the population. Over time, the number of infected individuals varies based on the values of β , γ , and initial conditions. The long-term behavior and equilibrium depend on the relationship between infection and recovery rates, influencing the duration and magnitude of outbreaks.

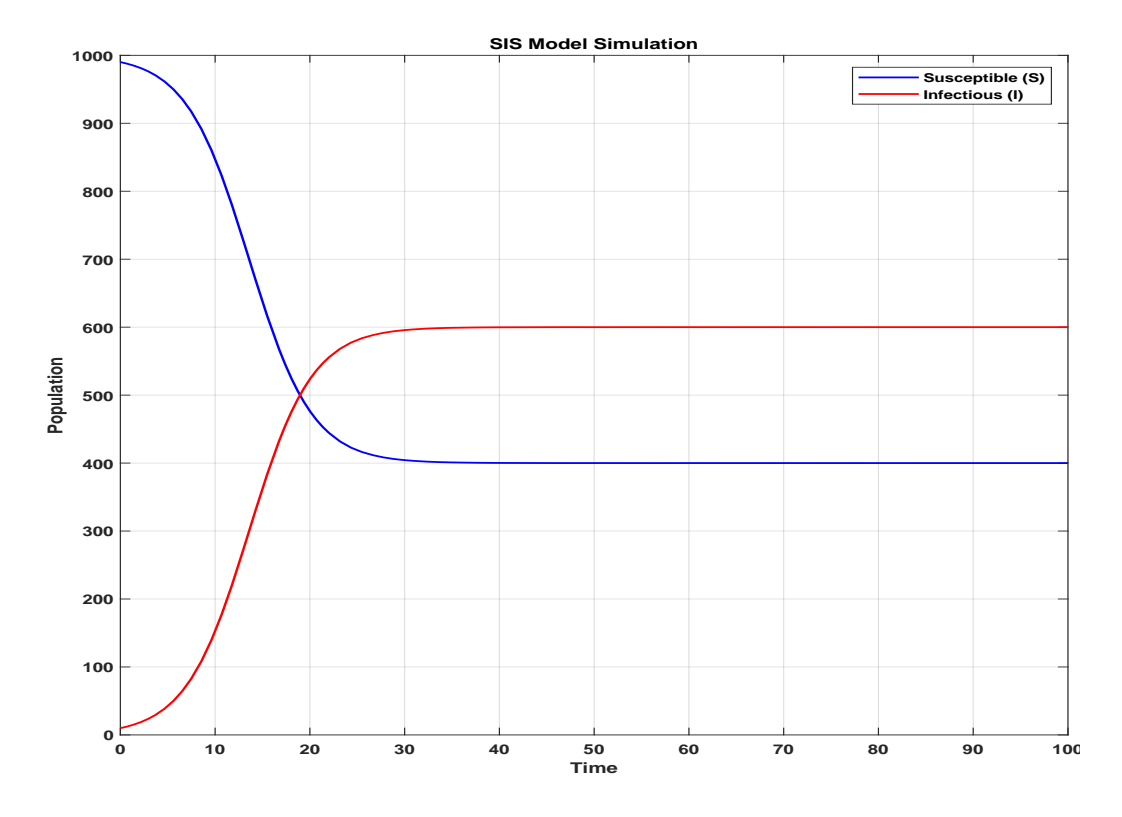


Figure 3.5: Numerical results from the SIS model with parameters $\beta = 0.5$ and $\gamma = 0.2$, initialized with S(0) = 990 susceptible individuals and I(0) = 10 infected individuals.

$3.5.3 \mid \mathcal{SIR} \mod \mathsf{el}$

This model was introduced by researchers W.O. Kermack and A.G. McKendrick; we consider the population to be constant. The main problem of the researchers was to understand the cause of the great epidemic. In 1918 the Spanish flu did not infect the entire population.

Assume that a population can be divided into three distinct groups:

- \blacksquare S: Those who are susceptible and vulnerable to contracting the disease.
- \blacksquare \mathcal{I} : The infectious cases, who are currently infectious and can pass on the disease.
- R: The class taken out, representing those who have recovered, developed immunity, or are quarantined until they recover.

3.5.3.1 | SIR model without vital dynamic

The spread of an infectious disease in a population without births or natural deaths is described by the classical SIR model through the following system of nonlinear ordinary differential equations (51):

$$\begin{cases} \dot{S} = -\beta S \frac{\mathcal{I}}{\mathcal{N}}, \\ \dot{\mathcal{I}} = \beta S \frac{\mathcal{I}}{\mathcal{N}} - \gamma \mathcal{I}, \\ \dot{\mathcal{R}} = \gamma \mathcal{I}. \end{cases}$$
(3.5)

Where the variables and parameters are defined as follows:

- \mathcal{N} : Total population size.
- *S*: The number of individuals who are susceptible to infection.
- \mathcal{I} : The number of individuals currently infected.
- \mathcal{R} : The number of individuals who have recovered.
- β : The rate at which the disease is transmitted.
- γ : The rate at which infected individuals recover.

The interactions among these compartments are illustrated in the flow diagram below:



Figure 3.6: Schematic representation of the \mathcal{SIR} model.

Since the total population remains constant, we have:

$$\mathcal{N} = \mathcal{S} + \mathcal{I} + \mathcal{R}$$
.

Taking the derivative of this equation gives:

$$\dot{\mathcal{N}} = \dot{\mathcal{S}} + \dot{\mathcal{I}} + \dot{\mathcal{R}} = 0, \tag{3.6}$$

confirming that the total population remains unchanged over time.

With initial conditions specified as:

$$S(0) = S_0$$
, $I(0) = I_0$, $R(0) = R_0$, where S_0 , I_0 , and R_0 are all positive.

We can focus on the system of equations for the susceptible and infected populations, since the equation for \mathcal{R} is independent of the others:

$$\begin{cases}
\dot{S} = -\beta S \frac{\mathcal{I}}{\mathcal{N}}, \\
\dot{\mathcal{I}} = \beta S \frac{\mathcal{I}}{\mathcal{N}} - \gamma \mathcal{I}.
\end{cases} (3.7)$$

By eliminating time dependence, we derive:

$$\frac{d\mathcal{I}}{d\mathcal{S}} = -1 + \frac{\rho \mathcal{N}}{\mathcal{S}},$$

where $\rho = \frac{\gamma}{\beta}$.

The phase plane representation of this equation is given in Figure 3.7.

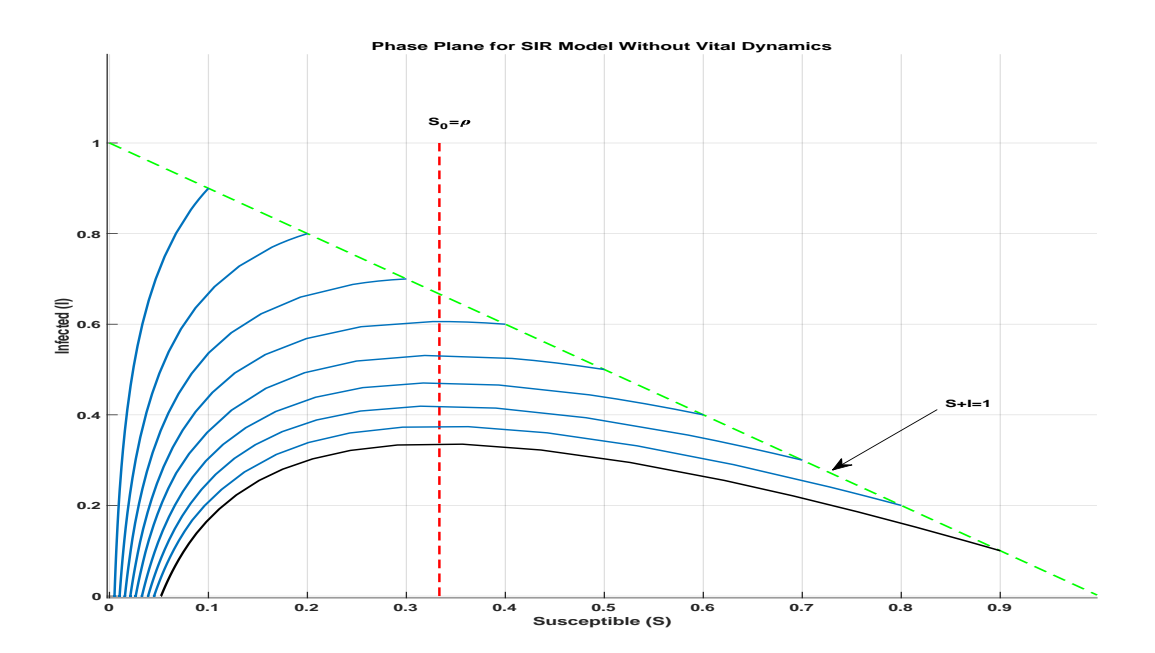


Figure 3.7: Phase plane trajectories of system (3.7) for $\gamma = 0.333333$ and $\beta = 1$.

From the phase plane, we identify a threshold at $S = \rho$, influencing the epidemic behavior:

- If $S(0) = S_0 > \rho$, the infection spreads.
- If $S(0) = S_0 < \rho$, the infection declines.

The fundamental threshold parameter, known as the basic reproduction number is

$$\mathcal{R}_0 = \frac{\beta}{\gamma}.$$

Its significance is as follows:

- $\mathcal{R}_0 > 1$: The disease will propagate through the population.
- \mathcal{R}_0 < 1: The disease will ultimately disappear.

To determine equilibrium points, we set $\dot{S} = \dot{I} = \dot{R} = 0$:

1. Disease-Free Equilibrium (DFE):

$$(\mathcal{S}, \mathcal{I}, \mathcal{R}) = (\mathcal{N}, 0, 0).$$

Here, the population remains entirely susceptible, with no infection.

2. Endemic Equilibrium (EE):

$$(\mathcal{S}, \mathcal{I}, \mathcal{R}) = \left(\frac{\gamma \mathcal{N}}{\beta}, \mathcal{N} - \frac{\gamma \mathcal{N}}{\beta}, \mathcal{N} - \mathcal{S} - \mathcal{I}\right).$$

This represents a scenario where the infection persists in the population at a steady level.

The numerical solution of the model is displayed in Figure 3.8, using the initial conditions $S_0 = 990$, $I_0 = 10$, and $I_0 = 0$. The parameters are assigned the values $\beta = 0.5$ and $\gamma = 0.2$. The graph demonstrates the epidemic cycle, showing an initial increase in infections, followed by a peak and subsequent decline due to recovery.

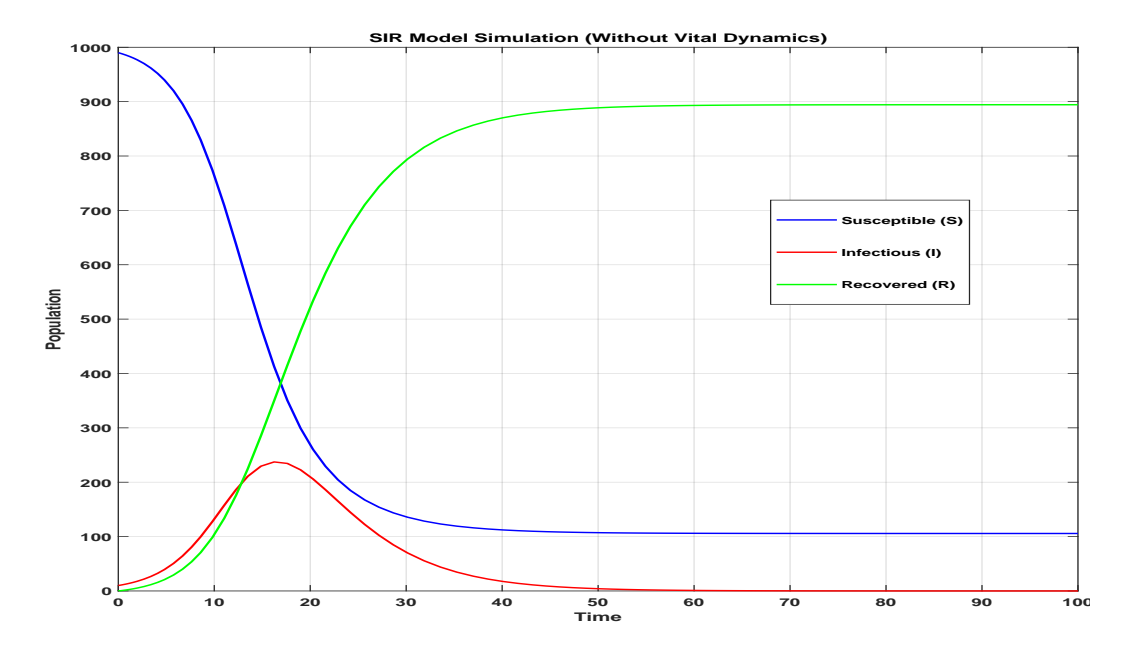


Figure 3.8: Numerical simulation of the SIR model without vital dynamics, illustrating the spread and decline of an epidemic with $\beta = 0.5$ and $\gamma = 0.2$.

3.5.3.2 | SIR model with vital dynamic

The dynamics of the SIR model, incorporating vital processes, are governed by the following system (21):

$$\begin{cases}
\frac{dS}{dt} = \lambda - \frac{\beta SI}{N} - \mu_1 S, \\
\frac{dI}{dt} = \frac{\beta SI}{N} - \mu_2 I - \gamma I, \\
\frac{dR}{dt} = \gamma I - \mu_3 R.
\end{cases} (3.8)$$

To simplify, we can rewrite it as follows:

$$\begin{cases}
\frac{dS}{dt} = -\frac{\beta SI}{N} + \mu_2 I + \mu_3 R, \\
\frac{dI}{dt} = \frac{\beta SI}{N} - \mu_2 I - \gamma I, \\
\frac{dR}{dt} = \gamma I - \mu_3 R.
\end{cases} (3.9)$$

By assuming that birth and mortality rates are balanced, we obtain:

$$\lambda = \mu_1 \mathcal{S} + \mu_2 \mathcal{I} + \mu_3 \mathcal{R}.$$

The structure of the model can be visualized as follows:

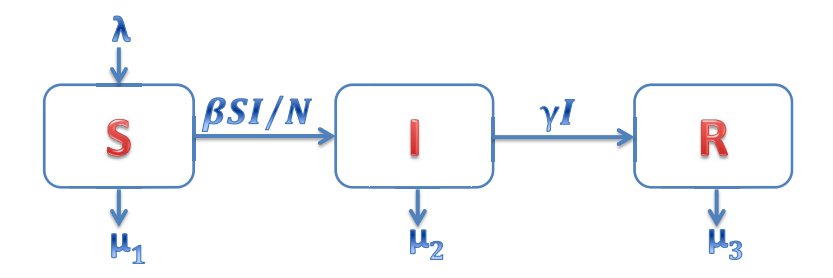


Figure 3.9: Schematic representation of the SIR model incorporating vital dynamics.

Since the total population remains unchanged over time, we have:

$$\mathcal{N} = \mathcal{S} + \mathcal{I} + \mathcal{R}$$
, leading to $\dot{\mathcal{N}} = \dot{\mathcal{S}} + \dot{\mathcal{I}} + \dot{\mathcal{R}} = 0$.

Thus, the total population remains constant.

By eliminating the recovered class equation, we obtain the following reduced system:

$$\begin{cases}
\frac{dS}{dt} = -\frac{\beta SI}{N} + \mu_2 I + \mu_3 (N - I - S), \\
\frac{dI}{dt} = \frac{\beta SI}{N} - (\mu_2 + \gamma) I.
\end{cases} (3.10)$$

Defining S/N and I/N as the proportions of susceptible and infected individuals, the system reduces to:

$$\begin{cases}
\frac{dS}{dt} = -\mu_3 + (\mu_2 - \mu_3)\mathcal{I} + \mu_3 S - \beta S \mathcal{I}, \\
\frac{d\mathcal{I}}{dt} = \beta S \mathcal{I} - (\mu_2 + \gamma) \mathcal{I}.
\end{cases} (3.11)$$

The system is constrained within the region $\Omega = \{(\mathcal{S}, \mathcal{I}) : \mathcal{S} \geq 0, \mathcal{I} \geq 0, \mathcal{S} + \mathcal{I} \leq 1\}$, which remains positively invariant and compact.

The fundamental reproductive ratio, determining the outbreak potential, is given by:

$$\mathcal{R}_0 = \frac{\beta}{\mu_2 + \gamma}.$$

The disease-free equilibrium (DFE) for the system is given by:

$$(S,0) = (1,0).$$

If $\mathcal{R}_0 \leq 1$, the DFE is globally asymptotically stable in the region Ω .

To analyze the stability of the DFE, we define a Lyapunov function $V(S, \mathcal{I}) = \mathcal{I}$. This function helps to determine the stability properties of the equilibrium.

The time derivative of the Lyapunov function along the trajectories of the system is given by:

$$\dot{V} = \dot{\mathcal{I}},$$

$$= \beta \mathcal{S} \mathcal{I} - (\mu_2 + \gamma) \mathcal{I},$$

$$= \mathcal{I} (\mathcal{R}_0 \mathcal{S} - 1) (\mu_2 + \gamma),$$

$$\leq 0.$$

The time derivative \dot{V} is non-positive ($\dot{V} \leq 0$), which indicates that the Lyapunov function $V(\mathcal{S}, \mathcal{I})$ is non-increasing over time. Specifically:

- $\dot{V}=0$ when either $\mathcal{I}=0$ (corresponding to the disease-free equilibrium) or $\mathcal{S}=\mathcal{S}^*$ and $\mathcal{R}_0=1$.

The largest invariant set where $\dot{V}=0$ contains only the DFE point. Application of La Salle's invariance principle implies that the DFE is globally asymptotically stable within the region Ω whenever $\mathcal{R}_0 \leq 1$.

Now, we shift focus to the endemic equilibrium, which exists when $\mathcal{R}_0 > 1$. The *EE* is characterized by the following expressions:

$$\bar{S} = \frac{\mu_2 + \gamma}{\beta} = \frac{1}{\mathcal{R}_0}, \quad \bar{\mathcal{I}} = \frac{\mu_3}{\mu_3 + \gamma} \left(1 - \frac{1}{\mathcal{R}_0} \right).$$

This equilibrium lies within the simplex Ω , defined as $0 \leq \bar{\mathcal{S}}$, $0 \leq \bar{\mathcal{I}}$, and $\bar{\mathcal{S}} + \bar{\mathcal{I}} \leq 1$, provided that $\mathcal{R}_0 > 1$. Clearly, $\bar{\mathcal{I}} \geq 0$ holds if and only if $\mathcal{R}_0 > 1$. Furthermore, we can express:

$$\bar{\mathcal{S}} + \bar{\mathcal{I}} = rac{\dfrac{\gamma}{\mathcal{R}_0} + \mu_3}{\gamma + \mu_3}.$$

When $\mathcal{R}_0 = 1$, the *EE* point coincides with the *DFE* point. Thus, a unique equilibrium exists within the interior of the simplex only if $\mathcal{R}_0 > 1$.

If $\mathcal{R}_0 > 1$, the *DFE* point becomes unstable, leading to the emergence of a unique endemic equilibrium $(\bar{\mathcal{S}}, \bar{\mathcal{I}})$, which is globally asymptotically stable in the region $\Omega \setminus ([0,1] \times \{0\})$.

To investigate stability, we consider the positively invariant compact set:

$$\Omega_1 = \{(\mathcal{S}, \mathcal{I}): \mathcal{S} \geq \frac{\mu_2 - \mu_3}{\beta}, \mathcal{I} \geq 0, \mathcal{S} + \mathcal{I} \leq 1\}.$$

We introduce a Lyapunov function $V(S, \mathcal{I})$ within Ω_1 :

$$V(\mathcal{S}, \mathcal{I}) = (\mathcal{S} - \bar{\mathcal{S}}) - \frac{\mu_3 + \gamma}{\beta} \log \frac{-\mu_2 + \mu_3 + \beta \mathcal{S}}{-\mu_2 + \mu_3 + \beta \bar{\mathcal{S}}} + (\mathcal{I} - \bar{\mathcal{I}}) - \bar{\mathcal{I}} \log \frac{\mathcal{I}}{\bar{\mathcal{I}}}.$$

- $V(S, \mathcal{I}) \geq 0$ for all $(S, \mathcal{I}) \in \Omega_1$, with equality holding only at $(S, \mathcal{I}) = (\bar{S}, \bar{\mathcal{I}})$.
- The function is positive definite, satisfying $V(\bar{S}, \bar{I}) = 0$.

The time derivative of $V(S, \mathcal{I})$ along system trajectories is computed as:

$$\begin{split} \dot{V}(\mathcal{S},\mathcal{I}) &= \dot{\mathcal{S}} - (\mu_{3} + \gamma) \frac{\mu_{3} + (\mu_{2} - \mu_{3})\mathcal{I} - \mu_{3} - \beta \mathcal{S}\mathcal{I}}{-\mu_{2} + \mu_{3} + \beta \mathcal{S}} + \\ & \beta \mathcal{S}\mathcal{I} - (\mu_{2} + \gamma)\mathcal{I} - \bar{\mathcal{I}}(\beta \mathcal{S} - (\mu_{2} + \gamma)) \\ &= \dot{\mathcal{S}} - (\mu_{3} + \gamma) \frac{(\mu_{3} - \mu_{3}\mathcal{S})}{-\mu_{2} + \mu_{3} + \beta \mathcal{S}} + (\mu_{3} + \gamma)\mathcal{I} + \beta \mathcal{S}\mathcal{I} - \\ & (\mu_{2} + \gamma)\mathcal{I} - \bar{\mathcal{I}}(\beta \mathcal{S} - (\mu_{2} + \gamma)) \\ &= \mu_{3}(1 - \mathcal{S}) - (\mu_{3} + \gamma) \frac{(\mu_{3} - \mu_{3}\mathcal{S})}{-\mu_{2} + \mu_{3} + \beta \mathcal{S}} - \bar{\mathcal{I}}(\beta \mathcal{S} - (\mu_{2} + \gamma))) \\ &= \mu_{3}(1 - \mathcal{S}) \left[1 - \frac{\mu_{3} + \gamma}{-\mu_{2} + \mu_{3} + \beta \mathcal{S}} \right] - \bar{\mathcal{I}}(\beta \mathcal{S} - (\mu_{2} + \gamma))) \\ &= \mu_{3}(1 - \mathcal{S}) - \left(\frac{-\beta \bar{\mathcal{S}} + \beta \mathcal{S}}{-\mu_{2} + \mu_{3} + \beta \mathcal{S}} \right) - \\ & \frac{\mu_{3}}{\mu_{3} + \gamma} (1 - \bar{\mathcal{S}})(\beta \mathcal{S} - \beta \bar{\mathcal{S}}) \\ &= -\mu_{3}\beta(\bar{\mathcal{S}} - \mathcal{S}) \left[\frac{1 - \mathcal{S}}{-\mu_{2} + \mu_{3} + \beta \mathcal{S}} - \frac{1 - \bar{\mathcal{S}}}{\mu_{3} + \gamma} \right] \\ &= \frac{-\beta \mu_{3}}{\mu_{3} + \gamma} \left[\frac{-\mu_{2} + \beta + \mu_{3}}{-\mu_{2} + \beta + \beta \mathcal{S}} \right] (\mathcal{S} - \bar{\mathcal{S}})^{2} \\ &< 0. \end{split}$$

Thus, the derivative \dot{V} with respect to time is negative semi-definite, verifying the global stability of the EE according to Lyapunov's stability theorem.

Using La Salle's invariance principle, we establish that the EE is attractive. The invariant set where $\dot{V}=0$ is given by:

$$E = \{(\mathcal{S}, \mathcal{I}) \in \mathring{\Omega}_1 : \mathcal{S} = \bar{\mathcal{S}}\}.$$

On this set, substituting $S = \bar{S}$ into the system dynamics results in $\dot{S} = 0$, implying $\mathcal{I} = \bar{\mathcal{I}}$. Consequently, the largest invariant set contained in $\{(S, \mathcal{I}) \in \mathring{\Omega}_1 : \dot{V} = 0\}$ is the equilibrium state in the endemic situation $(\bar{S}, \bar{\mathcal{I}})$.

This confirms that the equilibrium state in the endemic situation EE is globally asymptotically stable on Ω_1 . When $\mathcal{R}_0 > 1$, all system trajectories converge to the EE $(\bar{\mathcal{S}}, \bar{\mathcal{I}})$.

For regions outside Ω_1 , considering $S \leq \frac{\mu_2 - \mu_3}{\beta}$, the equation for \dot{S} is:

$$\dot{S} = \mu_3(1 - S) + (\mu_2 - \mu_3 - \beta S)\mathcal{I}.$$

For $\mathcal{R}_0 > 1$, this ensures $\dot{\mathcal{S}} > 0$, causing trajectories to enter $\mathring{\Omega}_1$. Additionally, all trajectories in $\mathring{\Omega} \setminus \mathring{\Omega}_1$ eventually enter $\mathring{\Omega}_1$, making it an absorbing set.

On the boundaries S = 0 and S + I = 1, the vector field directs inward, ensuring Ω remains invariant under the dynamics. Even though the S-axis is an invariant set, it does not impact the global stability of the endemic equilibrium.

Thus, the equilibrium state in the endemic situation (\bar{S}, \bar{I}) is globally asymptotically stable in Ω for $\mathcal{R}_0 > 1$. All trajectories converge to this equilibrium, confirming the system's tendency toward this steady state under the given conditions.

Figure 3.10 illustrates the dynamics of the \mathcal{SIR} model with birth and death rates, using parameters $\beta=0.5$, $\gamma=0.2$, $\mu_1=0.01$, $\mu_2=0.02$, and $\mu_3=0.015$. The initial conditions are set at $S_0=990$, $I_0=10$, and $I_0=0$. The simulation demonstrates the evolution of susceptible, infected, and recovered populations over time, incorporating birth and death effects. As depicted in Figure 3.10, the model shows how the disease propagates within the population and stabilizes at an endemic equilibrium. These results align with expectations based on the reproduction number \mathcal{R}_0 .

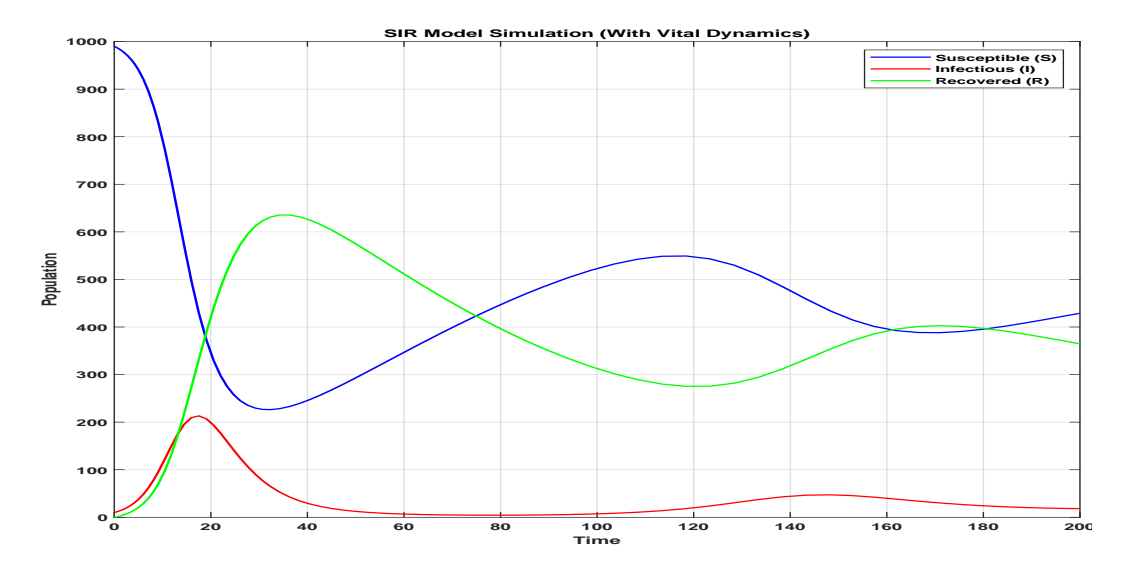


Figure 3.10: Numerical simulation of the \mathcal{SIR} model with birth and death dynamics using: $\beta = 0.5$, $\gamma = 0.2$, $\mu_1 = 0.01$, $\mu_2 = 0.02$, $\mu_3 = 0.015$, and initial conditions $\mathcal{S}(0) = 990$, $\mathcal{I}(0) = 10$, $\mathcal{R}(0) = 0$.

$3.5.4 \mid SIRS \mod el$

$3.5.4.1 \mid SIRS$ model without vital dynamic

The following model is given by (21):

$$\begin{cases} \frac{dS}{dt} = -\frac{\beta SI}{N} + \nu \mathcal{R}, \\ \frac{dI}{dt} = \frac{\beta SI}{N} - \gamma I, \\ \frac{d\mathcal{R}}{dt} = \gamma I - \nu \mathcal{R}. \end{cases}$$
(3.12)

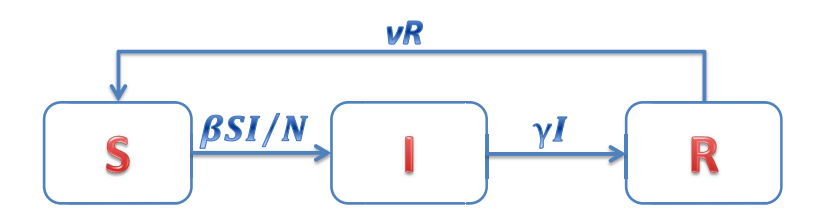


Figure 3.11: Flow diagram representing the SIRS model.

Since the total population size is given by $\mathcal{N}=\mathcal{S}+\mathcal{I}+\mathcal{R}$, differentiating both sides leads to:

$$\dot{\mathcal{N}} = \dot{\mathcal{S}} + \dot{\mathcal{I}} + \dot{\mathcal{R}} = 0.$$

This indicates that the total population stays unchanged over time. The system can thus be simplified as follows:

$$\begin{cases}
\frac{dS}{dt} = -\frac{\beta SI}{N} - \nu I + \nu (N - S), \\
\frac{dI}{dt} = \frac{\beta SI}{N} - \gamma I,
\end{cases} (3.13)$$

The equilibrium points of the system are:

$$(\mathcal{S}_1,\mathcal{I}_1) = (0,\mathcal{N}) \quad \text{and} \quad (\mathcal{S}_2,\mathcal{I}_2) = \left(\frac{\gamma}{\beta},\frac{\nu}{\gamma}\frac{\beta\mathcal{N}\gamma}{\gamma}\right).$$

To analyze stability, we compute the Jacobian matrix at the first equilibrium point:

$$J(S_1, \mathcal{I}_1) = \begin{pmatrix} -
u & -eta \mathcal{N} +
u \\ 0 & eta \mathcal{N} - \gamma \end{pmatrix}.$$

The eigenvalues are given by: $\lambda_1 = -\nu$ and $\lambda_2 = \beta \mathcal{N} - \gamma$.

For stability, both eigenvalues must be negative. The condition $\lambda_2 < 0$ holds when the fundamental reproductive ratio, defined as $\mathcal{R}_0 = \frac{\beta \mathcal{N}}{\gamma}$, is less than 1. Thus, the disease-free equilibrium $(\mathcal{S}_1, \mathcal{I}_1)$ is stable if $\mathcal{R}_0 < 1$, ensuring disease eradication in the population. If $\mathcal{R}_0 > 1$, the second equilibrium $(\mathcal{S}_2, \mathcal{I}_2)$ emerges, leading to endemic persistence.

Now, evaluating the Jacobian at (S_2, \mathcal{I}_2) :

$$J(\mathcal{S}_2, \mathcal{I}_2) = \begin{pmatrix} -(\beta \mathcal{I}_2 + \nu) & -(\beta + \nu) \\ \beta \mathcal{I}_2 & 0 \end{pmatrix}.$$

Since the trace is negative $tr(J(S_2, \mathcal{I}_2)) = -(\beta \mathcal{I}_2 + \nu) < 0$ and the determinant is positive $det(J(S_2, \mathcal{I}_2)) = -\beta(\beta + \nu)\mathcal{I}_2 > 0$, the equilibrium state in the endemic situation (S_2, \mathcal{I}_2) is locally asymptotically stable. This confirms that when $\mathcal{R}_0 > 1$, the disease persists, and the disease-free equilibrium (S_1, \mathcal{I}_1) becomes unstable as $\lambda_2 > 0$.

The following simulation illustrates the behavior of the system:

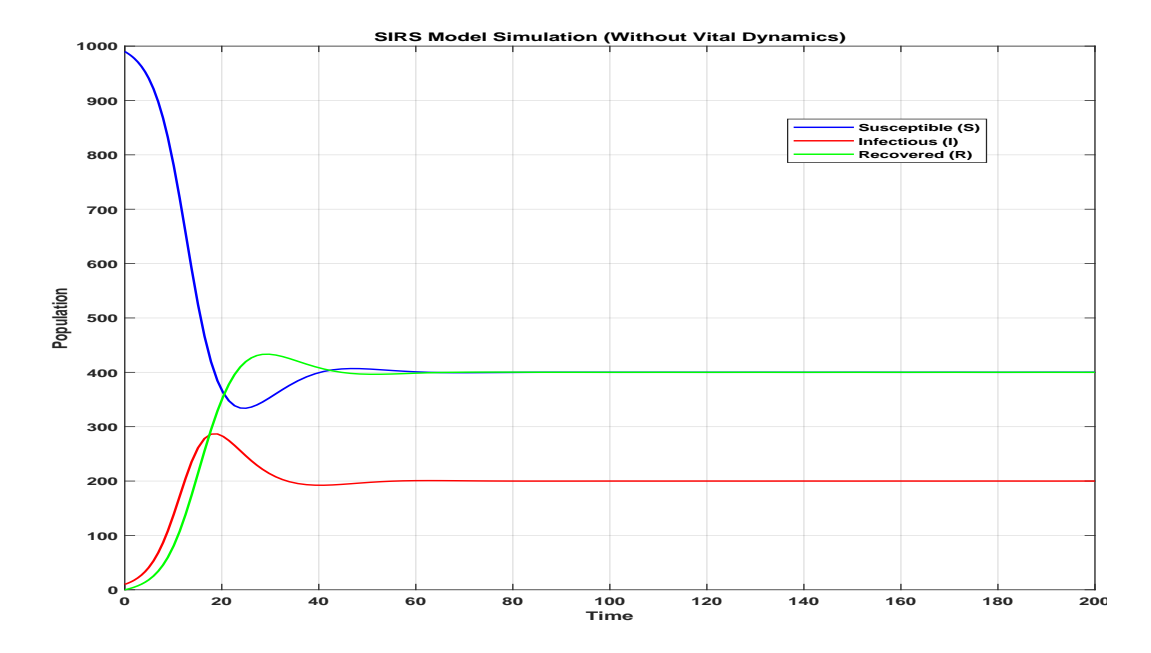


Figure 3.12: Numerical simulation of the \mathcal{SIRS} model without vital dynamics, using parameter values $\beta = 0.5$, $\gamma = 0.2$, and $\nu = 0.1$, with initial conditions $\mathcal{S}(0) = 990$, $\mathcal{I}(0) = 10$, and $\mathcal{R}(0) = 0$.

$3.5.4.2 \mid SIRS$ Model with Vital Dynamics

In this section, we investigate a SIRS model that incorporates birth and mortality rates. Using the previously defined notation, the system is expressed as follows (21):

$$\begin{cases}
\frac{dS}{dt} = \lambda - \frac{\beta SI}{N} - \mu_1 S + \nu R, \\
\frac{dI}{dt} = \frac{\beta SI}{N} - \mu_2 I - \gamma I, \\
\frac{dR}{dt} = \gamma I - (\mu_3 + \nu) R.
\end{cases} (3.14)$$

Rearranging the system, we obtain:

$$\begin{cases}
\frac{dS}{dt} = -\frac{\beta SI}{N} + \mu_2 I + (\mu_3 + \nu) \mathcal{R}, \\
\frac{dI}{dt} = \frac{\beta SI}{N} - \mu_2 I - \gamma I, \\
\frac{dR}{dt} = \gamma I - (\mu_3 + \nu) \mathcal{R}.
\end{cases} (3.15)$$

Notably, system (3.15) corresponds to system (3.9) with the parameter μ_3 replaced by $\mu_3 + \nu$.

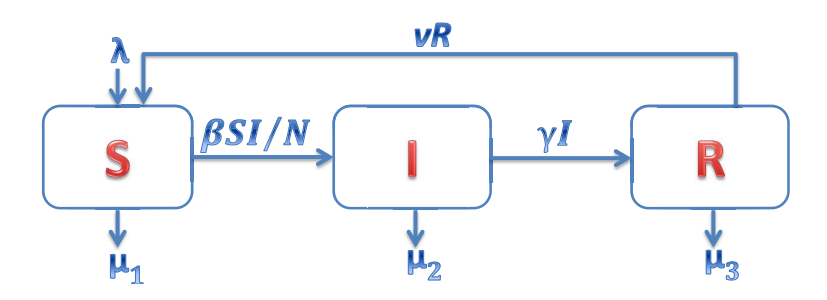


Figure 3.13: Flowchart representing the SIRS model with vital dynamics.

Figure 3.14 illustrates the simulation results using the parameter values $\beta=0.5$, $\gamma=0.2$, $\nu=0.1$, $\mu_1=0.01$, $\mu_2=0.02$, and $\mu_3=0.01$. The initial conditions are set as $\mathcal{S}(0)=990$, $\mathcal{I}(0)=10$, and $\mathcal{R}(0)=0$.

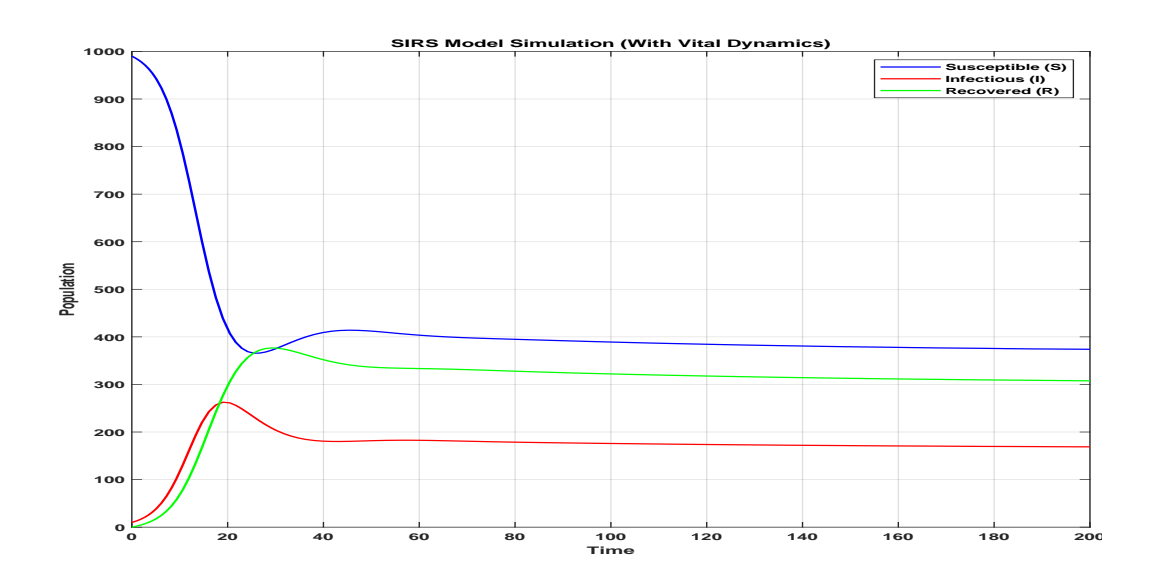


Figure 3.14: Numerical simulation of the \mathcal{SIRS} model with vital dynamics, illustrating the evolution of the compartments over time.

$3.5.5 \mid \mathcal{SEIR} \text{ Model}$

The SEIR model is commonly used to describe infectious disease dynamics, incorporating four compartments: Susceptible (S), Exposed (E), Infectious (I), and Recovered (I). This model accounts for an incubation phase before individuals become infectious (69). The governing equations are:

$$\begin{cases}
\frac{dS}{dt} = -\beta \frac{SI}{N}, \\
\frac{dE}{dt} = \beta \frac{SI}{N} - \delta \mathcal{E}, \\
\frac{dI}{dt} = \delta \mathcal{E} - \gamma \mathcal{I}, \\
\frac{dR}{dt} = \gamma \mathcal{I}.
\end{cases} (3.16)$$

The model parameters are defined as follows:

 β : Infection rate.

δ: Rate at which individuals progress from the exposed to the infectious state.

 γ : Rate of recovery.



Figure 3.15: Diagram illustrating the transitions in the SEIR model.

Since the total population remains unchanged, we have:

$$S + E + I + R = N \Rightarrow \dot{N} = \dot{S} + \dot{E} + \dot{I} + \dot{R} = 0.$$

The initial conditions are: $S(0) = S_0 = \mathcal{N} - I_0 > 0$, $\mathcal{E}(0) = 0$, $\mathcal{I}(0) = I_0 > 0$, $\mathcal{R}(0) = 0$.

Numerical simulation:

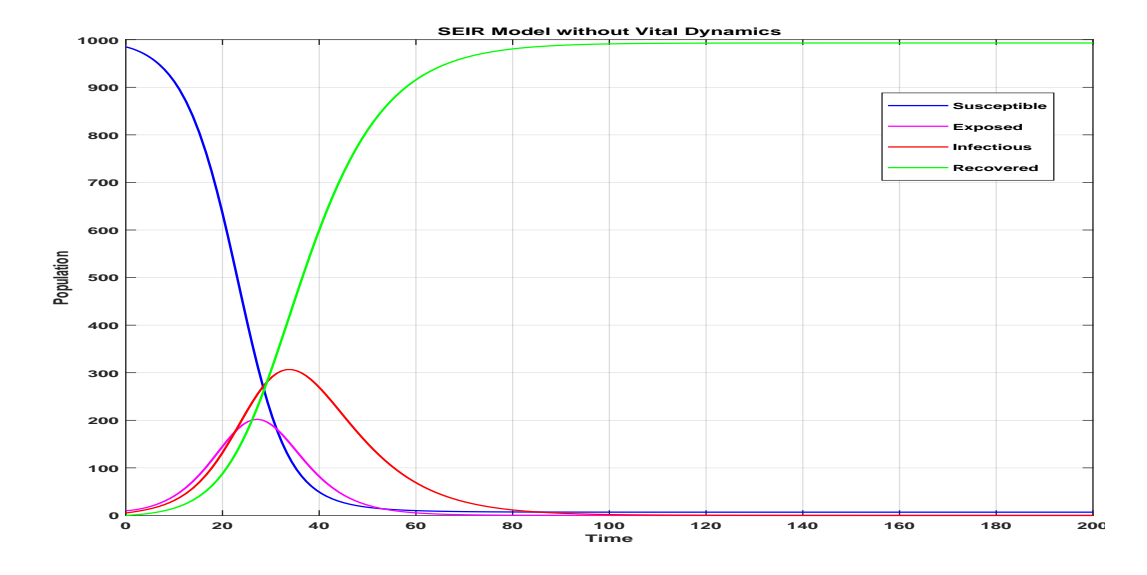


Figure 3.16: Numerical simulation of the \mathcal{SEIR} model without vital dynamics, using parameters $\beta=0.5$, $\gamma=0.1$, $\delta=0.2$, and initial values $\mathcal{N}=1000$, $\mathcal{S}(0)=985$, $\mathcal{E}(0)=10$, $\mathcal{I}(0)=5$, $\mathcal{R}(0)=0$.

3.6 | Case studies and applications of infectious disease modeling

3.6.1 | Dengue Fever and the SIR - SI model

Derouich et al. (20) propose an SIR - SI model that integrates the dynamics of both human and mosquito populations to analyze the spread of dengue fever. The fundamental reproductive ratio (R_0) is calculated to understand the epidemiological dynamics of the disease.

The impact of control strategies, such as reducing mosquito populations through insecticides or biological methods, is assessed. The results show that reducing the lifespan and density of infected mosquitoes significantly decreases the spread of dengue. This model highlights the importance of integrated vector management strategies for disease control.

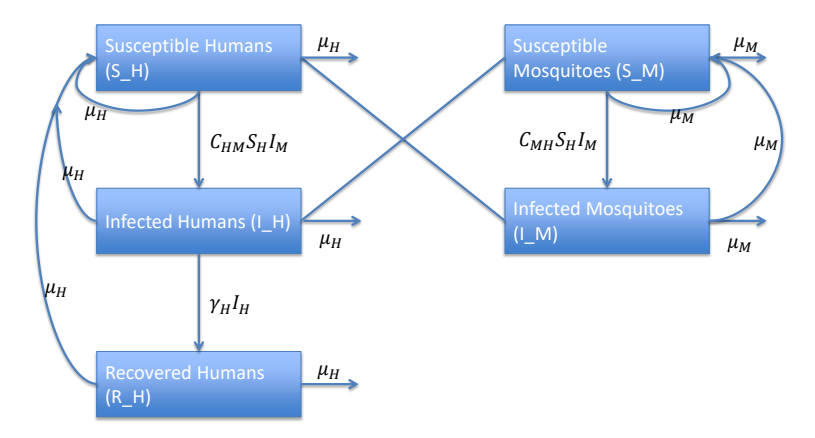


Figure 3.17: Diagram illustrating the transitions in the SIR - SI Dengue model.

The model equations are given by:

Human Population:

$$\begin{split} \frac{d\mathcal{S}_{H}}{dt} &= \Lambda_{H} - C_{MH}\mathcal{S}_{H}\mathcal{I}_{M} - \mu_{H}\mathcal{S}_{H}, \\ \frac{d\mathcal{I}_{H}}{dt} &= C_{MH}\mathcal{S}_{H}\mathcal{I}_{M} - (\gamma_{H} + \mu_{H})\mathcal{I}_{H}, \\ \frac{d\mathcal{R}_{H}}{dt} &= \gamma_{H}\mathcal{I}_{H} - \mu_{H}\mathcal{R}_{H}. \end{split}$$

Mosquito Population:

$$\begin{split} \frac{d\mathcal{S}_{M}}{dt} &= \Lambda_{M} - C_{HM}\mathcal{S}_{M}\mathcal{I}_{H} - \mu_{M}\mathcal{S}_{M}, \\ \frac{d\mathcal{I}_{M}}{dt} &= C_{HM}\mathcal{S}_{M}\mathcal{I}_{H} - \mu_{M}\mathcal{I}_{M}. \end{split}$$

The parameters are defined as follows:

- S_H , I_H , R_H : Susceptible, infected, and recovered humans.
- S_M , I_M : Susceptible and infected mosquitoes.
- \blacksquare Λ_H , Λ_M : Recruitment rates of humans and mosquitoes.
- $C_{MH} = p_{MH}b_i$: The rate at which mosquitoes transmit the disease to humans.
- $C_{HM} = p_{HM}b_s$: The rate at which humans transmit the disease to mosquitoes.
- \blacksquare γ_H : Recovery rate of infected humans.
- \blacksquare μ_H , μ_M : Natural mortality rates of humans and mosquitoes.
- \blacksquare p_{MH}, p_{HM} : Transmission probabilities from vector to human and vice versa.
- \bullet b_s , b_i : Biting rates of susceptible and infected mosquitoes.

3.6.2 | Ebola and the SEIR control model

Grigorieva and Khailov (30) propose an SEIR model to analyze Ebola outbreaks and determine optimal intervention strategies. The model integrates **quarantine measures** and vaccination tactics to mitigate disease transmission. The fundamental reproductive ratio (\mathcal{R}_0) is calculated to assess the epidemic's potential and evaluate control measures.

The study focuses on **optimal control strategies**, including:

- Isolation of exposed and infected individuals.
- Vaccination campaigns to increase immunity.
- Reducing human contact to lower transmission rates.



Figure 3.18: Diagram illustrating the transitions in the SEIR Ebola model with control strategies.

The model equations are given by:

Human Population:

$$\begin{split} \frac{d\mathcal{S}}{dt} &= \Lambda - \beta \mathcal{S}\mathcal{I} - u_1 \mathcal{S} - \mu \mathcal{S}, \\ \frac{d\mathcal{E}}{dt} &= \beta \mathcal{S}\mathcal{I} - (\sigma + \mu + u_2)\mathcal{E}, \\ \frac{d\mathcal{I}}{dt} &= \sigma \mathcal{E} - (\gamma + \mu + u_3)\mathcal{I}, \\ \frac{d\mathcal{R}}{dt} &= \gamma \mathcal{I} + u_1 \mathcal{S} + u_2 \mathcal{E} + u_3 \mathcal{I} - \mu \mathcal{R}. \end{split}$$

The parameters and are defined as follows:

- \blacksquare Λ : Rate of human population recruitment.
- \blacksquare β : Transmission rate of Ebola.
- \bullet σ : Incubation rate (rate at which exposed individuals become infectious).
- \blacksquare γ : Recovery rate of infected individuals.
- \blacksquare μ : Natural mortality rate of humans.
- \blacksquare u_1 : Vaccination rate of susceptible individuals.
- u_2 : Quarantine rate of exposed individuals.
- u_3 : Hospitalization rate of infected individuals.

This model provides insight into the effectiveness of different control measures and helps policymakers design optimal strategies to mitigate Ebola outbreaks.

Conclusion

Mathematical models are essential in understanding and managing epidemics, providing insights into disease spread and control. Models like SI, SIS, SIR, and SEIR help quantify key parameters, such as the fundamental reproductive ratio (\mathcal{R}_0), and assess the likelihood of disease outbreaks. Each model has unique applications depending on the disease's characteristics, such as the SIR-SI model for dengue and the SEIR model for Ebola. Mathematical epidemiology guides public health decisions, such as vaccination strategies and quarantine measures. Continued model refinement, incorporating factors like socioeconomic and mobility dynamics, is crucial for addressing emerging infectious threats and ensuring effective epidemic control.

Some methods of parameter estimation

Contents					
4.1	Maximum likelihood estimation				
	4.1.1	Likelihood function			
	4.1.2	Optimization			
	4.1.3	Bias and mean squared error (MSE) 72			
4.2	Nonli	near least squares method			
	4.2.1	Model fitting			
	4.2.2	Nonlinear least squares procedure			
	4.2.3	Distinction from linear least squares			
4.3	Metho	ods for solving nonlinear least squares problems 74			
	4.3.1	Gauss-Newton method			
	4.3.2	Levenberg-Marquardt algorithm			
	4.3.3	TNC algorithm			
	4.3.4	Trust Region Constrained method			
	4.3.5	Trust Region Reflective method			
Con	clusion				

Estimating parameters is essential for effectively applying mathematical models to predict and control epidemics. By aligning models with observed data, parameter estimation enables accurate predictions and effective intervention strategies. This chapter provides an overview of commonly used techniques, including Maximum Likelihood Estimation (MLE) and Nonlinear Least Squares, supported by optimization algorithms such as Gauss-Newton, Levenberg-Marquardt, and Trust-Region. The aim is to equip readers with the knowledge needed to apply these methods to complex epidemic systems.

4.1 | Maximum likelihood estimation

Maximum Likelihood Estimation (MLE) is a popular statistical approach for estimating the parameters of a probabilistic model. Its goal is to determine the parameter values that make the observed data most likely according to the model. By maximizing the likelihood function, MLE helps us find the best-fitting model for the data, offering an estimate of the unknown parameters based on available evidence. This method is commonly applied in various fields such as epidemiology, econometrics, and machine learning, where understanding the underlying parameters is essential for making predictions and inferences (15).

4.1.1 | Likelihood function

The likelihood function is a fundamental component of Maximum Likelihood Estimation (MLE), representing the probability of observing the given data under unknown parameters. Consider a set of independent random variables x_0, x_1, \ldots, x_n , each following a probability distribution defined by a parameter θ . The joint probability density function of these variables is denoted as $p(x_0, x_1, \ldots, x_n \mid \theta)$. Consequently, the likelihood function is expressed as:

$$L(\theta) = L(\theta \mid x_0, x_1, \dots, x_n) = p(x_0, x_1, \dots, x_n \mid \theta) = \prod_{i=0}^n p(x_i \mid \theta).$$
 (4.1)

The objective of Maximum Likelihood Estimation is to find the parameter θ that maximizes the likelihood function. This can be formulated as the following optimization problem:

$$\hat{\theta} = \arg\max_{\theta} L(\theta) \tag{4.2}$$

Maximizing the likelihood function directly can be challenging, so it is often more convenient to work with the logarithm of the likelihood, referred to as the log-likelihood function. Since maximizing the log-likelihood yields the same result as maximizing the likelihood, this approach simplifies calculations, particularly when dealing with products of probabilities.

Example 4.1 (Bernoulli distribution) A basic example involves each X_i being modeled as a Bernoulli-distributed variable with parameter θ , representing the probability of success. The corresponding probability mass function (PMF) is expressed as:

$$p(x_i \mid \theta) = \theta^{x_i} (1 - \theta)^{1 - x_i}.$$

For a set of n independent trials, the likelihood function becomes:

$$L(\theta) = \prod_{i=1}^n \theta^{x_i} (1-\theta)^{1-x_i}.$$

By applying the natural logarithm, we obtain the log-likelihood function:

$$\ell(\theta) = \sum_{i=1}^{n} (x_i \log(\theta) + (1 - x_i) \log(1 - \theta)).$$

To estimate $\hat{\theta}$ using maximum likelihood, we identify the value of θ that maximizes the log-likelihood function.

4.1.2 | Optimization

In parameter estimation, it is often preferable to work with the log-likelihood function instead of the likelihood function, as it simplifies the optimization process, especially for complex models or large datasets. The maximum likelihood estimator (MLE) is determined by solving:

$$\hat{\theta} = \arg \max_{\theta} \ell(\theta).$$

Alternatively, minimizing the negative log-likelihood yields the same result as maximizing the log-likelihood. The exact formulation of the log-likelihood depends on whether the system follows a discrete-time or continuous-time process.

In cases where a closed-form solution does not exist, numerical techniques such as the gradient ascent method, the Newton-Raphson method, or the Expectation-Maximization (EM) technique are employed. These iterative methods refine the parameter estimates to achieve optimal likelihood.

4.1.3 | Bias and mean squared error (MSE)

The accuracy of MLE-based parameter estimates can be assessed using *bias* and *Mean Squared Error (MSE)*. The *bias* of an estimator $\hat{\theta}$ is defined as the difference between its expected value and the true parameter:

$$Bias(\hat{\theta}) = E(\hat{\theta}) - \theta.$$

An estimator is unbiased if its bias is zero. If not, it may systematically overestimate or underestimate the true parameter. The *Mean Squared Error (MSE)* incorporates both variance and bias, providing a comprehensive measure of estimation accuracy:

$$MSE(\hat{\theta}) = E((\hat{\theta} - \theta)^2).$$

A lower MSE indicates a more accurate estimator. In epidemiology, it is important to evaluate both bias and MSE when using MLE, especially with small sample sizes or noisy data, to ensure the reliability of parameter estimates.

4.2 | Nonlinear least squares method

Nonlinear least squares is a method used to estimate model parameters when the relationship between variables is nonlinear. It generalizes the traditional least squares approach, which reduces the sum of squared differences between observed values and model estimates, to cases involving nonlinear dependencies (40).

In this approach, the experimental dataset consists of points $(x_i, y(x_i), \sigma_i)$, where:

- \blacksquare x_i denotes the independent variable,
- $y(x_i)$ represents the corresponding dependent variable, and
- \bullet σ_i is the standard error of the mean (SEM) associated with $y(x_i)$.

Each index i corresponds to a specific observation from a total of N data points. The goal is to estimate the parameters in the model function $f(x_i, \mathbf{a})$, where \mathbf{a} is the vector of unknown parameters.

4.2.1 | Model fitting

The primary objective of nonlinear least squares is to determine parameter values in **a** that allow the model function $f(x_i, \mathbf{a})$ to best approximate the observed data $y(x_i)$. This is accomplished by reducing the discrepancy between the predicted and actual values.

For example, in a kinetic experiment where optical density is measured over time, x_i represents time, and $y(x_i)$ is the optical density. A typical model might be an exponential function like:

$$y(x_i) \approx f(x_i, \mathbf{a}) = \text{amplitude} \times e^{-kx_i} + \text{baseline}.$$

where \mathbf{a} contains parameters such as amplitude, rate constant k, and baseline.

4.2.2 | Nonlinear least squares procedure

The nonlinear least squares method refines an initial parameter estimate, \mathbf{g} , through iterative adjustments to improve the model fit. The objective is to minimize the weighted sum of squared residuals, given by:

$$\chi^2 = \sum_{i=1}^N \left(\frac{r_i}{\sigma_i}\right)^2.$$

where r_i represents the residual, calculated as the difference between observed and predicted values: $r_i = y(x_i) - f(x_i, \mathbf{a})$, and σ_i denotes the standard error associated with $y(x_i)$. The parameter vector \mathbf{a} is updated iteratively until χ^2 reaches its minimum, signifying an optimal alignment between the model and the data.

4.2.3 | Distinction from linear least squares

Linear least squares apply to models where parameters appear linearly. A typical example is:

$$y = a_1 + a_2 x + a_3 x^2$$
.

where a_1 , a_2 , and a_3 are linear coefficients. In contrast, nonlinear least squares deals with models where parameters interact in a nonlinear manner, such as:

$$y = a \cdot e^{bx} + c.$$

where the parameters a, b, and c contribute to an exponential relationship with x. Due to these nonlinear dependencies, the optimization process requires more sophisticated numerical techniques, often involving higher-order derivatives.

4.3 | Methods for solving nonlinear least squares problems

Various numerical methods are used to solve nonlinear least squares problems, iteratively adjusting parameters to minimize the sum of squared residuals. Below are some of the commonly used techniques:

4.3.1 | Gauss-Newton method

The Gauss-Newton method is an optimization technique designed specifically for least-squares parameter estimation. It's known for being computationally efficient and relatively simple to implement (40).

4.3.1.1 | Algorithm steps

- 1. **Initial Parameter Selection**: Begin with an estimated starting value for the parameters \hat{a} .
- 2. **Taylor Series Expansion**: Approximate the fitting function $f(x_i, a)$ around the current parameter estimate g using a first-order Taylor series:

$$f(x_i, a) \approx f(x_i, g) + \frac{\partial f(x_i, g)}{\partial g}(a - g).$$

- 3. **Linear Approximation**: Compute the residual $D = Y(x_i) f(x_i, g)$, the difference between the observed data and model output.
- 4. **Jacobian Matrix**: Calculate the Jacobian matrix *A* of the first-order partial derivatives:

$$A = \frac{\partial f(x_i, g)}{\partial g}.$$

5. **Normal Equation**: Solve the normal equations to update the parameter estimates:

$$(A^T A)\Delta a = A^T D.$$

6. **Update Parameters**: Update the parameter estimates:

$$\hat{a} = \hat{a} + \Delta a$$
.

7. **Convergence Check**: Repeat until the changes in the least-squares norm and parameter estimates fall below a threshold.

4.3.1.2 | Advantages and disadvantages

- Advantages:
 - Efficient due to reliance on first-order derivatives.
 - Exhibits quadratic convergence as parameter estimates approach true values.
 - Simple to implement compared to other optimization methods.

■ Disadvantages:

- Limited to least-squares problems, less general than methods that minimize other norms.
- May not converge if the initial guess is far from the true parameters.
- Sensitive to poor initial guesses, which may lead to slow convergence or failure to find the optimal solution.
- Solving normal equations can be memory-intensive for large-scale problems.

4.3.2 | Levenberg-Marquardt algorithm

The Levenberg-Marquardt algorithm is an optimization method that merges elements of gradient descent and the Gauss-Newton approach to solve nonlinear least-squares problems. Particularly, it is effective for models with nonlinear functions (48; 55; 57).

4.3.2.1 | Algorithm steps

- 1. **Initialization**: Start with an initial estimate for the parameter vector x_0 and set an appropriate damping parameter λ .
- 2. Iterative Update: Update the parameters at each iteration using:

$$x_{k+1} = x_k - \left[\left(J^T J + \lambda I \right)^{-1} J^T f(x_k) \right].$$

3. **Jacobian Matrix**: Compute the Jacobian matrix *J*:

$$J_{ij} = \frac{\partial f_i(x)}{\partial x_i}.$$

- 4. Adjust Damping Parameter:
 - Decrease λ if the update improves the objective function.
 - Increase λ if the update does not improve the objective function.
- 5. **Convergence Check**: Repeat until the changes in *x* or the objective function fall below a threshold.

4.3.2.2 | Advantages and disadvantages

Advantages:

- Combines strengths of both gradient descent and the Gauss-Newton method.
- More robust to poor initial guesses due to adaptive damping.
- Effective for nonlinear problems where the Gauss-Newton method might struggle.

■ Disadvantages:

- More computationally expensive than gradient descent.
- The damping parameter λ can affect convergence and performance.

4.3.3 | TNC algorithm

The TNC (Truncated Newton Conjugate-Gradient) method is an optimization algorithm that employs a truncated Newton method with gradient information for constrained optimization. This method employs conjugate gradient techniques to estimate the inverse of the local Hessian matrix (34). The function is approximated using a quadratic model:

$$f(x) \approx f(x_0) + \nabla f(x_0) \cdot (x - x_0) + \frac{1}{2}(x - x_0)^T H(x_0)(x - x_0).$$

where $H(x_0)$ represents the Hessian matrix.

4.3.4 | Trust Region Constrained method

The trust-region constrained method is an optimization technique that relies on a quadratic approximation of the objective function. It addresses the following trust-region subproblem:

$$\min m_k(p) = f_k + g_k^T p + \frac{1}{2} p^T B_k p.$$

subject to $||p|| \le \Delta_k$, where Δ_k denotes the trust-region radius. This approach is especially useful for handling large-scale constrained problems, as it dynamically adjusts the trust-region size during the optimization process.

4.3.5 | Trust Region Reflective method

The Trust Region Reflective algorithm is used for optimization problems with bound constraints. It enforces first-order necessary conditions for local minimization and handles problems with or without constraints. It uses a diagonal matrix to simplify optimization, allowing efficient handling of bound-constrained problems (34).

Conclusion

This chapter underscores the significance of robust parameter estimation techniques in mathematical modeling of epidemics. By leveraging methods like MLE and Nonlinear Least Squares, in conjunction with optimization approaches, researchers can achieve precise parameter estimation, leading to models that better reflect real-world dynamics. These advancements enhance the reliability and predictive power of epidemic models, offering valuable insights for public health decision-making.

A novel compartmental \mathcal{VSLIT} model

Contents			
5.1	Background on tuberculosis		
5.2	Dynamic modeling and analysis		
	5.2.1 Formulating of the $VSLIT$ model 80		
	5.2.2 Preservation of the feasible set 83		
	5.2.3 Existence of equilibrium points and global stability 84		
5.3	Simulating numerically and estimating parameters 90		
5.4	Sensitivity analysis		
5.5	Discussion and results of numerical simulations		
Con	Plusion 96		

In recent years, the global rate of tuberculosis (TB) has risen considerably. This chapter examines how vaccinations and treatments have influenced the spread of TB in two countries—Ukraine and Algeria—which differ significantly in their demographic characteristics. To conduct this analysis, a mathematical model referred to as VSLIT is used. The stability of both the disease-free equilibrium and endemic equilibrium is assessed through qualitative methods. For the numerical simulations, parameter estimates are obtained using the least squares approach, with TB data from Algeria and Ukraine spanning from 1990 to 2020.

5.1 | Background on tuberculosis

Tuberculosis (TB) remains one of the leading causes of death from infectious diseases worldwide. According to the World Health Organization (WHO), approximately 2 bil-

lion people carry latent TB, with 1.7 million fatalities reported in 2009. Although TB incidence has declined in the United States, it continues to spread in many regions, and the emergence of drug-resistant strains poses a growing threat, particularly among individuals co-infected with HIV (88).

TB is caused by **Mycobacterium tuberculosis**, a member of the **M. tuberculosis** complex, which includes related species such as **M. africanum**, **M. bovis**, and **M. microti**. The disease primarily affects the lungs, accounting for nearly 85% of cases, though extrapulmonary TB can impact other organs. Diagnostic tools for TB include the Mantoux tuberculin skin test (PPD) and the interferon-gamma release assay (IGRA). When TB is suspected, sputum samples are analyzed using acid-fast bacilli (AFB) smear and culture tests. Treatment usually spans six months and involves a combination of antibiotics, with modifications based on drug resistance and patient-specific factors. Special treatment protocols exist for children, pregnant women, and individuals with HIV. Ongoing research aims to develop new treatment strategies and vaccines (36).

Historical overview of tuberculosis

Tuberculosis (TB) has a long history, with evidence of skeletal TB, such as Pott's disease, found in human remains from Neolithic Europe (8000 BCE), ancient Egypt (1000 BCE), and pre-Columbian America. By 400 BCE, Hippocrates had identified TB as a contagious illness, referring to it as phthisis, a Greek term meaning "to waste away". In historical English texts, pulmonary TB was often called consumption. A major breakthrough came in 1882 when German physician Robert Koch successfully isolated **Mycobacterium tuberculosis**.

As urbanization and population density grew, TB cases increased significantly. By the Industrial Revolution (circa 1750), the disease accounted for over 25% of adult deaths in Europe. Tuberculosis was the primary cause of death in the United States during the early 20th century. However, its incidence declined as public health measures, including patient isolation, were introduced (36).

5.2 | Dynamic modeling and analysis

5.2.1 | Formulating of the VSLIT model

This section presents a mathematical model developed to study the transmission dynamics of tuberculosis (TB) (13). The model categorizes the population into five distinct groups:

Model variables

V(t): Individuals who have been vaccinated,

S(t): Individuals susceptible to TB,

 $\mathcal{L}(t)$: Individuals in the latent (exposed) stage,

 $\mathcal{I}(t)$: Individuals actively infected with TB,

 $\mathcal{T}(t)$: Individuals undergoing treatment.

At any time *t*, the total population is given by:

$$\mathcal{N}(t) = \mathcal{V}(t) + \mathcal{S}(t) + \mathcal{L}(t) + \mathcal{I}(t) + \mathcal{T}(t). \tag{5.1}$$

A flowchart illustrating the model is shown in Figure 5.1.

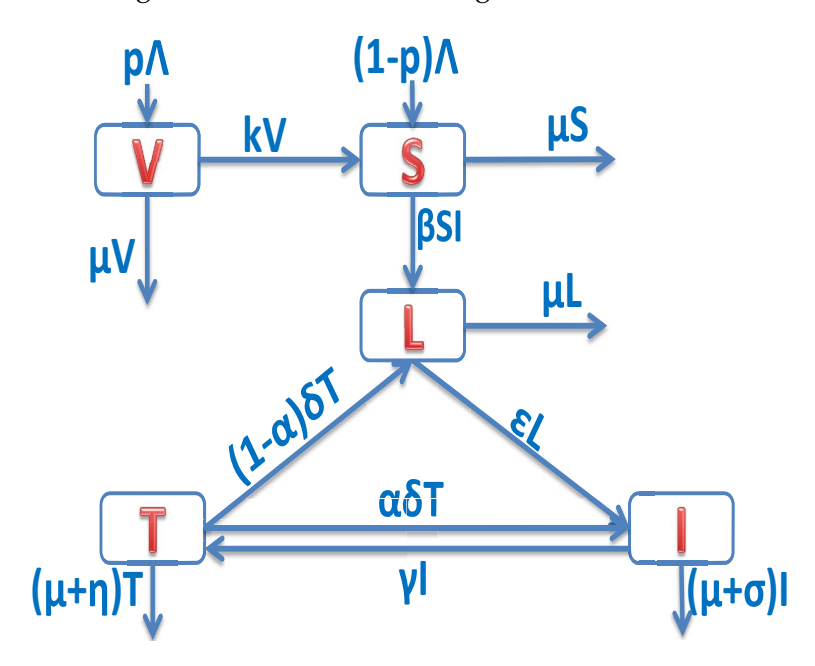


Figure 5.1: Flowchart of the proposed VSLIT model

The number of vaccinated individuals, denoted as V, increases due to a small proportion of newborns being immunized, represented by $p\Lambda$. However, this population declines as some vaccinated individuals lose immunity over time and back to the susceptible group at a rate k. These individuals remain free from infection during the period when immunity is intact, assuming the vaccine provides full immunity. The natural mortality rate within this group is represented by μ . Thus, the dynamics of the vaccinated population are governed by the following equation:

$$\dot{\mathcal{V}}(t) = p\Lambda - (k+\mu)\mathcal{V}(t).$$

The susceptible population, S, increases due to newborns who are not vaccinated against tuberculosis, which occurs at a rate of $(1-p)\Lambda$. Additionally, as vaccinated individuals who lose their immunity transition into this group at rate k. The susceptible population declines as individuals contract the infection through contact with infected individuals at a rate β and due to natural mortality at a rate μ . The dynamics of the susceptible population are described by:

$$\dot{S}(t) = (1 - p)\Lambda + kV(t) - \beta S(t)I(t) - \mu S(t).$$

The latent population, \mathcal{L} , grows when susceptible individuals are exposed to infected persons. This population decreases as individuals progress to the active stage of TB at rate ϵ or through natural mortality at rate μ . Additionally, a portion $\delta(1-\alpha)$ of treated individuals re-enter the latent stage, where α represents the treatment failure rate. When $\alpha=0$, all treated individuals transition back to latency, whereas $\alpha=1$ signifies complete treatment failure, preventing any movement to the latent group. The equation for the latent population is:

$$\dot{\mathcal{L}}(t) = \beta \mathcal{S}(t) \mathcal{I}(t) - (\epsilon + \mu) \mathcal{L}(t) + (1 - \alpha) \delta \mathcal{T}(t).$$

The infected population, \mathcal{I} , grows as latent individuals develop active TB and as some treated individuals relapse into the infectious stage at a rate $\alpha\delta$, which plays a significant role in sustaining infections. This population declines when individuals receive treatment at rate γ , succumb to natural mortality at rate μ , or die from TB-related complications at rate σ . The equation governing the infected population is:

$$\dot{\mathcal{I}}(t) = \epsilon \mathcal{L}(t) + \alpha \delta \mathcal{T}(t) - (\gamma + \mu + \sigma) \mathcal{I}(t).$$

Lastly, the treated population, \mathcal{T} , grows as individuals undergo treatment at a rate γ . However, it declines due to reinfection at rate δ , along with natural deaths occurring at rate μ and TB-related fatalities at rate η . The dynamics of the treated population are expressed as:

$$\dot{\mathcal{T}}(t) = \gamma \mathcal{I}(t) - (\mu + \delta + \eta) \mathcal{T}(t).$$

The TB infection dynamics are modeled using the following system of differential equations:

$$\begin{cases} \dot{\mathcal{V}}(t) = p\Lambda - (k+\mu)\mathcal{V}(t), \\ \dot{\mathcal{S}}(t) = (1-p)\Lambda + k\mathcal{V}(t) - \beta\mathcal{S}(t)\mathcal{I} - \mu\mathcal{S}(t), \\ \dot{\mathcal{L}}(t) = \beta\mathcal{S}(t)\mathcal{I} - (\epsilon + \mu)\mathcal{L}(t) + (1-\alpha)\delta\mathcal{T}(t), \\ \dot{\mathcal{I}}(t) = \epsilon\mathcal{L}(t) + \alpha\delta\mathcal{T}(t) - (\gamma + \mu + \sigma)\mathcal{I}, \\ \dot{\mathcal{T}}(t) = \gamma\mathcal{I}(t) - (\mu + \delta + \eta)\mathcal{T}(t). \end{cases}$$
(5.2)

The model assumes the following initial conditions:

$$\mathcal{V}(0) \ge 0$$
, $\mathcal{S}(0) \ge 0$, $\mathcal{L}(0) \ge 0$, $\mathcal{I}(0) \ge 0$, and $\mathcal{T}(0) \ge 0$.

Model Parameters:

- Λ : Rate of new individuals entering the population,
- *p*: Proportion of newborns receiving vaccination ($p \in [0,1]$),
- μ : Natural mortality rate,
- k: Rate at which vaccinated individuals lose immunity,
- β : Infection transmission rate,
- γ : Rate of recovery through treatment,
- ϵ : Rate at which latent TB becomes active,
- α: Probability of treatment failure,
- δ : Rate of transition out of the treated population,
- σ : TB-induced mortality rate in infected individuals (\mathcal{I}),
- η : TB-related mortality rate among treated individuals (\mathcal{T}).

5.2.2 | Preservation of the feasible set

We aim to analyze the TB model presented in equation (5.2) within a biologically feasible domain $\Omega \subset \mathbb{R}^5_+$, which is defined as:

$$\Omega = \left\{ (\mathcal{V}(t), \mathcal{S}(t), \mathcal{L}(t), \mathcal{I}(t), \mathcal{T}(t)) \in \mathbb{R}^5_+ : \mathcal{N}(t) \leq \frac{\Lambda}{\mu} \right\}.$$

This set represents a biologically feasible region.

Lemma 5.1 For the TB model described in equation (5.2), the solution remains non-negative for all t > 0, given that the initial conditions are non-negative. Moreover, if the total population satisfies $0 \le \mathcal{N}(0) \le \frac{\Lambda}{\mu}$ initially, then for all t > 0, the population size $\mathcal{N}(t)$ adheres to the constraint:

$$0 \le \mathcal{N}(t) \le \frac{\Lambda}{\mu}.$$

Proof 5.1 If V(t), S(t), L(t), L(t), and T(t) remain non-negative, then the following conditions hold:

$$\begin{cases}
\dot{\mathcal{V}} \mid_{\mathcal{V}=0} = p\Lambda \geq 0, \\
\dot{\mathcal{S}} \mid_{\mathcal{S}=0} = (1-p)\Lambda + k\mathcal{V} \geq 0, \\
\dot{\mathcal{L}} \mid_{\mathcal{L}=0} = \beta \mathcal{S}\mathcal{I} + (1-\alpha)\delta\mathcal{T} \geq 0, \\
\dot{\mathcal{I}} \mid_{\mathcal{I}=0} = \epsilon \mathcal{L} + \alpha\delta\mathcal{T} \geq 0, \\
\dot{\mathcal{T}} \mid_{\mathcal{T}=0} = \gamma \mathcal{I} \geq 0.
\end{cases} (5.3)$$

Thus, if the initial conditions are non-negative, the solution remains non-negative for all $t \ge 0$. By summing the equations of system (5.2), we obtain the total population equation:

$$\dot{\mathcal{N}}(t) = \dot{\mathcal{V}}(t) + \dot{\mathcal{S}}(t) + \dot{\mathcal{L}}(t) + \dot{\mathcal{I}}(t) + \dot{\mathcal{T}}(t).$$

This simplifies to:

$$\dot{\mathcal{N}}(t) = \Lambda - \mu \left(\mathcal{V}(t) + \mathcal{S}(t) + \mathcal{L}(t) + \mathcal{I}(t) + \mathcal{T}(t) \right) - (\sigma \mathcal{I}(t) + \eta \mathcal{T}(t)).$$

Rearranging, we obtain:

$$\dot{\mathcal{N}}(t) = \Lambda - \mu \mathcal{N}(t) - (\sigma \mathcal{I}(t) + \eta \mathcal{T}(t)) \le \Lambda - \mu \mathcal{N}(t).$$

This implies $\dot{\mathcal{N}}<0$ when $\mathcal{N}>\frac{\Delta}{\mu}$, which is avoided by assuming $\mathcal{N}(0)\leq\frac{\Delta}{\mu}$. Then, by comparison, $\mathcal{N}(t)\leq\frac{\Delta}{\mu}$ for all $t\geq0$. Thus, the region Ω is invariant.

5.2.3 | Existence of equilibrium points and global stability

To determine the equilibrium points of the system in equation (5.2), we set the time derivatives of all the model variables to zero:

$$\dot{\mathcal{V}} = \dot{\mathcal{S}} = \dot{\mathcal{L}} = \dot{\mathcal{I}} = \dot{\mathcal{T}} = 0.$$

This results in the identification of two equilibrium states: Disease-Free Equilibrium (\mathcal{DFE}):

$$E_{\mathcal{DFE}}^* = (\mathcal{V}_{\mathcal{DFE}}^*, \mathcal{S}_{\mathcal{DFE}}^*, \mathcal{L}_{\mathcal{DFE}}^*, \mathcal{I}_{\mathcal{DFE}}^*, \mathcal{T}_{\mathcal{DFE}}^*) = \left(\frac{p\Lambda}{k+\mu}, \frac{(k+\mu-\mu p)\Lambda}{\mu(k+\mu)}, 0, 0, 0\right).$$

Therefore, the total population at the disease-free equilibrium is:

$$\mathcal{N}_{\mathcal{DFE}}^* = \frac{\Lambda}{\mu}.$$

The endemic equilibrium ($\mathcal{E}\mathcal{E}$):

$$E_{\mathcal{E}\mathcal{E}}^* = (\mathcal{V}_{\mathcal{E}\mathcal{E}}^*, \mathcal{S}_{\mathcal{E}\mathcal{E}}^*, \mathcal{L}_{\mathcal{E}\mathcal{E}}^*, \mathcal{I}_{\mathcal{E}\mathcal{E}}^*, \mathcal{T}_{\mathcal{E}\mathcal{E}}^*),$$

where:

$$\mathcal{V}_{\mathcal{E}\mathcal{E}}^* = \frac{p\Lambda}{k+\mu'}, \quad \mathcal{S}_{\mathcal{E}\mathcal{E}}^* = \frac{(k+\mu-\mu p)\Lambda}{(k+\mu)(\beta I_2^* + \mu)'},$$

$$\mathcal{L}_{\mathcal{E}\mathcal{E}}^* = \frac{(\gamma+\mu+\sigma)(\mu+\delta+\eta) - \alpha\delta\gamma}{\epsilon(\mu+\delta+\eta)} \mathcal{I}_{\mathcal{E}\mathcal{E}}^*, \quad \mathcal{T}_{\mathcal{E}\mathcal{E}}^* = \frac{\gamma}{\mu+\delta+\eta} \mathcal{I}_{\mathcal{E}\mathcal{E}}^*.$$

The infected population I_2^* is given by:

$$\mathcal{I}_{\mathcal{E}\mathcal{E}}^* = \frac{(k+\mu-\mu p)\epsilon\Lambda(\mu+\delta+\eta)}{(k+\mu)\left((\epsilon+\mu)(\gamma+\mu+\sigma)(\mu+\delta+\eta)-(\epsilon+\mu)\alpha\delta\gamma-(1-\alpha)\gamma\delta\epsilon\right)} - \frac{\mu}{\beta},$$

or equivalently:

$$\mathcal{I}_{\mathcal{E}\mathcal{E}}^* = \frac{\mu}{\beta}(\mathcal{R}_0 - 1).$$

The total population at the endemic equilibrium can be expressed as:

$$\mathcal{N}_{\mathcal{E}\mathcal{E}}^* = \frac{\Lambda - (\sigma I_2^* + \eta T_2^*)}{\mu} < \frac{\Lambda}{\mu}.$$

The endemic equilibrium exists if $\mathcal{R}_0 > 1$.

5.2.3.1 | The fundamental reproduction rate \mathcal{R}_0

The fundamental reproduction rate, \mathcal{R}_0 , quantifies the expected number of secondary infections generated by a single infectious individual in a fully susceptible population (22).

- If \mathcal{R}_0 < 1, the disease will not persist in the population and will eventually be eradicated.
- If $\mathcal{R}_0 > 1$, the infection has the potential to spread and become endemic.

To determine \mathcal{R}_0 , we use the next-generation matrix method (83), given by:

$$\mathcal{R}_0 = \rho(FV^{-1}),$$

where *F* and *V* are the Jacobian matrices corresponding to new infections and transition terms in the infected compartments, respectively. These are defined as:

$$f = \begin{bmatrix} \beta \mathcal{S} \mathcal{I} \\ 0 \\ 0 \end{bmatrix}, \quad v = \begin{bmatrix} (\epsilon + \mu)\mathcal{L} - (1 - \alpha)\delta \mathcal{T} \\ -\epsilon \mathcal{L} - \alpha \delta \mathcal{T} + (\gamma + \mu + \sigma)\mathcal{I} \\ -\gamma \mathcal{I} + (\mu + \delta + \eta)\mathcal{T} \end{bmatrix} = \begin{bmatrix} c_1 \mathcal{L} - (1 - \alpha)\delta \mathcal{T} \\ -\epsilon \mathcal{L} - \alpha \delta \mathcal{T} + c_2 \mathcal{I} \\ -\gamma \mathcal{I} + c_3 \mathcal{T} \end{bmatrix}.$$

where $c_1 = \epsilon + \mu$, $c_2 = \gamma + \mu + \sigma$, and $c_3 = \mu + \delta + \eta$.

Evaluating the Jacobian matrices at the disease-free equilibrium E_{DFE}^* , we obtain:

$$J(f) = \begin{pmatrix} 0 & \beta S & 0 \\ 0 & 0 & 0 \\ 0 & 0 & 0 \end{pmatrix}, \quad J(v) = \begin{pmatrix} c_1 & 0 & -(1-\alpha)\delta \\ -\epsilon & c_2 & -\alpha\delta \\ 0 & -\gamma & c_3 \end{pmatrix}.$$

At $E_{D,F,\mathcal{E}}^*$, the matrices simplify to:

$$F = \begin{pmatrix} 0 & \frac{(k+\mu-\mu p)\Lambda\beta}{\mu(k+\mu)} & 0 \\ 0 & 0 & 0 \\ 0 & 0 & 0 \end{pmatrix}, \quad V = \begin{pmatrix} c_1 & 0 & -(1-\alpha)\delta \\ -\epsilon & c_2 & -\alpha\delta \\ 0 & -\gamma & c_3 \end{pmatrix}.$$

Finally, the basic reproduction number \mathcal{R}_0 is computed as the spectral radius of FV^{-1} :

$$\mathcal{R}_0 = \rho(FV^{-1}) = \frac{\epsilon(k + \mu - \mu p)\Lambda\beta c_3}{\mu(k + \mu)(c_1c_2c_3 - \alpha\gamma\delta c_1 - (1 - \alpha)\delta\gamma\epsilon)}.$$

5.2.3.2 | Analysis of the global stability of the \mathcal{DFE}

Proposition 5.1 Consider the vaccinated population equation of model (5.2):

$$\frac{d\mathcal{V}}{dt} = \nu \Lambda - (\kappa + \mu) \mathcal{V}.$$

If the initial condition $V(0) \geq 0$ is satisfied, then V(t) converges to $V^* = \frac{v\Lambda}{\kappa + \mu}$ as $t \to \infty$.

Proof 5.2 Starting with $V(0) \ge 0$, solve the differential equation:

$$\frac{d\mathcal{V}}{dt} = \nu \Lambda - (\kappa + \mu) \mathcal{V}.$$

This represents a linear differential equation, whose general solution is given by:

$$\mathcal{V}(t) = \mathcal{V}^* + (\mathcal{V}(0) - \mathcal{V}^*)e^{-(\kappa + \mu)t}.$$

Taking the limit as $t \to \infty$ *:*

$$\mathcal{V}(t) \to \frac{\nu \Lambda}{\kappa + \mu}.$$

Theorem 5.1 The disease-free equilibrium (E_{DFE}^*) of the model (5.2) is globally asymptotically stable when $\mathcal{R}_0 < 1$. However, if $\mathcal{R}_0 > 1$, the equilibrium becomes unstable.

Proof. For $\mathcal{R}_0 < 1$, the following inequality holds:

$$\frac{\epsilon(k+\mu-\mu p)\Lambda\beta c_3}{\mu(k+\mu)(c_1c_2c_3-\alpha\gamma\delta c_1-(1-\alpha)\delta\gamma\epsilon)}<1.$$

By the **Archimedean property** of \mathbb{R} , there exists $\gamma_0 > 0$ such that:

$$\epsilon c_3 \left(\frac{\Lambda \beta(k+\mu-\mu p)}{\mu(k+\mu)} + \gamma_0 \right) - (c_1 c_2 c_3 - \alpha \gamma \delta c_1 - (1-\alpha) \delta \gamma \epsilon) < 0.$$

Define the Lyapunov function:

$$L(t) = l_1 \mathcal{L} + l_2 \mathcal{I} + l_3 \mathcal{T}, \tag{5.4}$$

where the coefficients l_1 , l_2 , l_3 are positive constants that are yet to be determined. The time derivative of L(t) along the system trajectories is given by:

$$\frac{dL}{dt} = l_1 \frac{d\mathcal{L}}{dt} + l_2 \frac{d\mathcal{T}}{dt} + l_3 \frac{d\mathcal{T}}{dt},
\frac{dL}{dt} = l_1 \left[\beta \mathcal{S}\mathcal{I} - c_1 \mathcal{L} + (1 - \alpha)\delta \mathcal{T}\right] + l_2 \left[\epsilon \mathcal{L} + \alpha \delta \mathcal{T} - c_2 \mathcal{I}\right] + l_3 \left[\gamma \mathcal{I} - c_3 \mathcal{T}\right],$$
(5.5)

Also, by assumption, we have $\mathcal{N}_t \leq \frac{\Lambda}{u}$. Thus,

$$\mathcal{S}_t \leq \mathcal{N}_t - \mathcal{V}_t \leq \frac{\Lambda}{\mu} - \mathcal{V}^* + \gamma_0 \leq \frac{\Lambda}{\mu} - \frac{p\Lambda}{k+\mu} + \gamma_0 \leq \frac{(k+\mu-\mu p)\Lambda}{\mu(k+\mu)} + \gamma_0.$$

Thus, we obtain the inequality:

$$\frac{dL}{dt} \leq l_1 \left[\left(\frac{l_1 \Lambda \beta(k + \mu - \mu p)}{\mu(k + \mu)} + \gamma_0 \right) \mathcal{I} - c_1 \mathcal{L} + (1 - \alpha) \delta \mathcal{T} \right] + l_2 \left[\varepsilon \mathcal{L} + \alpha \delta \mathcal{T} - c_2 \mathcal{I} \right] + l_3 \left[\gamma \mathcal{I} - c_3 \mathcal{T} \right],$$

$$\leq \left[\frac{l_1 \Lambda \beta(k + \mu - \mu p)}{\mu(k + \mu)} + \gamma_0 - (l_2 c_2 - l_3 \gamma) \right] \mathcal{I} + \left[l_2 \varepsilon - l_1 c_1 \right] \mathcal{L}$$

$$+ \left[l_1 (1 - \alpha) \delta + l_2 \alpha \delta - l_3 c_3 \right] \mathcal{T}.$$
(5.6)

By selecting the constants:

$$l_1 = \epsilon c_3$$
, $l_2 = c_1 c_3$, $l_3 = ((1 - \alpha)\delta + \alpha \delta c_1)$,

we obtain:

$$\frac{dL}{dt} \le \left[\frac{\epsilon c_3 \Lambda \beta (k + \mu - \mu p)}{\mu (k + \mu)} + \gamma_0 - (c_1 c_2 c_3 - ((1 - \alpha)\delta + \alpha \delta c_1)\gamma) \right] \mathcal{I}. \tag{5.7}$$

Thus, if $\mathcal{R}_0 < 1$, then $\frac{dL}{dt}$ is negative. We conclude that $E_{\mathcal{DFE}}^*$ is globally asymptotically stable.

5.2.3.3 | Analysis of the global stability of the $\mathcal{E}\mathcal{E}$

In this part, we demonstrate the global asymptotic stability of the endemic equilibrium $(\mathcal{E}\mathcal{E})$ for the model described in (5.2). Utilizing the approach detailed in (87), we derive

the following results from the system (5.2) at the $\mathcal{E}\mathcal{E}$:

$$\begin{cases}
p\Lambda = (k+\mu)\mathcal{V}_{\mathcal{E}\mathcal{E}}^{*}, \\
k\mathcal{V}_{\mathcal{E}\mathcal{E}}^{*} = -(1-p)\Lambda + \beta\mathcal{S}_{\mathcal{E}\mathcal{E}}^{*}\mathcal{I}_{\mathcal{E}\mathcal{E}}^{*} + \mu\mathcal{S}_{\mathcal{E}\mathcal{E}}^{*}, \\
c_{1}\mathcal{L}_{\mathcal{E}\mathcal{E}}^{*} = \beta\mathcal{S}_{\mathcal{E}\mathcal{E}}^{*}\mathcal{I}_{\mathcal{E}\mathcal{E}}^{*} + (1-\alpha)\delta\mathcal{T}_{\mathcal{E}\mathcal{E}}^{*}, \\
c_{2}\mathcal{I}_{\mathcal{E}\mathcal{E}}^{*} = \varepsilon\mathcal{L}_{\mathcal{E}\mathcal{E}}^{*} + \alpha\delta\mathcal{T}_{\mathcal{E}\mathcal{E}}^{*}, \\
\gamma\mathcal{I}_{\mathcal{E}\mathcal{E}}^{*} = c_{3}\mathcal{T}_{\mathcal{E}\mathcal{E}}^{*}.
\end{cases} (5.8)$$

Theorem 5.2 The endemic equilibrium $\mathcal{E}_{\mathcal{E}\mathcal{E}}^*$ of the system (5.2) is globally asymptotically stable when $\mathcal{R}_0 > 1$.

Proof 5.3 To demonstrate the theorem, we examine the following Lyapunov function:

$$\mathcal{D} = k \left[\mathcal{V}(t) - \mathcal{V}_{\mathcal{E}\mathcal{E}}^* - \mathcal{V}_{\mathcal{E}\mathcal{E}}^* \ln \frac{\mathcal{V}(t)}{\mathcal{V}_{\mathcal{E}\mathcal{E}}^*} \right] + \epsilon \left[\mathcal{S}(t) - \mathcal{S}_{\mathcal{E}\mathcal{E}}^* - \mathcal{S}_{\mathcal{E}\mathcal{E}}^* \ln \frac{\mathcal{S}(t)}{\mathcal{S}_{\mathcal{E}\mathcal{E}}^*} \right]$$

$$+ \epsilon \left[\mathcal{L}(t) - \mathcal{L}_{\mathcal{E}\mathcal{E}}^* - \mathcal{L}_{\mathcal{E}\mathcal{E}}^* \ln \frac{\mathcal{L}(t)}{\mathcal{L}_{\mathcal{E}\mathcal{E}}^*} \right] + c_1 \left[\mathcal{I}(t) - \mathcal{I}_{\mathcal{E}\mathcal{E}}^* - \mathcal{I}_{\mathcal{E}\mathcal{E}}^* \ln \frac{\mathcal{I}(t)}{\mathcal{I}_{\mathcal{E}\mathcal{E}}^*} \right]$$

$$+ \frac{\delta \mathcal{T}_{\mathcal{E}\mathcal{E}}^* \left(c_1 \alpha + \epsilon (1 - \alpha) \right)}{\gamma \mathcal{I}_{\mathcal{E}\mathcal{E}}^*} \left[\mathcal{T}(t) - \mathcal{T}_{\mathcal{E}\mathcal{E}}^* - \mathcal{T}_{\mathcal{E}\mathcal{E}}^* \ln \frac{\mathcal{T}(t)}{\mathcal{T}_{\mathcal{E}\mathcal{E}}^*} \right].$$

$$(5.9)$$

By computing derivative of $\mathcal{D}(t)$ with respect to the time along the trajectories of system (5.2), we derive

$$\begin{split} \dot{\mathcal{D}} = & k \left[\left(1 - \frac{\mathcal{V}_{\mathcal{E}\mathcal{E}}^*}{\mathcal{V}} \right) \dot{\mathcal{V}} \right] + \epsilon \left[\left(1 - \frac{\mathcal{S}_{\mathcal{E}\mathcal{E}}^*}{\mathcal{S}} \right) \dot{\mathcal{S}} + \left(1 - \frac{\mathcal{L}_{\mathcal{E}\mathcal{E}}^*}{\mathcal{L}} \right) \dot{\mathcal{L}} \right] + c_1 \left[\left(1 - \frac{\mathcal{I}_{\mathcal{E}\mathcal{E}}^*}{\mathcal{I}} \right) \dot{\mathcal{I}} \right] \\ & + \frac{\delta \mathcal{T}_{\mathcal{E}\mathcal{E}}^* \left(c_1 \alpha + \epsilon (1 - \alpha) \right)}{\gamma \mathcal{I}_{\mathcal{E}\mathcal{E}}^*} \left[\left(1 - \frac{\mathcal{T}_{\mathcal{E}\mathcal{E}}^*}{\mathcal{T}} \right) \dot{\mathcal{T}} \right]. \end{split}$$

From a simple calculation, it follows that

$$k\left(1 - \frac{\mathcal{V}_{\mathcal{E}\mathcal{E}}^*}{\mathcal{V}}\right)\dot{\mathcal{V}} = k\left(1 - \frac{\mathcal{V}_{\mathcal{E}\mathcal{E}}^*}{\mathcal{V}}\right)\left[p\Lambda - (k+\mu)\mathcal{V}\right]$$
$$= k(k+\mu)\mathcal{V}_{\mathcal{E}\mathcal{E}}^*\left(2 - \frac{\mathcal{V}_{\mathcal{E}\mathcal{E}}^*}{\mathcal{V}} - \frac{\mathcal{V}}{\mathcal{V}_{\mathcal{E}\mathcal{E}}^*}\right).$$

$$\begin{split} \epsilon \left(1 - \frac{\mathcal{S}_{\mathcal{E}\mathcal{E}}^*}{\mathcal{S}}\right) \dot{\mathcal{S}} &= \epsilon \left(1 - \frac{\mathcal{S}_{\mathcal{E}\mathcal{E}}^*}{\mathcal{S}}\right) \left[(1 - p)\Lambda + k\mathcal{V} - \beta \mathcal{S}\mathcal{I} - \mu \mathcal{S}\right] \\ &= \epsilon \mu \mathcal{S}_{\mathcal{E}\mathcal{E}}^* \left(2 - \frac{\mathcal{S}_{\mathcal{E}\mathcal{E}}^*}{\mathcal{S}} - \frac{\mathcal{S}}{\mathcal{S}_{\mathcal{E}\mathcal{E}}^*}\right) + \epsilon \beta \mathcal{S}_{\mathcal{E}\mathcal{E}}^* \mathcal{I}_{\mathcal{E}\mathcal{E}}^* \left(1 - \frac{\mathcal{S}_{\mathcal{E}\mathcal{E}}^*}{\mathcal{S}} + \frac{\mathcal{I}}{\mathcal{I}_{\mathcal{E}\mathcal{E}}^*}\right) - \epsilon \beta \mathcal{S}\mathcal{I}. \end{split}$$

$$\begin{split} \varepsilon \left(1 - \frac{\mathcal{L}_{\mathcal{E}\mathcal{E}}^*}{\mathcal{L}} \right) \dot{\mathcal{L}} &= \varepsilon \left(1 - \frac{\mathcal{L}_{\mathcal{E}\mathcal{E}}^*}{\mathcal{L}} \right) \left[\beta \mathcal{S} \mathcal{I} - c_1 \mathcal{L} + (1 - \alpha) \delta \mathcal{T} \right] \\ &= \varepsilon \beta \mathcal{S} \mathcal{I} - \varepsilon \beta \mathcal{S} \mathcal{I} \frac{\mathcal{L}_{\mathcal{E}\mathcal{E}}^*}{\mathcal{L}} - c_1 \varepsilon \mathcal{L} + \varepsilon \beta \mathcal{S}_{\mathcal{E}\mathcal{E}}^* \mathcal{I}_{\mathcal{E}\mathcal{E}}^* + (1 - \alpha) \delta \varepsilon \mathcal{T}_{\mathcal{E}\mathcal{E}}^* + (1 - \alpha) \varepsilon \delta \mathcal{T} \\ &- (1 - \alpha) \delta \varepsilon \frac{\mathcal{T} \mathcal{L}_{\mathcal{E}\mathcal{E}}^*}{\mathcal{L}}. \end{split}$$

$$\begin{split} c_{1}\left(1-\frac{\mathcal{I}_{\mathcal{E}\mathcal{E}}^{*}}{\mathcal{I}}\right)\dot{\mathcal{I}} &= c_{1}\left(1-\frac{\mathcal{I}_{\mathcal{E}\mathcal{E}}^{*}}{\mathcal{I}}\right)\left[\varepsilon\mathcal{L}+\alpha\delta\mathcal{T}-c_{2}\mathcal{I}\right] \\ &= c_{1}\varepsilon\mathcal{L}-\varepsilon\beta\mathcal{S}_{\mathcal{E}\mathcal{E}}^{*}\mathcal{I}_{\mathcal{E}\mathcal{E}}^{*}\frac{\mathcal{L}\mathcal{I}_{\mathcal{E}\mathcal{E}}^{*}}{\mathcal{L}_{\mathcal{E}\mathcal{E}}^{*}\mathcal{I}}-(1-\alpha)\varepsilon\delta\mathcal{T}_{\mathcal{E}\mathcal{E}}^{*}\frac{\mathcal{L}\mathcal{I}_{\mathcal{E}\mathcal{E}}^{*}}{\mathcal{L}_{\mathcal{E}\mathcal{E}}^{*}\mathcal{I}}+c_{1}\alpha\delta\mathcal{T}-c_{1}\alpha\delta\mathcal{T}\frac{\mathcal{I}_{\mathcal{E}\mathcal{E}}^{*}}{\mathcal{I}} \\ &+\varepsilon\beta\mathcal{S}_{\mathcal{E}\mathcal{E}}^{*}\mathcal{I}_{\mathcal{E}\mathcal{E}}^{*}+c_{1}\alpha\delta\mathcal{T}_{\mathcal{E}\mathcal{E}}^{*}+\varepsilon(1-\alpha)\delta\mathcal{T}_{\mathcal{E}\mathcal{E}}^{*}-\varepsilon\beta\mathcal{S}_{\mathcal{E}\mathcal{E}}^{*}\mathcal{I}_{\mathcal{E}\mathcal{E}}^{*}\frac{\mathcal{I}}{\mathcal{I}_{\mathcal{E}\mathcal{E}}^{*}}-(1-\alpha)\varepsilon\delta\mathcal{T}_{\mathcal{E}\mathcal{E}}^{*}\frac{\mathcal{I}}{\mathcal{I}_{\mathcal{E}\mathcal{E}}^{*}} \\ &-c_{1}\alpha\delta\mathcal{T}_{\mathcal{E}\mathcal{E}}^{*}\frac{\mathcal{I}}{\mathcal{I}_{\mathcal{E}\mathcal{E}}^{*}}. \end{split}$$

$$\begin{split} \frac{\delta \mathcal{T}_{\mathcal{E}\mathcal{E}}^{*}\left(c_{1}\alpha+\varepsilon(1-\alpha)\right)}{\gamma \mathcal{I}_{\mathcal{E}\mathcal{E}}^{*}}\left(1-\frac{\mathcal{T}_{\mathcal{E}\mathcal{E}}^{*}}{T}\right)\left[\gamma \mathcal{I}-c_{3}\mathcal{T}\right] &= \frac{\delta \mathcal{T}_{\mathcal{E}\mathcal{E}}^{*}\left(c_{1}\alpha+\varepsilon(1-\alpha)\right)}{\mathcal{I}_{\mathcal{E}\mathcal{E}}^{*}}\left(1-\frac{\mathcal{T}_{\mathcal{E}\mathcal{E}}^{*}}{\mathcal{T}}\right)\left[\mathcal{I}-\frac{\mathcal{I}_{\mathcal{E}\mathcal{E}}^{*}}{\mathcal{T}_{\mathcal{E}\mathcal{E}}^{*}}\mathcal{T}\right] \\ &= \delta \alpha c_{1}\mathcal{T}_{\mathcal{E}\mathcal{E}}^{*}\frac{\mathcal{I}}{\mathcal{I}_{\mathcal{E}\mathcal{E}}^{*}}+\delta(1-\alpha)\varepsilon\mathcal{T}_{\mathcal{E}\mathcal{E}}^{*}\frac{\mathcal{I}}{\mathcal{I}_{\mathcal{E}\mathcal{E}}^{*}}-\delta \alpha c_{1}\mathcal{T}_{\mathcal{E}\mathcal{E}}^{*}\frac{\mathcal{I}\mathcal{T}_{\mathcal{E}\mathcal{E}}^{*}}{\mathcal{I}_{\mathcal{E}\mathcal{E}}^{*}}\mathcal{T} \\ &-\delta(1-\alpha)\varepsilon\mathcal{T}_{\mathcal{E}\mathcal{E}}^{*}\frac{\mathcal{I}\mathcal{T}_{\mathcal{E}\mathcal{E}}^{*}}{\mathcal{I}_{\mathcal{E}\mathcal{E}}^{*}}\mathcal{T}-\delta \alpha c_{1}\mathcal{T}-\delta(1-\alpha)\varepsilon\mathcal{T} \\ &+\delta \alpha c_{1}\mathcal{T}_{\mathcal{E}\mathcal{E}}^{*}+\delta(1-\alpha)\varepsilon\mathcal{T}_{\mathcal{E}\mathcal{E}}^{*}. \end{split}$$

Using the previous equations we get

$$\dot{\mathcal{D}} = k(k+\mu)\mathcal{V}_{\mathcal{E}\mathcal{E}}^{*} \left(2 - \frac{\mathcal{V}_{\mathcal{E}\mathcal{E}}^{*}}{\mathcal{V}} - \frac{\mathcal{V}}{\mathcal{V}_{\mathcal{E}\mathcal{E}}^{*}}\right) + \epsilon\mu\mathcal{S}_{\mathcal{E}\mathcal{E}}^{*} \left(2 - \frac{\mathcal{S}_{\mathcal{E}\mathcal{E}}^{*}}{\mathcal{S}} - \frac{\mathcal{S}}{\mathcal{S}_{\mathcal{E}\mathcal{E}}^{*}}\right) \\
+ \epsilon\beta\mathcal{S}_{\mathcal{E}\mathcal{E}}^{*}\mathcal{I}_{\mathcal{E}\mathcal{E}}^{*} \left(3 - \frac{\mathcal{S}_{\mathcal{E}\mathcal{E}}^{*}}{\mathcal{S}} - \frac{\mathcal{I}}{\mathcal{I}_{\mathcal{E}\mathcal{E}}^{*}} - \frac{\mathcal{L}\mathcal{I}_{\mathcal{E}\mathcal{E}}^{*}}{\mathcal{L}_{\mathcal{E}\mathcal{E}\mathcal{I}}^{*}} - \frac{\mathcal{S}\mathcal{I}\mathcal{L}_{\mathcal{E}\mathcal{E}}^{*}}{\mathcal{S}_{\mathcal{E}\mathcal{E}\mathcal{E}}^{*}}\mathcal{I}_{\mathcal{E}\mathcal{E}\mathcal{E}}^{*} \left(1 - \frac{\mathcal{L}\mathcal{S}_{\mathcal{E}\mathcal{E}}^{*}}{\mathcal{L}_{\mathcal{E}\mathcal{E}\mathcal{E}}^{*}}\right)\right) \\
+ (1 - \alpha)\epsilon\delta\mathcal{T}_{\mathcal{E}\mathcal{E}}^{*} \left(3 - \frac{\mathcal{I}_{\mathcal{E}\mathcal{E}}^{*}\mathcal{L}}{\mathcal{I}\mathcal{L}_{\mathcal{E}\mathcal{E}}^{*}} - \frac{\mathcal{L}_{\mathcal{E}\mathcal{E}}^{*}\mathcal{I}}{\mathcal{L}\mathcal{T}_{\mathcal{E}\mathcal{E}}^{*}} - \frac{\mathcal{T}_{\mathcal{E}\mathcal{E}}^{*}\mathcal{I}}{\mathcal{I}\mathcal{I}_{\mathcal{E}\mathcal{E}}^{*}}\right) \\
+ \delta\alpha c_{1}\mathcal{T}_{\mathcal{E}\mathcal{E}}^{*} \left(2 - \frac{\mathcal{I}_{\mathcal{E}\mathcal{E}}^{*}\mathcal{I}}{\mathcal{I}\mathcal{T}_{\mathcal{E}\mathcal{E}}^{*}} - \frac{\mathcal{I}\mathcal{T}_{\mathcal{E}\mathcal{E}}^{*}}{\mathcal{I}_{\mathcal{E}\mathcal{E}}^{*}}\right). \tag{5.10}$$

By employing the arithmetic-geometric mean inequality in Eq. (5.10), we derive the following

inequalities:

$$\begin{cases}
\left(2 - \frac{\mathcal{V}}{\mathcal{V}_{\mathcal{E}\mathcal{E}}^{*}} - \frac{\mathcal{V}_{\mathcal{E}\mathcal{E}}^{*}}{\mathcal{V}}\right) \leq 0 \\
\left(2 - \frac{\mathcal{S}}{\mathcal{S}_{\mathcal{E}\mathcal{E}}^{*}} - \frac{\mathcal{S}_{\mathcal{E}\mathcal{E}}^{*}}{\mathcal{S}}\right) \leq 0 \\
\left(3 - \frac{\mathcal{S}_{\mathcal{E}\mathcal{E}}^{*}}{\mathcal{S}} - \frac{\mathcal{I}}{\mathcal{I}_{\mathcal{E}\mathcal{E}}^{*}} - \frac{\mathcal{L}\mathcal{I}_{\mathcal{E}\mathcal{E}}^{*}}{\mathcal{L}_{\mathcal{E}\mathcal{E}}^{*}}\mathcal{I} - \frac{\mathcal{S}\mathcal{I}\mathcal{L}_{\mathcal{E}\mathcal{E}}^{*}\mathcal{N}_{\mathcal{E}}^{*}}{\mathcal{S}_{\mathcal{E}\mathcal{E}}^{*}}\mathcal{I}_{\mathcal{E}\mathcal{E}}^{*}\mathcal{N}_{\mathcal{E}}^{*}}\left(1 - \frac{\mathcal{L}\mathcal{S}_{\mathcal{E}\mathcal{E}}^{*}}{\mathcal{L}_{\mathcal{E}\mathcal{E}\mathcal{E}}^{*}}\right) \leq 0, \\
\left(3 - \frac{\mathcal{I}_{\mathcal{E}\mathcal{E}}^{*}\mathcal{L}}{\mathcal{I}\mathcal{L}_{\mathcal{E}\mathcal{E}}^{*}} - \frac{\mathcal{L}_{\mathcal{E}\mathcal{E}}^{*}\mathcal{I}}{\mathcal{L}\mathcal{I}_{\mathcal{E}\mathcal{E}}^{*}} - \frac{\mathcal{T}_{\mathcal{E}\mathcal{E}}^{*}\mathcal{I}}{\mathcal{I}\mathcal{I}_{\mathcal{E}\mathcal{E}}^{*}}\right) \leq 0, \\
\left(2 - \frac{\mathcal{I}_{\mathcal{E}\mathcal{E}}^{*}\mathcal{I}}{\mathcal{I}\mathcal{I}_{\mathcal{E}\mathcal{E}}^{*}} - \frac{\mathcal{I}\mathcal{I}_{\mathcal{E}\mathcal{E}}^{*}}{\mathcal{I}_{\mathcal{E}\mathcal{E}}^{*}\mathcal{I}}\right) \leq 0.
\end{cases} (5.11)$$

The parameters are all positive, so it follows that $\dot{\mathcal{D}} \leq 0$ when $\mathcal{R}_0 > 1$. Consequently, applying LaSalle's Invariance Principle (refer to 2.2.2.5), $(\mathcal{V}, \mathcal{S}, \mathcal{L}, \mathcal{I}, \mathcal{T}) \rightarrow (\mathcal{V}_{\mathcal{E}\mathcal{E}}^*, \mathcal{S}_{\mathcal{E}\mathcal{E}}^*, \mathcal{L}_{\mathcal{E}\mathcal{E}}^*, \mathcal{I}_{\mathcal{E}\mathcal{E}}^*, \mathcal{T}_{\mathcal{E}\mathcal{E}}^*)$ as $t \rightarrow \infty$.

5.3 | Simulating numerically and estimating parameters

This section focuses on estimating six key model parameters using data extracted from the WHO Global Tuberculosis Report (76) covering the years 1990–2020 (see Table 5.1). The remaining parameters are obtained from statistical sources available in the literature.

The mortality rate μ is calculated as the average annual death rate from 1990 to 2020, based on population statistics for Algeria and Ukraine (63; 64). The estimated values are $\mu=0.00498$ for Algeria and $\mu=0.0150875$ for Ukraine. Similarly, the recruitment rate Λ , representing the mean number of births per year during the same period, is determined as $\Lambda=811,085$ for Algeria and $\Lambda=434,687$ for Ukraine.

The BCG vaccination rate corresponds to the proportion of infants aged 12–23 months who have received the BCG vaccine. Figures 5.2 and 5.3 illustrate the percentage of one-year-old children vaccinated in Algeria and Ukraine between 1990 and 2020, according to data from the World Bank (80; 81). The mean vaccination coverage is estimated as p = 0.977 for Algeria and p = 0.899 for Ukraine. The BCG vaccine is reported to have an efficacy of 70%–80% in preventing severe childhood tuberculosis, such as meningitis and miliary TB (41). Given this, the transition rate from $\mathcal V$ to $\mathcal S$ is assumed to correspond to the immunization failure rate, calculated as k = 1 - 0.75 = 0.25.

Treatment success rates from 2000 to 2020 (78; 79) provide estimates for treatment failure probabilities. These are determined as $\alpha = 1 - 0.8905 = 0.1095$ for Algeria and $\alpha = 1 - 0.59 = 0.4033$ for Ukraine.

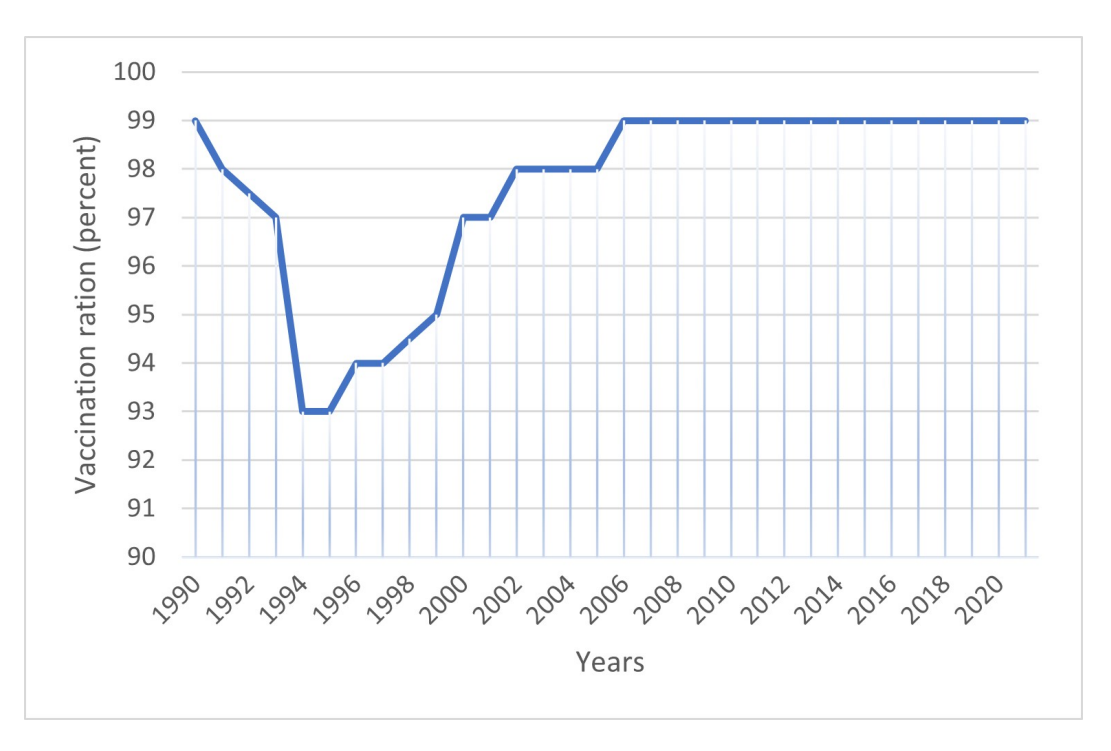


Figure 5.2: Proportion of one-year-old children in Algeria who received the BCG vaccine from 1990 to 2020.

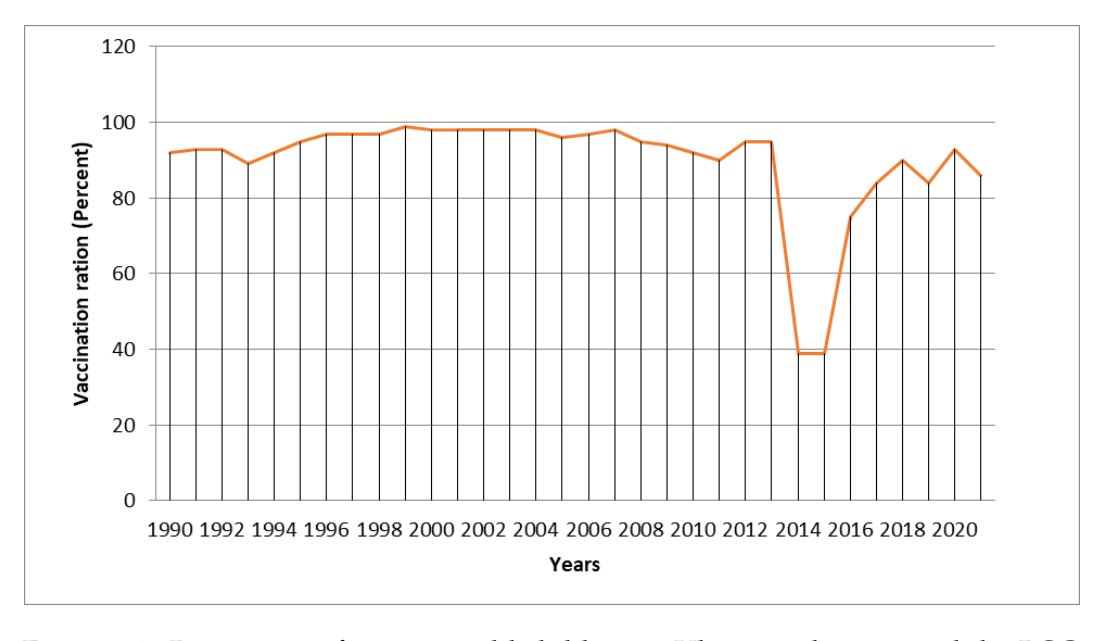


Figure 5.3: Proportion of one-year-old children in Ukraine who received the BCG vaccine from 1990 to 2020.

The initial conditions were selected based on demographic data and epidemiological considerations. The total initial population, $\mathcal{N}(0)$, is set at 25,518,074 for Algeria and 51,589,817 for Ukraine, reflecting their respective populations in 1990 as reported in (63). The number of initially infected individuals, $\mathcal{I}(0)$, was derived from estimates provided in the WHO Global Tuberculosis Report (76). Additionally, initial values for the latent ($\mathcal{L}(0)$), treated ($\mathcal{T}(0)$), and vaccinated ($\mathcal{V}(0)$) populations were assumed. Given these values, the initial number of susceptible individuals was determined using the equation:

$$S(0) = \mathcal{N}(0) - \mathcal{L}(0) - \mathcal{I}(0) - \mathcal{T}(0) - \mathcal{V}(0).$$

These initial conditions were chosen to ensure consistency and reliability in the numerical simulations.

The parameters β , γ , ϵ , σ , α , δ , k, and η were estimated by fitting the model to real-world TB incidence data, aiming to minimize the discrepancy between the simulated and observed values in (5.2). The estimation process involved optimizing the following objective function:

$$\psi = \sum_{i=1}^n \left(\mathcal{I}_{t_i} - \mathcal{I}_{t_i}^*\right)^2$$
 ,

where $\mathcal{I}_{t_i}^*$ denotes the recorded number of TB cases, \mathcal{I}_{t_i} is the model's predicted value at time t_i , and n represents the total number of data points considered. To perform this optimization, the nonlinear regression problem was solved using the Levenberg-Marquardt algorithm, implemented via the 'fitnlm' function in MATLAB R2020b (3.5). Figure 5.4 displays the incidence data alongside the model-fitted curve, generated using

Parameters	Description	Algerian Value	References	Ukrainian Value	References
$\mathcal{V}(0)$	The initial number of vaccinated	8,109,389	Assumed	5,980,291	Assumed
S(0)	The initial number of susceptible	17,368,226	Calculated	45,564,208	Calculated
$\mathcal{L}(0)$	The initial number of latent	8,852	Assumed	8,852	Assumed
$\mathcal{I}(0)$	The initial number of infected	11,607	(76)	16,465	(76)
$\mathcal{T}(0)$	The initial number of treated	20,000	Assumed	20,000	Assumed
Λ	The recruitment rate	811,085	(63)	344214	(64)
μ	The natural death rate	0.00498	(63)	0.0121	(64)
k	The rate of moving from $\mathcal V$ to $\mathcal S$	0.25	(80)	0.25	(81)
β	The transmission rate	6.6752×10^{-11}	Fitted	5.83×10^{-10}	Fitted
γ	The recovery rate	0.0043	Fitted	0.00012	Fitted
ϵ	The progression rate	0.0656	Fitted	0.225	Fitted
α	Treatment failure rate	0.1095	(78)	0.4033	(79)
δ	The rate at which the treated	0.1325	Fitted	0.208	Fitted
	population leave the class T				
σ	The disease death rate in I	0.0136	Fitted	0.019	Fitted
η	The disease death rate in T	4.2327×10^{-6}	Fitted	0.0006	Fitted
p	The vaccination rate	0.977	(80)	0.899	(81)

Table 5.1: Model parameters and initial data for equation (5.2).

the parameters listed in Table 5.1.

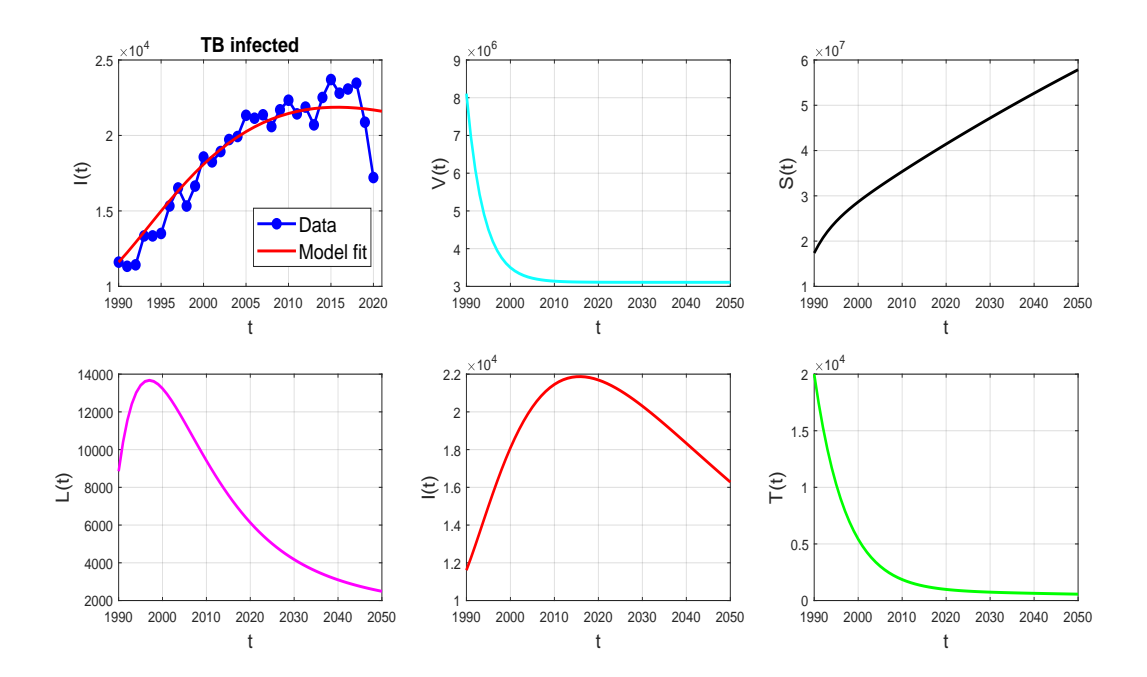


Figure 5.4: Fitting the data for tuberculosis cases in Algeria.

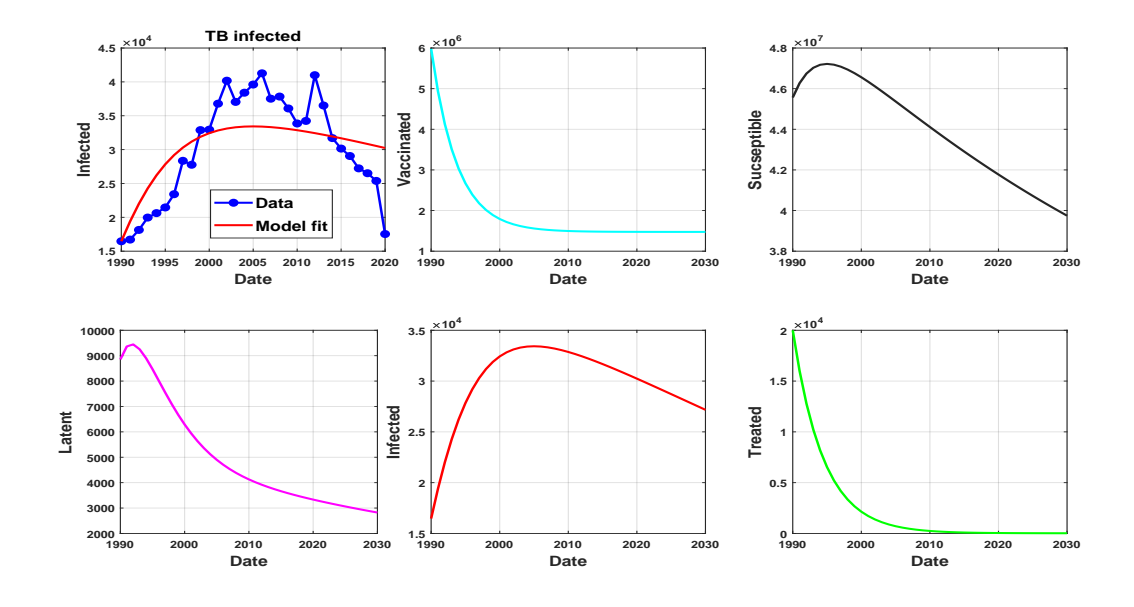


Figure 5.5: Fitting the data for tuberculosis cases in Ukraine.

5.4 | Sensitivity analysis

Understanding disease transmission dynamics necessitates evaluating the sensitivity of each parameter. This method is widely applied to assess the robustness of model predictions, accounting for possible inaccuracies in data collection and parameter assumptions. By analyzing the influence of various parameters on model outcomes, we can determine their relative impact on disease spread.

The partial derivatives of the basic reproduction number \mathcal{R}_0 are analyzed concerning the model parameters β , γ , k, and ϵ . Given that $\frac{\partial \mathcal{R}_0}{\partial \beta} > 0$, it can be inferred that reducing the transmission rate (for instance, through isolation strategies) can stabilize the endemic-free equilibrium, thereby controlling the spread of the disease. Conversely, since $\frac{\partial \mathcal{R}_0}{\partial \gamma}$ < 0, we conclude that increasing the treatment rate γ can help manage tuberculosis infections. A higher immunization failure rate, k, leads to an increase in \mathcal{R}_0 , as shown by $\frac{\partial \mathcal{R}_0}{\partial k} > 0$, which contributes to a faster spread of the disease. Additionally, since $\frac{\partial \mathcal{R}_0}{\partial \alpha} > 0$, lowering the treatment failure rate, α , helps reduce the overall number

To evaluate the impact of parameter variations on a given variable, the sensitivity index is employed.

For a parameter δ , the normalized sensitivity index of \mathcal{R}_0 is defined as:

$$S_{\delta}^{\mathcal{R}_0} = \frac{\delta}{\mathcal{R}_0} \frac{\partial \mathcal{R}_0}{\partial \delta}.$$
 (5.12)

Table 5.2 presents the computed sensitivity indices for the basic reproduction number \mathcal{R}_0 , based on the baseline model parameters and derived using equation (5.12).

As shown in Table 5.2, the values of $S^{\mathcal{R}_0}_{\beta}$ and $S^{\mathcal{R}_0}_{\Lambda}$ are both equal to +1. This indicates that an increase in \mathcal{R}_0 is directly proportional to increases in both β and Λ . Moreover, the parameters k, ϵ , α , and δ are positively correlated with \mathcal{R}_0 , as indicated by the positive sensitivity indices $S_k^{\mathcal{R}_0} > 0$, $S_{\epsilon}^{\mathcal{R}_0} > 0$, $S_{\alpha}^{\mathcal{R}_0} > 0$, and $S_{\delta}^{\mathcal{R}_0} > 0$.

Conversely, the negative sensitivity indices $S_{\mu}^{\mathcal{R}_0} < 0$, $S_{\gamma}^{\mathcal{R}_0} < 0$, $S_{\sigma}^{\mathcal{R}_0} < 0$, and

 $S_n^{\mathcal{R}_0} < 0$ suggest that the parameters μ , γ , σ , p, and η are inversely related to \mathcal{R}_0 .

Discussion and results of numerical simulations

Table 5.1 presents the estimated parameter values, while Figures 5.4 and 5.5 illustrate the tuberculosis incidence data for Algeria and Ukraine, respectively, alongside the model-

Parameter	Sensitivity index For Algeria	Sensitivity index For Ukraine
Λ	+1	+1
μ	-1.6502	-0.2053
k	+0.0012	+0.0035
β	+1	+1
γ	-0.1671	-3.0296
ϵ	+0.0005	+0.06294
α	$+2.1364 \times 10^{-10}$	$+8.7236 \times 10^{-05}$
δ	$+1.4003 \times 10^{-09}$	$+8.1145 \times 10^{-10}$
σ	-0.4043	-0.5647
η	-2.5311×10^{-11}	-3.3821×10^{-11}
p	-0.0194	-0.0527

Table 5.2: Sensitivity index for the model (5.2) in Algeria and Ukraine.

generated curves based on these estimates. The coefficient of determination (\mathbb{R}^2) values of 0.9016 for Algeria and 0.6036 for Ukraine indicate a satisfactory alignment between the model and the observed data.

With these estimated parameters, the basic reproduction numbers are computed as $\mathcal{R}_0 = 0.5228$ for Algeria and $\mathcal{R}_0 = 0.4306$ for Ukraine, both being below 1. This suggests that sustained treatment and isolation strategies, as depicted in the model projections for 2020–2050 in Figures 5.4 and 5.5, could help in controlling or eradicating the disease.

To explore the influence of key parameters on disease transmission, Figure 5.6 presents the variation of \mathcal{R}_0 with respect to six different parameters. The results highlight that β , ϵ , and α exhibit a direct correlation with \mathcal{R}_0 , implying that an increase in these parameters would enhance disease transmission.

Conversely, the parameters γ , p, and μ show an inverse relationship with \mathcal{R}_0 , indicating that their increase would contribute to reducing the spread of the infection. These findings align with empirical observations.

The findings indicate that four key factors should be considered in any strategy aimed at halting the spread of tuberculosis:

- Enhancing the accuracy and comprehensiveness of TB diagnoses to ensure that infected individuals receive appropriate care.
- Enforcing isolation protocols for infected individuals and closely monitoring their households to minimize exposure to contagious cases.
- Maintaining a high vaccination coverage among children to enhance their immunity and protection.

- Ensuring a high vaccination rate among children to provide them with adequate protection.
- Improving the treatment rate by training qualified healthcare professionals, procuring effective medications, and establishing facilities specifically designed for the treatment of this disease.

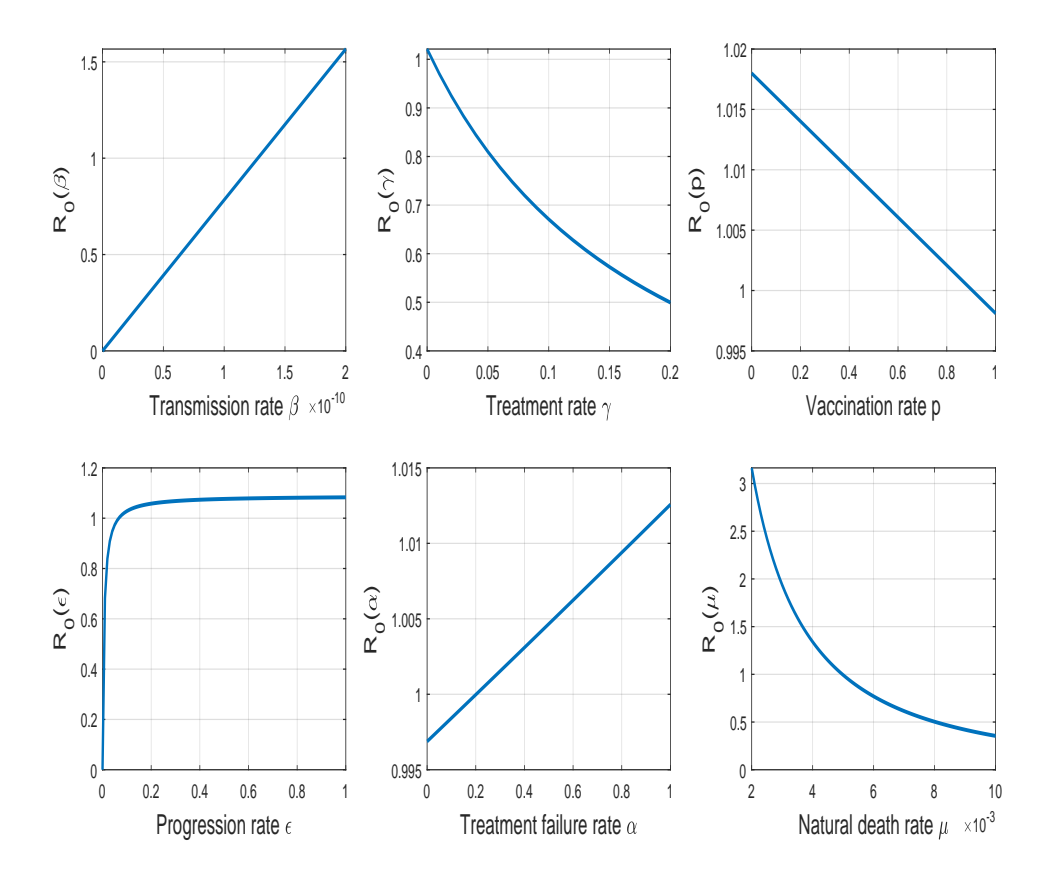


Figure 5.6: Effect of the parameters α , β , γ , μ , ϵ , and p on the fundamental reproduction rate \mathcal{R}_0 .

Conclusion

To examine tuberculosis (TB) transmission dynamics in Algeria and Ukraine, we constructed a mathematical VSLIT model incorporating key biological aspects of TB along with reasonable assumptions. Model parameters were estimated using the least-squares method based on available

infection data. The analysis underscores the significance of specific parameters in TB control. Specifically, the focus is on the contact rate β , the treatment rate γ , and the vaccination rate p. With the estimated parameters for both countries, we found that the basic reproduction number \mathcal{R}_0 was below one, suggesting that TB could be eliminated with sustained efforts in vaccination, treatment, and isolation measures. The study also highlights differences in TB management between Algeria and Ukraine. Algeria exhibited a higher vaccination rate (p) and recovery rate (γ) along with a lower transmission rate (β) compared to Ukraine, reflecting progress in TB control. However, Algeria's \mathcal{R}_0 was higher than Ukraine's, indicating that Ukraine may have better prospects for TB elimination. This is linked to Ukraine's significantly higher reported annual infections, which ranged from 33,000 to 41,000 between 2001 and 2013, peaking during this period. Conversely, Algeria implemented stricter control measures that initially reduced infections but delayed the epidemic peak, which continued to rise until 2018 before declining. These findings provide valuable insights for enhancing TB prevention and treatment strategies, aiding efforts to mitigate the disease's impact in Algeria, Ukraine, and other affected regions.

Discrete-Time modeling of tuberculosis epidemics: chemoprophylaxis strategies for combating MDR and XDR TB in Russia and India

Contents			
6.1	Formulation of discrete TB model		
6.2	The feasible region		
6.3	Disease-free equilibrium		
	6.3.1 Existence of the DFE		
	6.3.2 Basic reproduction number \mathcal{R}_0		
	6.3.3 Global stability investigation of the DFE 105		
6.4	Endemic equilibrium		
	6.4.1 Existence of EE		
	6.4.2 Global stability investigation of the EE		
6.5	Data fitting for discrete model		
6.6	Analyzing the sensitivity of \mathcal{R}_0		
6.7	Numerical results		
Con	clusion		

Tuberculosis (TB) is a bacterial infection that mainly affects the lungs and is transmitted through airborne particles expelled by infected individuals during coughing, sneezing, or spitting. Although tuberculosis is preventable and treatable, around 25% of the global population carries latent TB bacteria, with 5-10% of these individuals eventually developing active disease

(89). The persistent existence of TB, particularly the multidrug-resistant (MDR-TB) and extensively drug-resistant (XDR-TB) strains, poses significant challenges to global health. MDR-TB resists two primary first-line drugs, isoniazid and rifampicin, while XDR-TB exhibits additional resistance to fluoroquinolones and injectables (90). Factors such as improper treatment regimens, patient nonadherence, and systemic healthcare failures contribute to the rise of drug resistance, complicating TB management and control efforts. This highlights the urgent need for innovative and region-specific strategies. Mathematical modeling has become a critical tool for analyzing TB dynamics and exploring intervention strategies. While differential equation models have traditionally dominated epidemiological research, discrete-time models have gained prominence for capturing certain dynamics more effectively (2; 95). Building on foundational TB models, such as those by Waaler and Anderson (85), recent advancements have incorporated multidrug-resistant dynamics and interventions like chemoprophylaxis and vaccination (32; 43). This study develops a discrete-time epidemic model using data from India and Russia between 2000 and 2022 (76) to analyze TB dynamics, including MDR-TB and XDR-TB cases. The model employs Euler discretization with a step size of h = 1 to examine the effects of interventions such as chemoprophylaxis and BCG vaccination on susceptible, infected, MDR, and XDR populations. Through parameter estimation and sensitivity analysis, the study identifies critical factors influencing TB transmission and highlights region-specific recommendations for controlling the disease. The findings emphasize the more severe TB crisis in India compared to Russia, underscoring the need for targeted public health interventions to address TB and its drug-resistant forms effectively.

6.1 | Formulation of discrete TB model

In this section, we present a continuous-time model for tuberculosis (TB), building on the foundational work of Chennaf et al. (12), which incorporates both MDR-TB and XDR-TB populations. Our goal is to develop an analytically manageable model that enhances the understanding of TB transmission dynamics. Additionally, we investigate the impact of chemoprophylaxis on controlling TB and its resistant strains, with a particular focus on the socio-economic effects of varying intervention levels. This analysis highlights how different chemoprophylaxis rates influence TB spread and drug resistance, offering valuable insights into the broader socio-economic implications of TB control strategies.

The Bacillus Calmette-Guérin (BCG) vaccine is widely administered to infants in regions with a high TB burden. While it provides strong protection against severe child-hood TB, its effectiveness in preventing pulmonary TB the most common form in adults

is considerably lower.

People are usually infected with Mycobacterium tuberculosis (MTB) through exposure to those with active TB, entering an exposed phase. Some individuals then progress to active TB and become contagious. With timely treatment, they can recover and transition to the treatment phase. Discontinuing treatment increases the risk of developing multidrug-resistant tuberculosis (MDR-TB), which leads to a classification of resistance. Patients who recover from MDR-TB typically return to the treatment phase; however, if their MDR-TB treatment is unsuccessful, they may progress to extensively drug-resistant tuberculosis (XDR-TB). Similarly, individuals recovering from XDR-TB also reenter the treatment phase.

The population is categorized into seven distinct groups:

V(t): Vaccinated,

S(t): Susceptible,

 $\mathcal{E}(t)$: Exposed (latent),

 $\mathcal{I}(t)$: Infected (active TB),

 $\mathcal{D}(t)$: Multidrug-resistant TB,

 $\mathcal{X}(t)$: Extensively drug-resistant TB,

 $\mathcal{T}(t)$: Under treatment.

The dynamic behavior of the model is described by the following ordinary differential system (ODEs):

$$\begin{cases}
\dot{\mathcal{V}}(t) = \nu \Lambda - (\alpha + \mu) \mathcal{V}(t), \\
\dot{\mathcal{S}}(t) = (1 - \nu) \Lambda + \alpha \mathcal{V}(t) - \beta \mathcal{S}(t) \mathcal{I} - \mu \mathcal{S}(t), \\
\dot{\mathcal{E}}(t) = \beta \mathcal{S}(t) \mathcal{I} - (\epsilon + \mu + \omega) \mathcal{E}(t), \\
\dot{\mathcal{I}}(t) = \epsilon \mathcal{E}(t) - (\tau + \zeta + \gamma + \mu + \sigma) \mathcal{I}, \\
\dot{\mathcal{D}}(t) = \tau \mathcal{I}(t) - (\theta + \mu + \delta) \mathcal{D}(t), \\
\dot{\mathcal{X}}(t) = \zeta \mathcal{I}(t) - (\xi + \mu + \eta) \mathcal{X}(t), \\
\dot{\mathcal{T}}(t) = \gamma \mathcal{I}(t) + \omega \mathcal{E}(t) + \theta \mathcal{D}(t) + \xi \mathcal{X}(t) - \mu \mathcal{T}(t).
\end{cases} (6.1)$$

with suitable non-negative initial conditions: $\mathcal{V}(0) = \mathcal{V}_0 \geq 0$, $\mathcal{S}(0) = \mathcal{S}_0 \geq 0$, $\mathcal{E}(0) = \mathcal{E}_0 \geq 0$, $\mathcal{I}(0) = \mathcal{I}_0 \geq 0$, $\mathcal{D}(0) = \mathcal{D}_0 \geq 0$, $\mathcal{X}(0) = \mathcal{X}_0 \geq 0$, $\mathcal{T}(0) = \mathcal{T}_0 \geq 0$.

Model Parameters:

 \blacksquare Λ : The number of births,

- \blacksquare μ : The natural mortality rate,
- \blacksquare α : The moving rate from V to S,
- \blacksquare β : The transmission rate,
- \blacksquare γ : The rate of treatment from I,
- \bullet : The progression rate,
- \blacksquare ω : The chemoprophylaxis treatment rate,
- \blacksquare τ : The rate at which resistance to the first line of treatment develops,
- \blacksquare ζ : The rate at which resistance to the second line of treatment develops,
- \bullet ξ : The Rate of treatment for XDR-TB,
- \bullet : The rate of treatment for MDR-TB,
- \bullet δ : The mortality rate from disease in D,
- \bullet σ : The mortality rate from disease in I,
- \blacksquare η : The mortality rate from disease in X,
- ν : The vaccination rate.

Figure 6.1 illustrates the flowchart of the model.

All parameters and variables in system (6.1) are non-negative, consistent with the discrete model's portrayal of human dynamics. By applying the Euler forward difference method (39; 56) with a step size of h = 1, system (6.1) is converted into the following set of discrete equations:

$$\begin{cases}
\mathcal{V}_{t+1} = \mathcal{V}_t + \nu \Lambda - (\alpha + \mu) \mathcal{V}_t, \\
\mathcal{S}_{t+1} = \mathcal{S}_t + (1 - \nu) \Lambda + \alpha \mathcal{V}_t - \beta \mathcal{S}_t \mathcal{I}_t - \mu \mathcal{S}_t, \\
\mathcal{E}_{t+1} = \mathcal{E}_t + \beta \mathcal{S}_t \mathcal{I}_t - (\epsilon + \mu + \omega) \mathcal{E}_t, \\
\mathcal{I}_{t+1} = \mathcal{I}_t + \epsilon \mathcal{E}_t - (\tau + \zeta + \gamma + \mu + \sigma) \mathcal{I}_t, \\
\mathcal{D}_{t+1} = \mathcal{D}_t + \tau \mathcal{I}_t - (\theta + \mu + \delta) \mathcal{D}_t, \\
\mathcal{X}_{t+1} = \mathcal{X}_t + \zeta \mathcal{I}_t - (\xi + \mu + \eta) \mathcal{X}_t, \\
\mathcal{T}_{t+1} = \mathcal{T}_t + \gamma \mathcal{I}_t + \omega \mathcal{E}_t + \theta \mathcal{D}_t + \xi \mathcal{X}_t - \mu \mathcal{T}_t.
\end{cases} (6.2)$$

with non-negative initial conditions:

$$\mathcal{V}_0 \geq 0, \mathcal{S}_0 \geq 0, \mathcal{E}_0 \geq 0, \mathcal{I}_0 \geq 0, \mathcal{D}_0 \geq 0, \mathcal{X}_0 \geq 0, \mathcal{T}_0 \geq 0.$$

6.2 | The feasible region

Proposition 6.1 The feasible region for the discrete tuberculosis model represented by system (6.2) is defined as:

$$\Gamma = \left\{ (\mathcal{V}_t, \mathcal{S}_t, \mathcal{E}_t, \mathcal{I}_t, \mathcal{D}_t, \mathcal{X}_t, \mathcal{T}_t) \in \mathbb{R}_+^7 \mid \mathcal{N}_t \leq \frac{\Lambda}{\mu} \right\},$$

and this region remains positively invariant.

Proof. We begin by noting that:

$$\mathcal{N}_{t+1} = \mathcal{V}_{t+1} + \mathcal{E}_{t+1} + \mathcal{E}_{t+1} + \mathcal{I}_{t+1} + \mathcal{D}_{t+1} + \mathcal{X}_{t+1} + \mathcal{T}_{t+1},$$

$$= \Lambda - \mu [\mathcal{V}_t + \mathcal{E}_t + \mathcal{E}_t + \mathcal{I}_t + \mathcal{D}_t + \mathcal{X}_t + \mathcal{T}_t]$$

$$- \sigma \mathcal{I}_t - \delta \mathcal{D}_t + \eta \mathcal{X}_t + \mathcal{V}_t + \mathcal{E}_t + \mathcal{E}_t + \mathcal{I}_t + \mathcal{D}_t + \mathcal{X}_t + \mathcal{T}_t,$$

$$= \Lambda - \mu \mathcal{N}_t - \sigma \mathcal{I}_t - \delta \mathcal{D}_t + \eta \mathcal{X}_t + \mathcal{N}_t,$$

$$\mathcal{N}_{t+1} - \mathcal{N}_t = \Lambda - \mu \mathcal{N}_t - \sigma \mathcal{I}_t - \delta \mathcal{D}_t + \eta \mathcal{X}_t,$$

$$\leq \Lambda - \mu \mathcal{N}_t.$$
(6.3)

Now, note that:

$$\Lambda - \mu \mathcal{N}_t < 0$$
 if and only if $\mathcal{N}_t > \frac{\Lambda}{\mu}$.

Therefore, the total population decreases whenever it exceeds $\frac{\Lambda}{\mu}$, and remains bounded by this value if it starts below or equal to it.

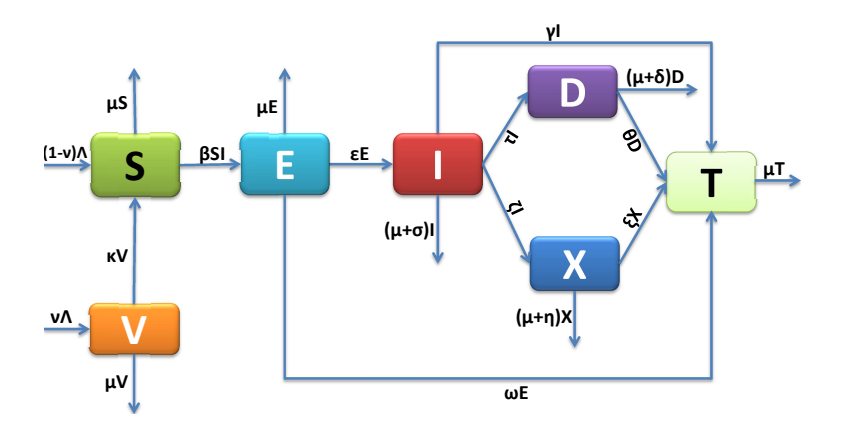


Figure 6.1: Flow diagram of the discrete model (6.2) depicting the transitions between various compartments in the system

Hence, for any initial condition satisfying $0 \le \mathcal{N}_0 \le \frac{\Lambda}{\mu}$, we conclude that:

$$0 \le \mathcal{N}_t \le \frac{\Lambda}{\mu}$$
, for all $t \ge 0$.

Thus, the feasible region Γ is positively invariant under the dynamics of the discrete model. \Box

6.3 | Disease-free equilibrium

This section examines the identification and analysis of a stable solution referred to as the Disease-Free Equilibrium (DFE) within the model.

6.3.1 | Existence of the DFE

At the **DFE**, the disease is entirely absent from the population. This equilibrium is typically established by equating the left-hand side of system (6.2) to V_t , S_t , E_t , I_t

$$\mathcal{V}_{t} = \mathcal{V}_{t} + \nu \Lambda - (\alpha + \mu) \mathcal{V}_{t},
S_{t} = S_{t} + (1 - \nu) \Lambda + \alpha \mathcal{V}_{t} - \beta S_{t} \mathcal{I}_{t} - \mu S_{t},
\mathcal{E}_{t} = \mathcal{E}_{t} + \beta S_{t} \mathcal{I}_{t} - (\epsilon + \mu + \omega) \mathcal{E}_{t},
\mathcal{I}_{t} = \mathcal{I}_{t} + \epsilon \mathcal{E}_{t} - (\tau + \zeta + \gamma + \mu + \sigma) \mathcal{I}_{t},
\mathcal{D}_{t} = \mathcal{D}_{t} + \tau \mathcal{I}_{t} - (\theta + \mu + \delta) \mathcal{D}_{t},
\mathcal{X}_{t} = \mathcal{X}_{t} + \zeta \mathcal{I}_{t} - (\xi + \mu + \eta) \mathcal{X}_{t},
\mathcal{T}_{t} = \mathcal{T}_{t} + \gamma \mathcal{I}_{t} + \omega \mathcal{E}_{t} + \theta \mathcal{D}_{t} + \xi \mathcal{X}_{t} - \mu \mathcal{T}_{t}.$$
(6.4)

The **DFE** is determined by solving the system (6.4), yielding:

$$\mathbf{DFE} = (\mathcal{V}^*, \mathcal{S}^*, \mathcal{E}^*, \mathcal{I}^*, \mathcal{D}^*, \mathcal{X}^*, \mathcal{T}^*) = \left(\frac{\nu \Lambda}{\alpha + \mu}, \frac{(\alpha + \mu - \mu \nu) \Lambda}{\mu (\alpha + \mu)}, 0, 0, 0, 0, 0, 0\right),$$
 where $\mathcal{N} = \frac{\Lambda}{\mu}$.

6.3.2 | Basic reproduction number \mathcal{R}_0

The computation of the basic reproduction number, \mathcal{R}_0 , for the discrete TB model is performed using the method described in (22; 83). This approach involves constructing

essential matrices to derive the threshold parameter, \mathcal{R}_0 (6; 37), expressed as:

$$\mathcal{R}_0 = \rho(FV^{-1}),$$

where FV^{-1} is the next-generation matrix. Here, F and V are $m \times m$ matrices, with m representing the number of infected compartments. The spectral radius of FV^{-1} , denoted $\rho(FV^{-1})$, determines the value of \mathcal{R}_0 .

The equations for the infected classes in the model (6.2) are:

$$\mathcal{E}_{t+1} = \mathcal{E}_t + \beta \mathcal{S}_t \mathcal{I}_t - (\epsilon + \mu + \omega) \mathcal{E}_t,$$

$$\mathcal{I}_{t+1} = \mathcal{I}_t + \epsilon \mathcal{E}_t - (\tau + \zeta + \gamma + \mu + \sigma) \mathcal{I}_t,$$

$$\mathcal{D}_{t+1} = \mathcal{D}_t + \tau \mathcal{I}_t - (\theta + \mu + \delta) \mathcal{D}_t,$$

$$\mathcal{X}_{t+1} = \mathcal{X}_t + \zeta \mathcal{I}_t - (\xi + \mu + \eta) \mathcal{X}_t.$$
(6.5)

The next-generation matrices *F* and *V* are derived as:

$$V = \begin{pmatrix} (\epsilon + \mu + \omega) & 0 & 0 & 0 \\ -\epsilon & (\tau + \zeta + \gamma + \mu + \sigma) & 0 & 0 \\ 0 & -\tau & (\theta + \mu + \delta) & 0 \\ 0 & -\zeta & 0 & (\xi + \mu + \eta) \end{pmatrix}.$$

The matrix FV^{-1} is computed as:

The eigenvalues of FV^{-1} are obtained by solving $|FV^{-1} - \lambda I_4| = 0$, yielding:

$$\lambda_1 = 0$$
, $\lambda_2 = 0$, $\lambda_3 = 0$, and
$$\lambda_4 = \frac{\epsilon \beta (\alpha + \mu - \mu \nu) \Lambda}{\mu (\alpha + \mu) (\epsilon + \mu + \omega) (\tau + \zeta + \gamma + \mu + \sigma)}.$$

The dominant eigenvalue, λ_4 , represents the basic reproduction number:

$$\mathcal{R}_0 = \rho(FV^{-1}) = \frac{\epsilon \beta(\alpha + \mu - \mu \nu) \Lambda}{\mu(\alpha + \mu)(\epsilon + \mu + \omega)(\tau + \zeta + \gamma + \mu + \sigma)}.$$

6.3.3 | Global stability investigation of the **DFE**

Proposition 6.2 *Consider the first equation of model (6.2):*

$$\mathcal{V}_{t+1} = \mathcal{V}_t + \nu \Lambda - (\alpha + \mu) \mathcal{V}_t.$$

If the initial condition $V_0 \geq 0$ is satisfied, then V_t converges to $V^* = \frac{v\Lambda}{\alpha + u}$ as $t \to \infty$.

Proof. Starting with $V_0 \ge 0$, substitute this into the recurrence relation to find V_1 :

$$V_1 = V_0 + \nu \Lambda - (\alpha + \mu) V_0.$$

This can be rewritten as:

$$\mathcal{V}_1 = \mathcal{V}_0(1 - (\alpha + \mu)) + \nu \Lambda.$$

Let us prove that V_t converges to a unique fixed point V^* . we express the recurrence relation as

$$\mathcal{V}_{t+1} = \mathcal{V}_t(1 - (\alpha + \mu)) + \nu \Lambda.$$

At equilibrium, $V_{t+1} = V_t = V^*$, substituting this into the equation results in:

$$\mathcal{V}^* = \mathcal{V}^*(1 - (\alpha + \mu)) + \nu \Lambda.$$

Simplify to find:

$$\mathcal{V}^* = \frac{\nu \Lambda}{\alpha + \mu}.$$

Now consider the difference from the equilibrium V^* , denoted as $\Delta_t = V_t - V^*$. Using the recurrence relation, we have:

$$\Delta_{t+1} = \mathcal{V}_{t+1} - \mathcal{V}^* = (\mathcal{V}_t - \mathcal{V}^*)(1 - (\alpha + \mu)).$$

This simplifies to:

$$\Delta_{t+1} = \Delta_t (1 - (\alpha + \mu)).$$

Since $1 - (\alpha + \mu)$ lies in the interval (0, 1), $\Delta_t \to 0$ as $t \to \infty$. Therefore:

$$\mathcal{V}_t \to \mathcal{V}^* = \frac{\nu \Lambda}{\alpha + \mu}.$$

Hence, V_t converges to V^* without assuming a priori boundedness.

Theorem 6.1 The disease-free equilibrium (**DFE**) of the model described by system (6.2) is globally asymptotically stable (GAS) if $\mathcal{R}_0 \leq 1$.

Proof. For $\mathcal{R}_0 < 1$, the following inequality holds:

$$\epsilon\beta\left(\frac{(\alpha+\mu-\mu\nu)\Lambda}{\mu(\alpha+\mu)}\right)-(\epsilon+\mu+\omega)(\tau+\zeta+\gamma+\mu+\sigma)<0.$$

According to the **Archimedean property** of \mathbb{R} , a positive constant $\gamma_0 > 0$ can be found such that:

$$\epsilon\beta\left(\frac{(\alpha+\mu-\mu\nu)\Lambda}{\mu(\alpha+\mu)}+\gamma_0\right)-(\epsilon+\mu+\omega)(\tau+\zeta+\gamma+\mu+\sigma)<0.$$

To prove the GAS of the discrete model (6.2), define the Lyapunov function:

$$F_t = b_1 \mathcal{E}_t + b_2 \mathcal{I}_t,$$

where the backward difference ΔF is given by:

$$\Delta F = F_{t+1} - F_t = b_1(\mathcal{E}_{t+1} - \mathcal{E}_t) + b_2(\mathcal{I}_{t+1} - \mathcal{I}_t).$$

This becomes:

$$\Delta F = b_1(\beta \mathcal{S}_t \mathcal{I}_t - (\epsilon + \mu + \omega) \mathcal{E}_t) + b_2(\epsilon \mathcal{E}_t - (\tau + \zeta + \gamma + \mu + \sigma) \mathcal{I}_t).$$

To establish an upper bound for S_t , we refer to Proposition 6.2, which implies the existence of t_0 such that for all $t > t_0$, the inequality $|\mathcal{V}_t - \mathcal{V}^*| < \gamma_0$ holds.

The inequality $|\mathcal{V}_t - \mathcal{V}^*| < \gamma_0$ implies that:

$$\mathcal{V}^* - \gamma_0 < \mathcal{V}_t$$

which leads to:

$$-\mathcal{V}_t < -\mathcal{V}^* + \gamma_0$$
.

Also, by assumption, we have $\mathcal{N}_t \leq \frac{\Lambda}{\mu}$.

Thus,

$$\mathcal{S}_t \leq \mathcal{N}_t - \mathcal{V}_t \leq \frac{\Lambda}{u} - \mathcal{V}^* + \gamma_0 \leq \frac{\Lambda}{u} - \frac{\nu\Lambda}{\alpha + u} + \gamma_0 \leq \frac{(\alpha + \mu - \mu\nu)\Lambda}{u(\alpha + u)} + \gamma_0.$$

Thus, we obtain the inequality:

$$\Delta F \leq b_1 \left(\beta \left(\frac{(\alpha + \mu - \mu \nu)\Lambda}{\mu(\alpha + \mu)} + \gamma_0\right) \mathcal{I}_t - (\epsilon + \mu + \omega)\mathcal{E}_t\right) + b_2 \left(\epsilon \mathcal{E}_t - (\tau + \zeta + \gamma + \mu + \sigma)\mathcal{I}_t\right).$$

We can then bound this expression as:

$$\Delta F \leq \left(b_1 \beta \left(\frac{(\alpha + \mu - \mu \nu) \Lambda}{\mu(\alpha + \mu)} + \gamma_0\right) - b_2(\tau + \zeta + \gamma + \mu + \sigma)\right) \mathcal{I}_t + \left(b_1(\epsilon + \mu + \omega) - b_2\epsilon\right) \mathcal{E}_t.$$

Choosing $b_1 = \epsilon$ and $b_2 = (\epsilon + \mu + \omega)$, we get:

$$\Delta F \leq \left(\epsilon\beta \left(\frac{(\alpha+\mu-\mu\nu)\Lambda}{\mu(\alpha+\mu)} + \gamma_0\right) - (\epsilon+\mu+\omega)(\tau+\zeta+\gamma+\mu+\sigma)\right)\mathcal{I}_t.$$

If $\mathcal{R}_0 < 1$, then $\Delta F < 0$, with equality only when $\mathcal{E}_{t+1} = \mathcal{I}_{t+1} = 0$. This implies $(\mathcal{E}, \mathcal{I}) \to (0, 0)$ as $t \to \infty$.

Substituting $\mathcal{E} = \mathcal{I} = 0$ into the first two equations of (6.2), we find:

$$V \to \frac{\nu\Lambda}{\alpha + \mu}$$
, $S \to \frac{(\alpha + \mu - \mu\nu)\Lambda}{\mu(\alpha + \mu)}$ as $t \to \infty$.

Thus, the **DFE** is the maximal invariant set in $\{(\mathcal{V}_t, \mathcal{S}_t, \mathcal{E}_t, \mathcal{I}_t, \mathcal{D}_t, \mathcal{X}_t, \mathcal{T}_t) : F_t = 0\}$. By LaSalle's Invariance Principle (see Theorem 2.2.2.5), every solution of (6.2) converges to the **DFE** as $t \to \infty$.

6.4 | Endemic equilibrium

This section examines the conditions for the existence and stability of an endemic equilibrium (EE) for model (6.2).

6.4.1 | Existence of **EE**

The following lemma guarantees the existence of EE:

Lemma 6.1 *Model (6.2) admits a unique EE if* $\mathcal{R}_0 > 1$.

Proof. At steady-state, solving the equations of system (6.2) results in the following ex-

pressions:

$$\begin{split} \mathcal{V}^{**} &= \frac{\nu \Lambda}{\alpha + \mu'}, \\ \mathcal{S}^{**} &= \frac{(\epsilon + \mu + \omega)(\tau + \zeta + \gamma + \mu + \sigma)}{\beta \epsilon}, \\ \mathcal{E}^{**} &= \frac{(\tau + \zeta + \gamma + \mu + \sigma)}{\epsilon} \mathcal{I}^{**}, \\ \mathcal{I}^{**} &= \frac{(\alpha + \mu - \mu \nu) \epsilon \Lambda}{(\alpha + \mu)(\epsilon + \mu + \omega)(\tau + \zeta + \gamma + \mu + \sigma)} - \frac{\mu}{\beta}, \\ &= \frac{\mu}{\beta} (\mathcal{R}_0 - 1), \\ \mathcal{D}^{**} &= \frac{\tau}{\theta + \mu + \delta} \mathcal{I}^{**}, \\ \mathcal{X}^{**} &= \frac{\zeta}{\xi + \mu + \eta} \mathcal{I}^{**}, \\ \mathcal{T}^{**} &= \left[\gamma + \frac{\omega(\tau + \zeta + \gamma + \mu + \sigma)}{\epsilon} + \frac{\theta \tau}{\theta + \mu + \delta} + \frac{\xi \zeta}{\xi + \mu + \eta} \right] \mathcal{I}^{**}. \end{split}$$

6.4.2 | Global stability investigation of the **EE**

The global asymptotic stability (GAS) of the unique **EE** is demonstrated in the following theorem:

Theorem 6.2 The unique **EE** of model (6.2) is globally asymptotically stable (GAS) if $\mathcal{R}_0 \ge 1$ and $\mu \le 1$.

Proof. Consider system (6.2). Define the nonlinear Lyapunov function:

$$\begin{split} U_t &= \frac{1}{2} \left[(\mathcal{V}_t - \mathcal{V}^{**}) + (\mathcal{S}_t - \mathcal{S}^{**}) + (\mathcal{E}_t - \mathcal{E}^{**}) + (\mathcal{I}_t - \mathcal{I}^{**}) + (\mathcal{D}_t - \mathcal{D}^{**}) + (\mathcal{X}_t - \mathcal{X}^{**}) + (\mathcal{T}_t - \mathcal{T}^{**}) \right]^2, \\ &= \frac{1}{2} \left[(\mathcal{V}_t + \mathcal{S}_t + \mathcal{L}_t + \mathcal{D}_t + \mathcal{X}_t + \mathcal{T}_t) - (\mathcal{V}^{**} + \mathcal{S}^{**} + \mathcal{L}^{**} + \mathcal{I}^{**} + \mathcal{D}^{**} + \mathcal{X}^{**} + \mathcal{T}^{**}) \right]^2, \\ &= \frac{1}{2} (\mathcal{N}_t - \mathcal{N}^{**})^2. \end{split}$$

The backward difference of U_t is:

$$\Delta U = U_{t+1} - U_t,
= \frac{1}{2} \left[(\mathcal{N}_{t+1} - \mathcal{N}^{**})^2 - (\mathcal{N}_t - \mathcal{N}^{**})^2 \right],
= \frac{1}{2} (\mathcal{N}_{t+1} - \mathcal{N}_t) (\mathcal{N}_{t+1} + \mathcal{N}_t - 2\mathcal{N}^{**}),
= -\frac{1}{2} (\mathcal{N}_{t+1} - \mathcal{N}_t)^2 + (\mathcal{N}_{t+1} - \mathcal{N}^{**}) (\mathcal{N}_{t+1} - \mathcal{N}_t),
\leq (\mathcal{N}_{t+1} - \mathcal{N}^{**}) (\mathcal{N}_{t+1} - \mathcal{N}_t).$$

Summing the equations of system (6.2) yields:

$$\mathcal{N}_{t+1} - \mathcal{N}_t = \Lambda - (\sigma \mathcal{I}^{**} + \delta \mathcal{D}^{**} + \eta \mathcal{X}^{**}) - \mu \mathcal{N}_t.$$

At steady-state, $\Lambda - (\sigma \mathcal{I}^{**} + \delta \mathcal{D}^{**} + \eta \mathcal{X}^{**}) = \mu \mathcal{N}^{**}$, so:

$$\Delta U = (\mathcal{N}_t - \mu \mathcal{N}_t + \mu \mathcal{N}^{**} - \mathcal{N}^{**})(\mu \mathcal{N}^{**} - \mu \mathcal{N}_t),$$

$$\leq (\mu^2 - \mu)(\mathcal{N}_t - \mathcal{N}^{**})^2.$$

Hence, $\Delta U \leq 0$ if $\mu \leq 1$. Therefore, **EE** is GAS when $\mathcal{R}_0 \geq 1$ and $\mu \leq 1$.

6.5 | Data fitting for discrete model

This section focuses on estimating seven model parameters using data from the WHO's Global Tuberculosis Report, which provides global TB incidence data from 2000 to 2022 (76) (refer to Table 6.1). Additional statistical data from the literature is used to infer the remaining parameters.

The death rate, μ , is calculated as the average annual death rate for the period 2000–2022, based on population data for India and Russia from (65; 66). Similarly, the annual average birth rate during the same period is used to estimate the birth rate, Λ , as shown in Table 6.1.

For India, the total population in 2000 was $\mathcal{N}=1\,059\,633\,675$ (65). The initial number of reported TB cases, $\mathcal{I}_0=1\,115\,718$, was obtained from WHO data (76), along with the initial counts of MDR- and XDR-TB cases. The number of vaccinated individuals was calculated using:

 $V_0 = \text{Number of births} \times \text{Vaccination rate.}$

The number of exposed individuals was assumed to be:

$$\mathcal{E}_0 = 8852$$
,

while the treated individuals were assumed to be:

$$T_0 = 2000.$$

Thus, the initial susceptible population was computed as:

$$S_0 = \mathcal{N} - (\mathcal{V}_0 + \mathcal{E}_0 + \mathcal{I}_0 + \mathcal{D}_0 + \mathcal{X}_0 + \mathcal{T}_0) = 851497070.$$

The initial conditions for Russia were found to be the same as those for India.

The vaccination rate, ν , was determined using data on Bacillus Calmette-Guérin (BCG) vaccination coverage for children aged 12 to 23 months from World Bank statistics (82; 93). The treatment rates for MDR-TB (θ) and XDR-TB (ξ) were derived as the annual average treatment success rates for MDR- and XDR-TB, respectively, during 2000–2022. These rates are calculated as:

Treatment success rate for MDR-TB each year

 $= \frac{\text{Number of individuals treated successfully for MDR-TB each year}}{\text{Number of individuals with MDR-TB each year}}$

Treatment success rate for XDR-TB each year =

 $\frac{\text{Number of individuals treated successfully for XDR-TB each year}}{\text{Number of individuals with XDR-TB each year}}.$

Similarly, the disease-specific death rates for MDR-TB (δ) and XDR-TB (η) were calculated as the annual average death rates during 2000–2022:

 $\label{eq:Death rate for MDR-TB each year} Death \ rate \ for \ MDR-TB \ each \ year = \frac{Number \ of \ MDR-TB \ deaths \ each \ year}{Number \ of \ individuals \ with \ MDR-TB \ each \ year}'$

Death rate for XDR-TB each year = $\frac{\text{Number of XDR-TB deaths each year}}{\text{Number of individuals with XDR-TB each year}}$.

The remaining parameters $(\beta, \gamma, \epsilon, \sigma, \omega, \tau, \alpha, \zeta)$ were estimated by minimizing the error between the model's predicted TB incidence and the observed data. The objective function used was:

$$\Phi = \sum_{i=1}^n (\mathcal{I}_{t_i} - \mathcal{I}_{t_i}^*)^2,$$

where $\mathcal{I}_{t_i}^*$ represents the observed TB cases at time t_i , \mathcal{I}_{t_i} represents the model-predicted cases, and n is the number of data points. This minimization was performed using the Levenberg-Marquardt algorithm and MATLAB's fitnlm function.

Figures 6.2 and 6.3 show the TB incidence data for Russia and India, respectively, along with the fitted model curves based on the estimated parameters (Table 6.1).

Table 6.1: Initial conditions and model parameters for Russia and India.

Parameters	Russia	References	India	References
$\mathcal{V}(0)$	13,791,833	(93)	180,967,005	(82)
$\mathcal{S}(0)$	132,653,507	Calculated	851,497,070	Calculated
$\mathcal{E}(0)$	8,852	Assumed	8,852	Assumed
$\mathcal{I}(0)$	140,677	(76)	1,115,718	(76)
$\mathcal{D}(0)$	0	(76)	0	(76)
$\mathcal{X}(0)$	0	(76)	0	(76)
$\mathcal{T}(0)$	2,000	Assumed	2,000	Assumed
Λ	1,720,142.287	(66)	26, 469, 994.76	(65)
μ	0.015	(66)	0.007	(65)
ν	0.96	(93)	0.858	(82)
α	0.0012	Fitted	0.160	Fitted
β	1.45×10^{-6}	Fitted	1.27×10^{-8}	Fitted
γ	1×10^{-14}	Fitted	0.043	Fitted
ϵ	0.0003	Fitted	0.004	Fitted
ω	0.254	Fitted	0.542	Fitted
τ	0.048	Fitted	4.17×10^{-6}	Fitted
ζ	0.028	Fitted	3.02×10^{-6}	Fitted
ζ ξ θ	0.36	Calculated	0.356	Calculated
θ	0.49	Calculated	0.504	Calculated
δ	0.15	Calculated	0.189	Calculated
σ	2.81×10^{-6}	Fitted	0.006	Fitted
η	0.21	Calculated	0.319	Calculated

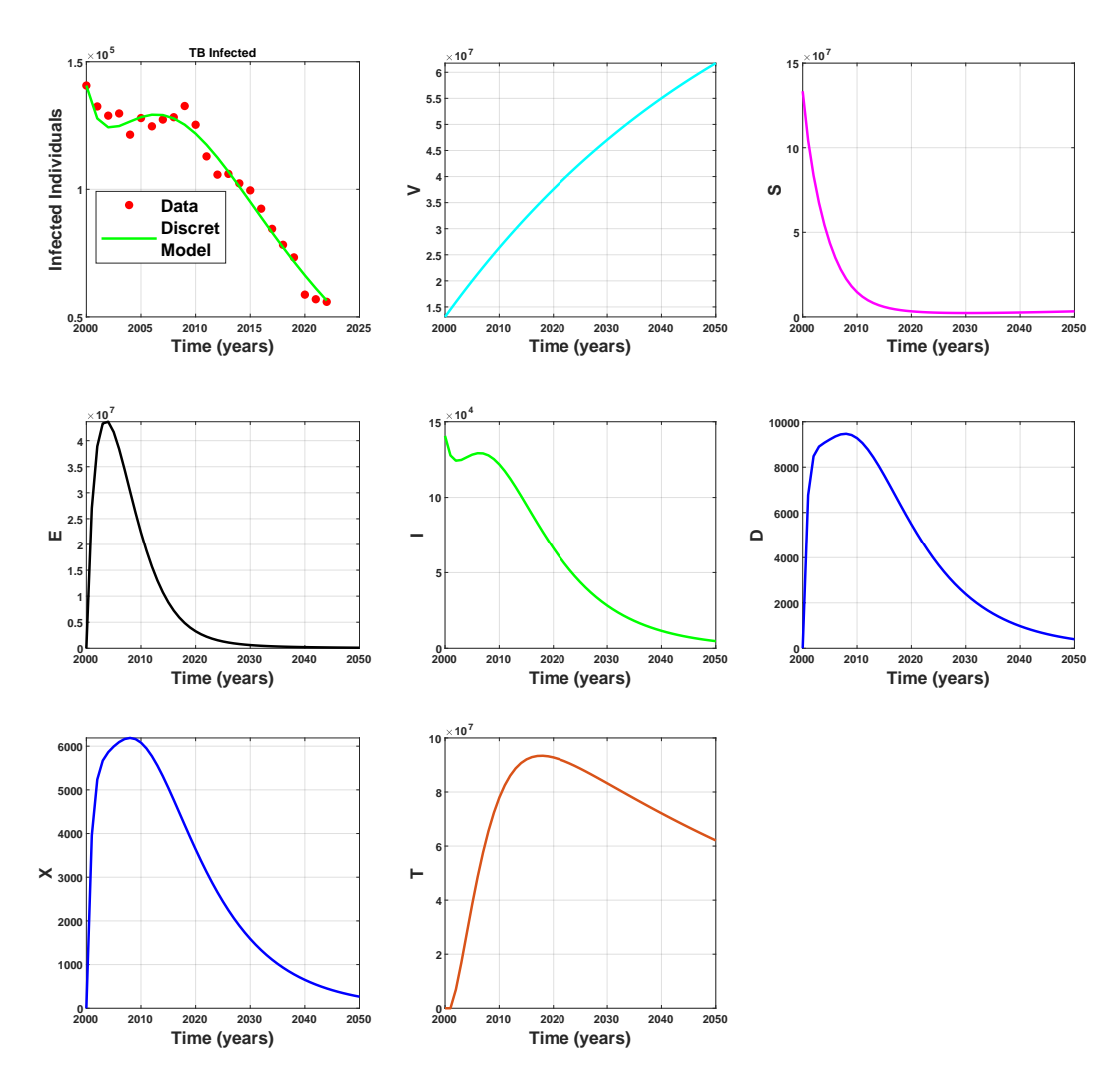


Figure 6.2: TB incidence data and model fit for Russia. The data points are shown in green, while the fitted model is depicted in red. The basic reproduction number, $\mathcal{R}_0 = 0.22 < 1$.

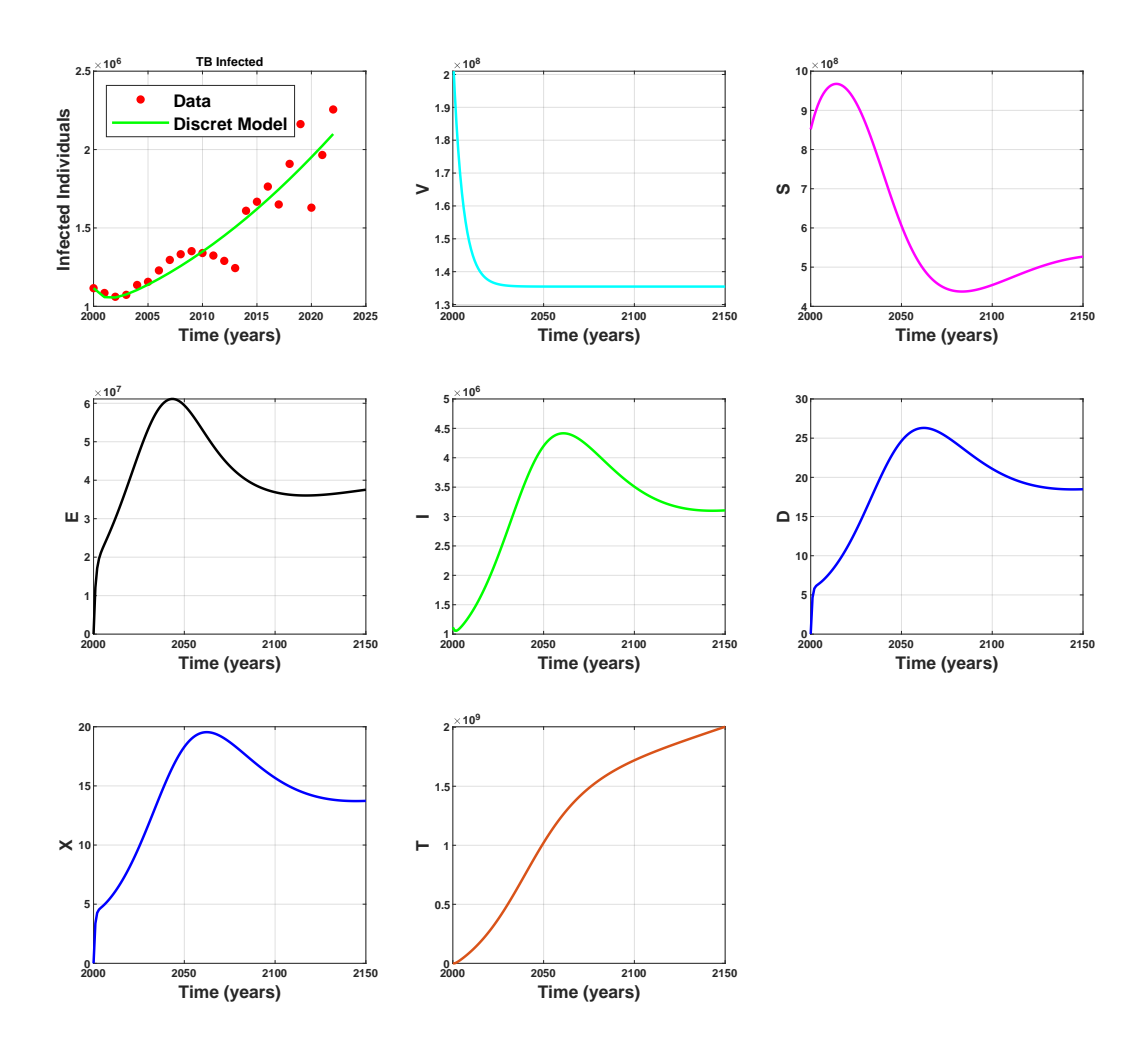


Figure 6.3: TB incidence data and model fit for India. The data points are shown in green, while the fitted model is depicted in red. The basic reproduction number, $\mathcal{R}_0 = 6.42 > 1$.

6.6 | Analyzing the sensitivity of \mathcal{R}_0

This section examines the sensitivity of the basic reproduction number \mathcal{R}_0 with respect to the model parameters. First, the partial derivatives of \mathcal{R}_0 with respect to the parameters β , γ , ε , ω , τ , ζ , σ , α , μ , and ν are derived. These derivatives are evaluated using the following definition of the normalized sensitivity index:

Definition 6.1 The normalized sensitivity index of \mathcal{R}_0 with respect to a parameter ρ is defined

as:

$$S_{\rho}^{\mathcal{R}_0} = \frac{\rho}{\mathcal{R}_0} \frac{\partial \mathcal{R}_0}{\partial \rho}.$$

Using this definition, the partial derivatives of \mathcal{R}_0 with respect to the parameters are calculated as follows:

Constrainted as follows:
$$S^{\mathcal{R}_0}_{\beta} = \frac{\beta}{\mathcal{R}_0} \frac{\partial \mathcal{R}_0}{\partial \beta} = 1 > 0,$$

$$S^{\mathcal{R}_0}_{\gamma} = \frac{\gamma}{\mathcal{R}_0} \frac{\partial \mathcal{R}_0}{\partial \gamma} = \frac{-\gamma}{(\gamma + \mu + \sigma + \tau + \zeta)},$$

$$S^{\mathcal{R}_0}_{\epsilon} = \frac{\varepsilon}{\mathcal{R}_0} \frac{\partial \mathcal{R}_0}{\partial \epsilon} = 1 - \frac{\varepsilon}{(\omega + \epsilon + \mu)},$$

$$S^{\mathcal{R}_0}_{\omega} = \frac{\omega}{\mathcal{R}_0} \frac{\partial \mathcal{R}_0}{\partial \omega} = \frac{-\omega}{(\omega + \epsilon + \mu)},$$

$$S^{\mathcal{R}_0}_{\tau} = \frac{\tau}{\mathcal{R}_0} \frac{\partial \mathcal{R}_0}{\partial \tau} = \frac{-\tau}{(\gamma + \mu + \sigma + \tau + \zeta)},$$

$$S^{\mathcal{R}_0}_{\zeta} = \frac{\zeta}{\mathcal{R}_0} \frac{\partial \mathcal{R}_0}{\partial \zeta} = \frac{-\zeta}{(\gamma + \mu + \sigma + \tau + \zeta)},$$

$$S^{\mathcal{R}_0}_{\rho} = \frac{p}{\mathcal{R}_0} \frac{\partial \mathcal{R}_0}{\partial \nu} = \frac{-(\mu \nu)}{(\alpha + \mu - \mu \nu)},$$

$$S^{\mathcal{R}_0}_{\alpha} = \frac{\alpha}{\mathcal{R}_0} \frac{\partial \mathcal{R}_0}{\partial \alpha} = \frac{(\alpha \mu \nu)}{((\alpha + \mu)(\alpha + \mu - \mu \nu))},$$

$$S^{\mathcal{R}_0}_{\sigma} = \frac{\sigma}{\mathcal{R}_0} \frac{\partial \mathcal{R}_0}{\partial \sigma} = \frac{-\sigma}{(\gamma + \mu + \sigma + \tau + \zeta)},$$

$$S^{\mathcal{R}_0}_{\mu} = \frac{\mu}{\mathcal{R}_0} \frac{\partial \mathcal{R}_0}{\partial \mu} = -(\frac{\mu}{(\gamma + \mu + \sigma + \tau + \zeta)} + \frac{\mu}{(\omega + \epsilon + \mu)} + \frac{\mu}{(\alpha + \mu)} + 1 + \frac{\mu((\nu - 1))}{(\alpha + \mu - \mu \nu)}).$$

Table 6.2: Sensitivity Index for the Basic Reproduction Number \mathcal{R}_0 .

Parameter	Sensitivity Index
μ	-1.6712
ν	-9.5533
α	+0.5449
β	+1.0000
γ	-6.8240×10^{-14}
ϵ	+0.9963
ω	-0.9759
au	-0.5153
ζ	-0.3788
σ	-1.1943×10^{-4}

6.7 | Numerical results

The results of the parameter estimation are presented in Table 6.1. The TB incidence data, along with the model's fitted curve, are shown in Figures 6.2 and 6.3, which were generated using the parameter values from Table 6.1. The model provides a good fit, demonstrated by high coefficients of determination: $\mathcal{R}^2 = 0.8709$ for India and $\mathcal{R}^2 = 0.977$ for Russia. These values suggest that the model accurately reflects the observed data patterns.

Based on the estimated parameter values, the calculated \mathcal{R}_0 for India is 6.42 (greater than 1), which indicates that the **DFE** is unstable, while the $\mathcal{E}\mathcal{E}$ is asymptotically stable, as depicted in Figure 6.3. In contrast, for Russia, the calculated \mathcal{R}_0 is 0.22 (less than 1), suggesting that the **DFE** is asymptotically stable, while the $\mathcal{E}\mathcal{E}$ is unstable, as shown in Figure 6.2.

To better understand the impact of specific parameters on disease transmission, Figures 6.4 and 6.5 provide graphical representations of R_0 in relation to ten parameters. The basic reproduction number, \mathcal{R}_0 , demonstrates a strong positive correlation with β , α , and ϵ . This suggests that an increase in these parameters results in a higher \mathcal{R}_0 , thereby promoting more rapid disease spread.

In contrast, an inverse relationship is found between \mathcal{R}_0 and the other parameters $\gamma, \nu, \tau, \zeta, \omega, \sigma$, and μ . Increased values of these parameters lead to a lower \mathcal{R}_0 , suggesting a slower rate of disease transmission. These findings align with real-world observations. The original model presented by Gupta et al. (32) did not account for the effects of chemoprophylaxis on individuals with latent TB infections, nor did it consider the treatment for those with active TB. To improve this, D. B. Kitaro et al. (43) enhanced the model by incorporating chemoprophylaxis for latent infections and treatment for those with active TB. As a result, this study focused on estimating parameters and evaluated the impact of chemoprophylaxis and vaccination on the infected, MDR, and XDR classes. The analysis used TB incidence data from India and Russia to assess the effectiveness of these interventions.

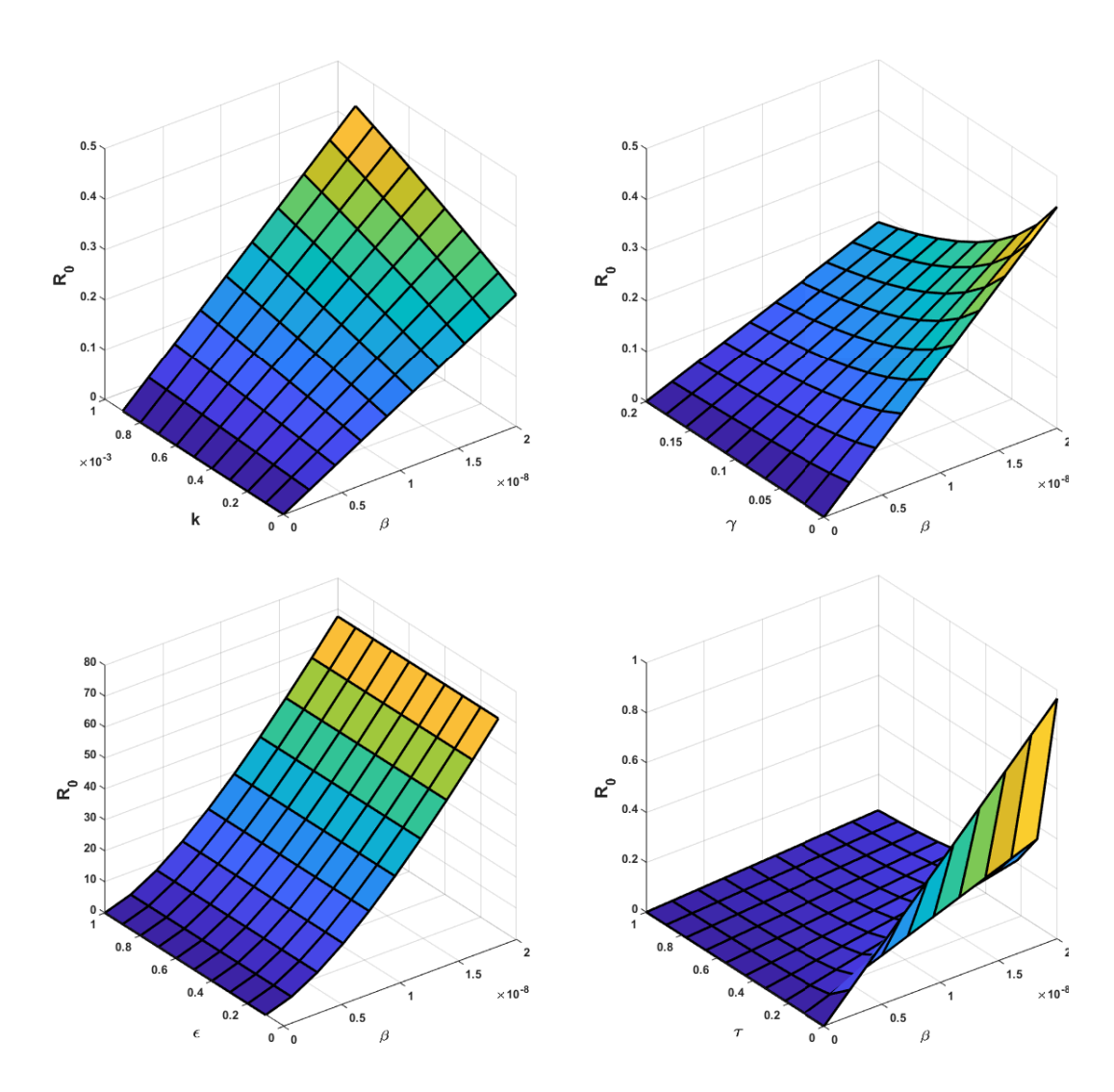


Figure 6.4: Representation of \mathcal{R}_0 versus β , τ , γ , ϵ and α .

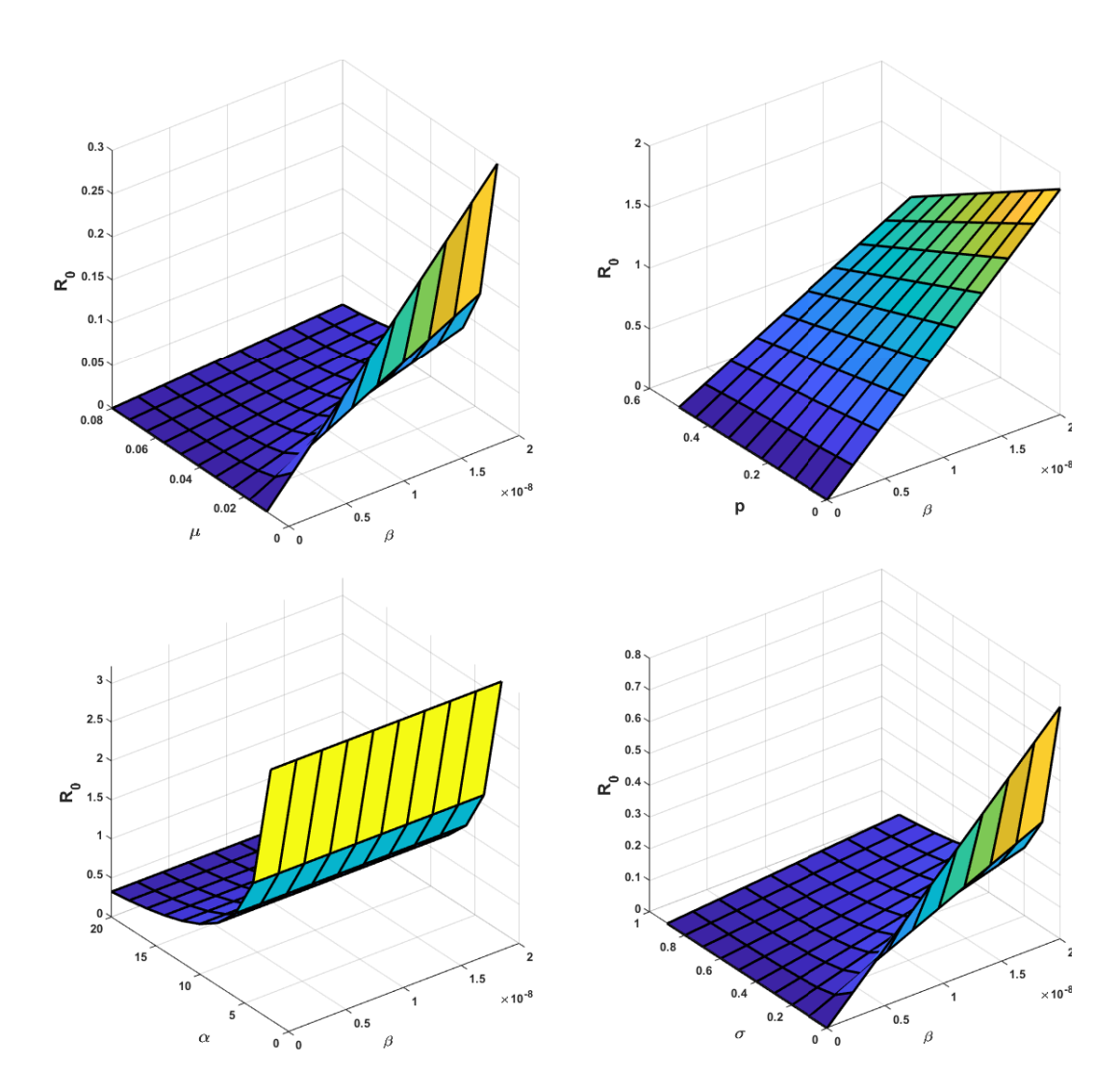


Figure 6.5: Representation of \mathcal{R}_0 versus β , ν , ω , σ , and μ .

An analysis of Figure 6.6 reveals that the number of individuals in the infected categories, MDR and XDR, who are not receiving chemoprophylaxis treatment exceeds those who are receiving it among the exposed groups. Additionally, as the chemoprophylaxis treatment parameter ω increases, it becomes clear that providing chemoprophylaxis to exposed individuals substantially reduces the transmission of tuberculosis.

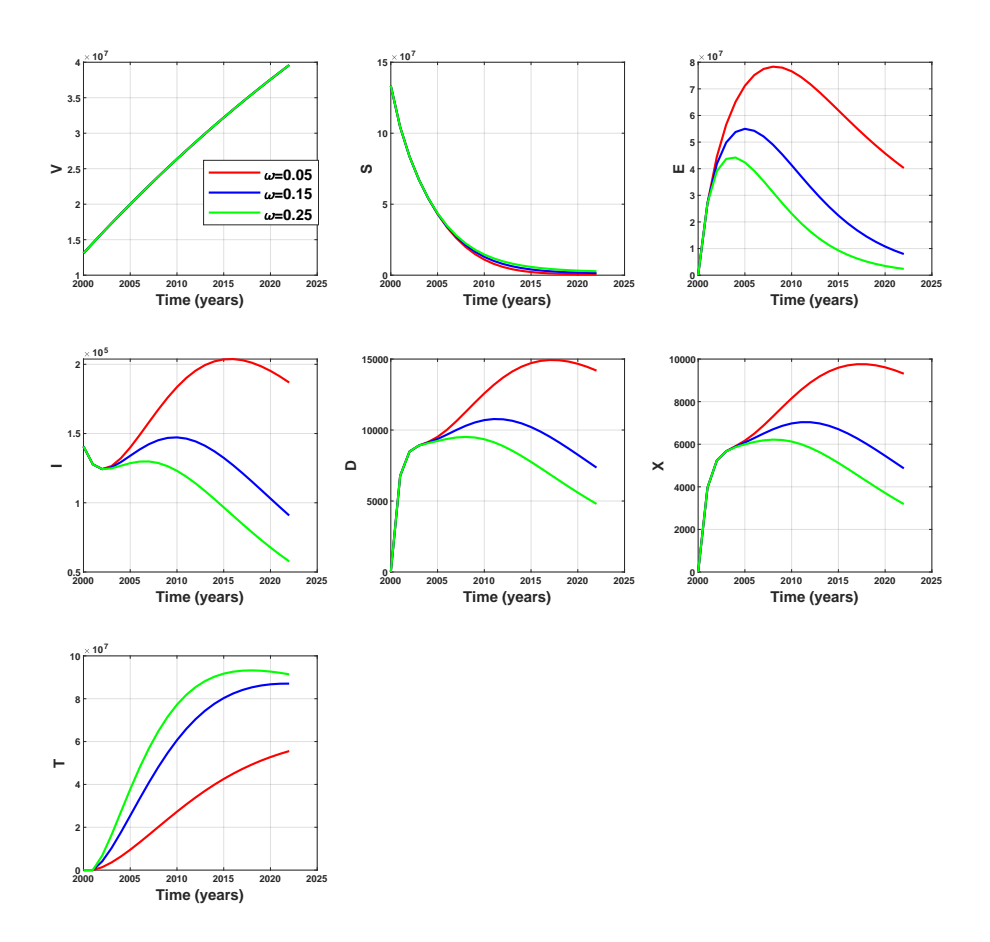


Figure 6.6: Effect of the chemoprophylaxis treatment rate on the compartments of the discrete model (6.2).

Figure 6.7 illustrates that as the BCG vaccination rate increases, the number of individuals in the infected, MDR, and XDR classes decreases, which can be attributed to the protective effects of the vaccine. The BCG (Bacillus Calmette-Guérin) vaccine, commonly used against TB, offers partial protection against specific strains of the TB-causing bacteria.

As more individuals are vaccinated with BCG, the overall immunity within the population increases, making it harder for the TB bacteria, including **MDR** and **XDR** strains, to infect those who have received the vaccine. Consequently, the spread of these drugresistant strains is diminished, leading to a reduction in the number of infected individuals in these categories.

In conclusion, the effectiveness of BCG vaccination in lowering the prevalence of **MDR-TB** and **XDR-TB** is reflected in the negative correlation between vaccination rate and the size of these infected classes, as shown in Figure 6.7.

Overall, the numerical analysis provides evidence that incorporating the chemoprophylaxis treatment parameter ω and the vaccination rate parameter ν into the model significantly enhances the reduction in TB transmission, especially within the **MDR** and **XDR** compartments. This improvement is evident when compared to the model that does not include chemoprophylaxis treatment for Exposed individuals or consider the vaccination rate. Figure 6.8 presents a comparison between the discrete and contin-

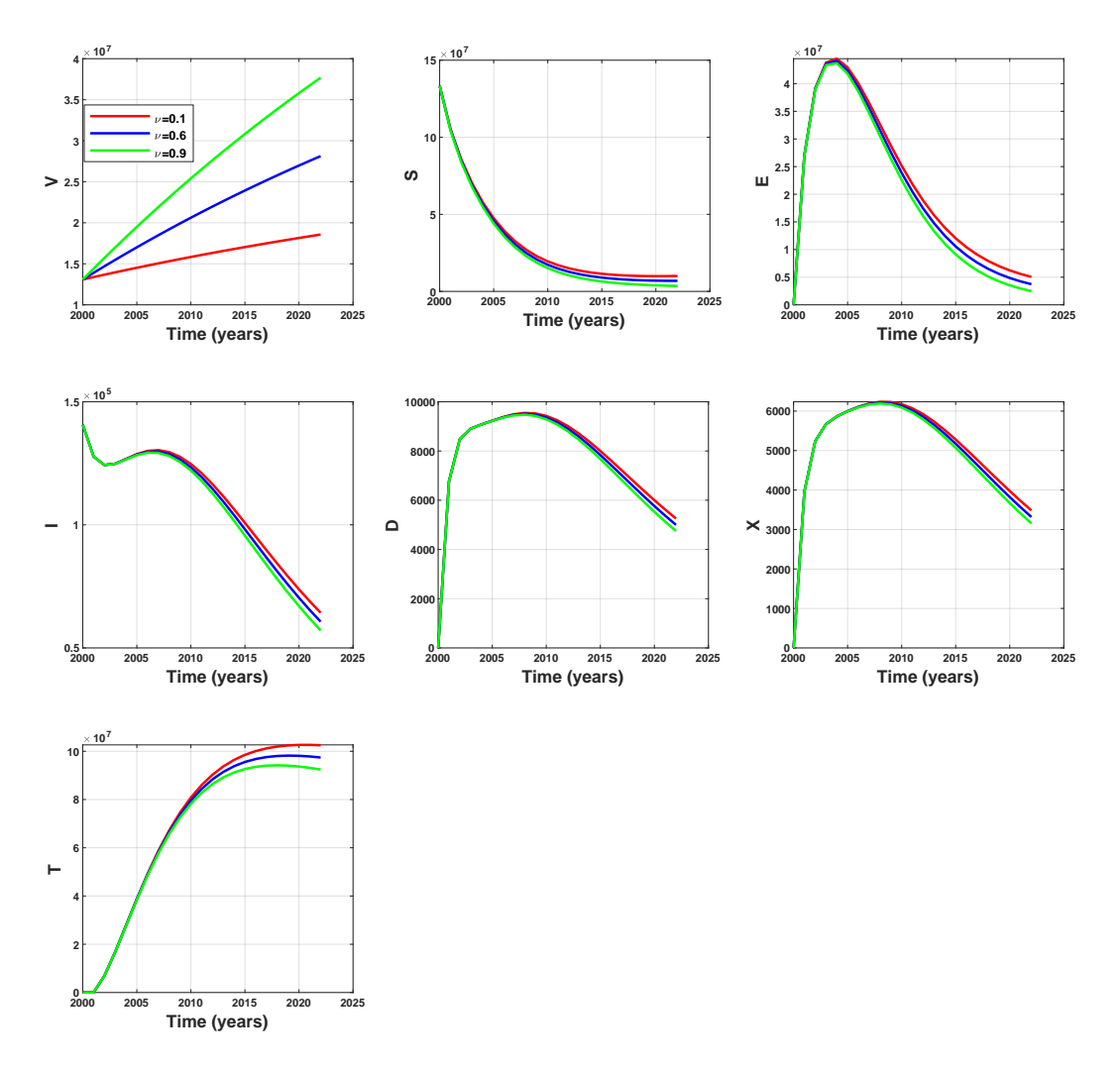


Figure 6.7: Effect of the vaccination rate on the compartments of the discrete model (6.2).

uous models in terms of the number of infected cases in Russia. The discrete model provides a strong fit, as indicated by a high coefficient of determination, $\mathcal{R}^2=0.98$. In contrast, the continuous model has a lower coefficient of determination, $\mathcal{R}^2=0.93$, suggesting a less accurate fit compared to the discrete model.

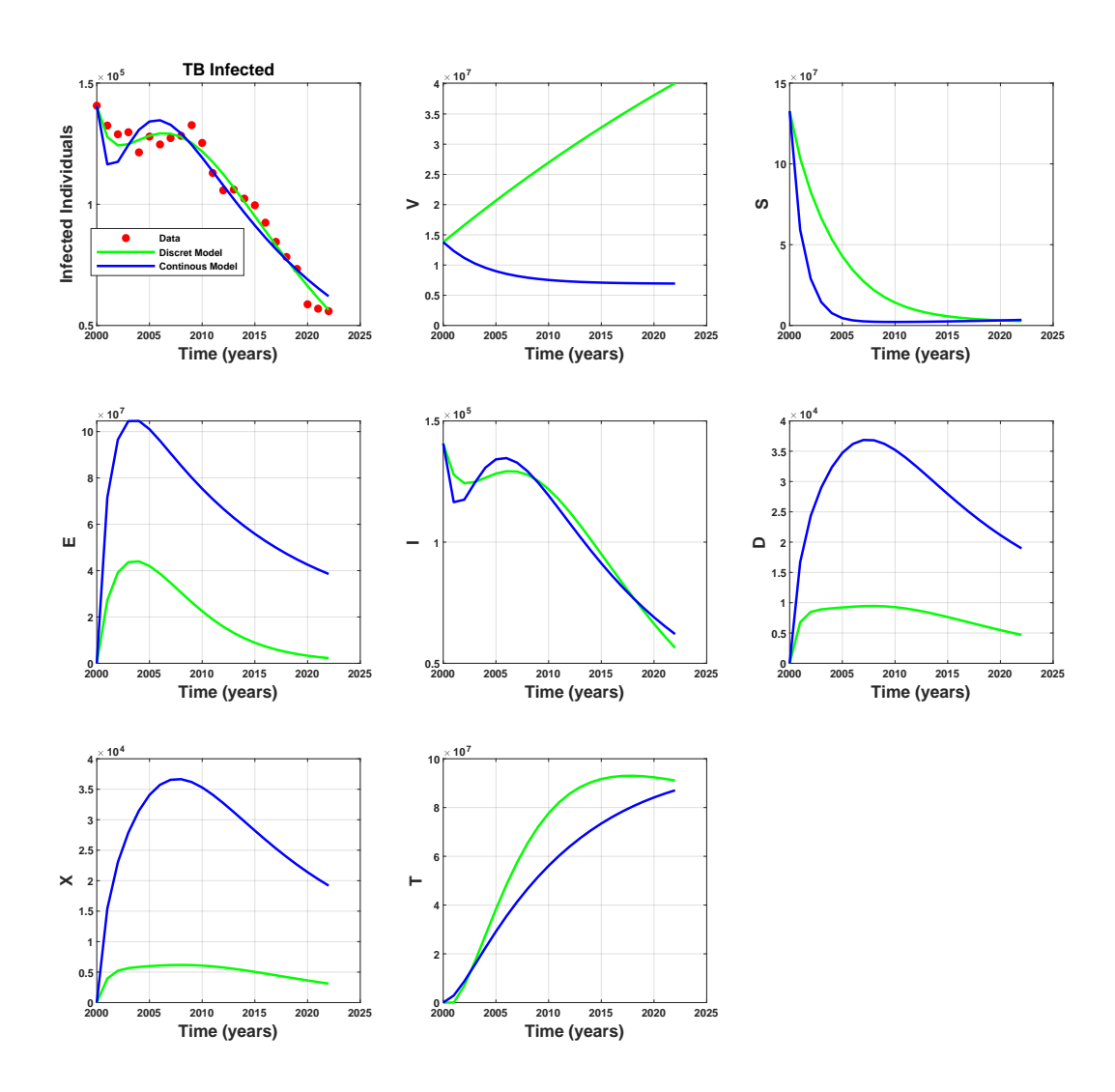


Figure 6.8: Comparision of the discrete model and continuous model vs Russia's Data.

The discrete model provides a better fit because its framework is particularly effective at capturing the dynamics of time-stepped data, especially when the data is recorded in discrete intervals, like daily case counts. Moreover, when real-world data has inherent discrete characteristics or experiences abrupt changes over time, the discrete model can adapt to these variations more easily. Additionally, discrete models are more adept at representing nonlinear behaviors and sudden shifts, such as bifurcations, resulting in a more precise reflection of the observed data.

Conclusion

This research developed and analyzed a discrete mathematical model for tuberculosis (TB) transmission, emphasizing multidrug-resistant (MDR-TB) and extensively drug-resistant (XDR-TB) cases. The model originated from a continuous-time framework and was discretized using the Euler forward method with a step size of h = 1. It incorporates the effects of chemoprophylaxis for the Exposed group and vaccination coverage. The next-generation matrix method was utilized to determine the basic reproduction number, \mathcal{R}_0 , and to assess the stability of both the disease-free and endemic equilibrium points. Model parameters were calibrated using real TB incidence data from India and Russia, yielding \mathcal{R}_0 values of 6.42 for India and 0.22 for Russia, indicating a significantly higher risk of TB transmission in India. The model's projections showed strong agreement with observed TB cases, demonstrating its reliability for predicting the disease's trajectory. Sensitivity analysis highlighted that increasing chemoprophylaxis for exposed individuals effectively reduces progression to MDR-TB and XDR-TB, while BCG vaccination enhances immunity and curtails transmission rates. Considering TB's greater prevalence in India compared to Russia, the study emphasizes the urgent need for enhanced interventions in India. Recommendations include improved treatment strategies, strengthening healthcare infrastructure, and conducting widespread public awareness campaigns to mitigate the impact of TB.

Game theory in tuberculosis vaccination: analyzing Nash equilibria for optimal strategies in Algeria

Contents

7.1	Material and methods	
7.2	Equilibrium points	
7.3	Basic reproduction number	
7.4	Herd immunity threshold vaccination rate $\ \ldots \ \ldots \ \ 125$	
7.5	Nash equilibrium vaccination strategy 126	
7.6	Uncertainty and sensitivity analysis	
Conc	lusion	

This chapter analyzes tuberculosis (TB) vaccination strategies using mathematical modeling and game theory. It covers the methods used to develop the model, explores equilibrium points, and examines key concepts such as the fundamental reproduction rate (R_0) and the threshold for herd immunity. The Nash equilibrium vaccination strategy is also analyzed, followed by a sensitivity analysis to assess the model's robustness.

Introduction

Tuberculosis continues to be a significant global health issue, particularly in nations like Algeria, where the disease burden remains high. Caused by the bacterium Mycobacterium tuberculosis, TB primarily affects the lungs, although it can also spread to other organs of the body (92). In Algeria, similar to many other nations, efforts to control

TB heavily depend on vaccination programs, with the Bacillus Calmette-Guérin (BCG) vaccine being instrumental in preventing severe TB in children (4). Despite the high coverage of BCG vaccination, TB transmission continues to pose a significant threat, necessitating innovative approaches to enhance control measures.

The vaccination decisions, particularly in the context of TB, often involve a complex interplay of individual incentives, societal norms, and public health strategies. Game theory, a mathematical framework that studies strategic interactions, has been increasingly applied to understand and optimize vaccination decisions. In this context, individuals' decisions to vaccinate or not vaccinate depend not only on their perceived risk of infection but also on the vaccination choices of others in the population (9).

In Algeria, while the vaccination rate for BCG is relatively high, gaps in TB transmission dynamics and individual vaccination decisions remain (91). Game theory provides a powerful tool to model the strategic decision-making process of individuals regarding vaccination. By analyzing the Nash equilibrium in the context of TB vaccination, we can determine the optimal vaccination rate that balances individual costs and benefits with the public health goal of reducing TB transmission (74).

This chapter aims to develop a game-theoretic model of TB vaccination in Algeria, where the decisions of individuals to vaccinate are influenced by the vaccination decisions of others in the population. We incorporate a simple epidemiological model to describe the spread of TB and analyze the conditions under which individuals will choose to vaccinate. By doing so, we explore the potential for achieving optimal vaccination rates through voluntary participation and assess the role of public health interventions in influencing these decisions. Through this model, we aim to provide insights into how game theory can guide TB vaccination strategies in Algeria and similar contexts.

7.1 | Material and methods

Our mathematical model is based on the compartmental approach to TB dynamics proposed by Chennaf et al. (12) and examined in Chapter 4. This framework categorizes the population into five distinct compartments: vaccinated individuals $(\mathcal{V}(t))$, susceptible individuals $(\mathcal{S}(t))$, latent individuals $(\mathcal{L}(t))$, infected individuals $(\mathcal{I}(t))$, and treated individuals $(\mathcal{T}(t))$, allowing for a systematic analysis of disease transmission and progression. The evolution of each compartment is determined by a system of differential equations, which represent the transitions of individuals between different states over time.

The differential equations governing the model are as follows:

$$\begin{cases} \frac{d\mathcal{V}(t)}{dt} = p\Lambda - (k+\mu)\mathcal{V}(t), \\ \frac{d\mathcal{S}(t)}{dt} = (1-p)\Lambda + k\mathcal{V}(t) - \beta\mathcal{S}(t)\mathcal{I}(t) - \mu\mathcal{S}(t), \\ \frac{d\mathcal{L}(t)}{dt} = \beta\mathcal{S}(t)\mathcal{I}(t) - (\epsilon + \mu)\mathcal{L}(t) + (1-\alpha)\delta\mathcal{T}(t), \\ \frac{d\mathcal{I}(t)}{dt} = \epsilon\mathcal{L}(t) + \alpha\delta\mathcal{T}(t) - (\gamma + \mu + \sigma)\mathcal{I}(t), \\ \frac{d\mathcal{T}(t)}{dt} = \gamma\mathcal{I}(t) - (\mu + \delta + \eta)\mathcal{T}(t). \end{cases}$$

(7.1)

Here, Λ is the population birth rate, k is the rate of vaccination, and μ is the natural mortality rate. The parameters β , ϵ , α , γ , δ , and η represent various transmission, progression, and treatment rates specific to TB. p is the proportion of the population that chooses to vaccinate.

A diagram of the model is shown in Figure 7.1, illustrating the interactions between the compartments.

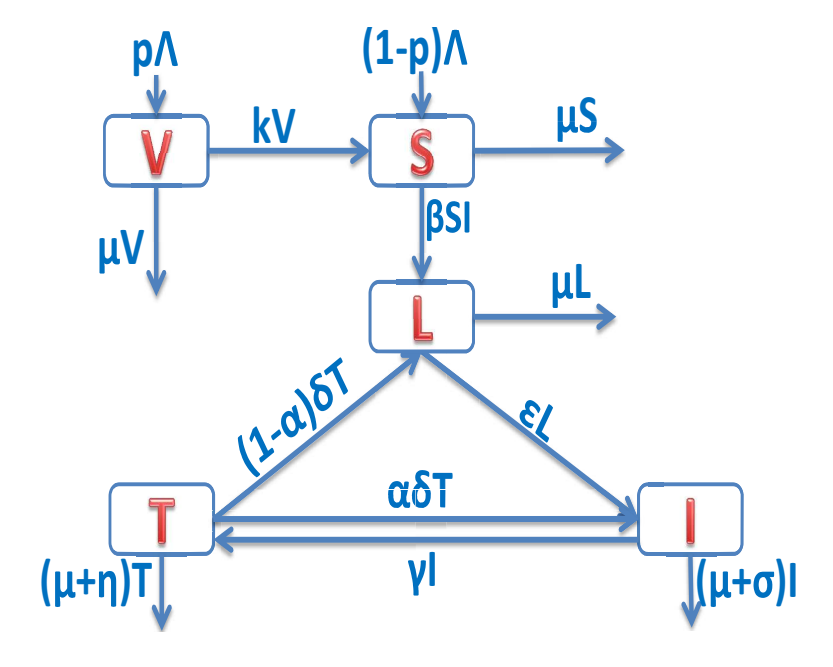


Figure 7.1: Model diagram showing the interactions between compartments in the \mathcal{VSLIT} tuberculosis model

7.2 | Equilibrium points

To assess the long-term behavior of the system 7.1, we compute its equilibrium points. The first of these is the disease-free equilibrium (DFE), which occurs when no individuals are infected. The DFE is expressed as:

$$E_{1} = (\mathcal{V}_{1}^{*}, \mathcal{S}_{1}^{*}, \mathcal{L}_{1}^{*}, \mathcal{I}_{1}^{*}, \mathcal{T}_{1}^{*}) = \left(\frac{p\Lambda}{k+\mu}, \frac{(k+\mu-\mu p)\Lambda}{\mu(k+\mu)}, 0, 0, 0\right).$$

The second equilibrium point is the endemic equilibrium (EE), which occurs when the disease remains in the population. The endemic equilibrium is given by:

$$E_2 = \left(\frac{p\Lambda}{k+\mu}, \frac{(k+\mu-\mu p)\Lambda}{(k+\mu)(\beta I_2^* + \mu)}, \frac{(\gamma+\mu+\sigma)(\mu+\delta+\eta) - \alpha\delta\gamma}{\epsilon(\mu+\delta+\eta)} \mathcal{I}_2^*, \mathcal{I}_2^*, \frac{\gamma}{\mu+\delta+\eta} \mathcal{I}_2^*\right).$$

The condition for the existence of the endemic equilibrium is $\mathcal{R}_0 > 1$, meaning that the disease will spread in the population. If $\mathcal{R}_0 \leq 1$, the disease will eventually die out.

7.3 | Basic reproduction number

The fundamental reproduction rate \mathcal{R}_0 serves as a key threshold parameter in epidemiology, determining whether an infection will persist in a population. It quantifies the expected number of secondary infections caused by a single infected individual in a fully susceptible population. The expression for \mathcal{R}_0 in our model is given by:

$$\mathcal{R}_0 = \frac{\epsilon(k+\mu-\mu p)\Lambda\beta k_3}{\mu(k+\mu)(k_1k_2k_3-\alpha\gamma\delta k_1-(1-\alpha)\delta\gamma\epsilon)}.$$

where
$$k_1 = (\epsilon + \mu)$$
, $k_2 = (\gamma + \mu + \sigma)$, and $k_3 = (\mu + \delta + \eta)$.

When \mathcal{R}_0 exceeds 1, the disease is likely to spread within the population. Conversely, if \mathcal{R}_0 remains below 1, the infection will gradually decline and eventually be eradicated.

7.4 | Herd immunity threshold vaccination rate

Achieving herd immunity requires a sufficiently high vaccination rate to reduce the fundamental reproduction rate \mathcal{R}_0 to below 1. The vaccination rate needed to achieve herd immunity, denoted as $p_{\rm HI}$, is the rate at which vaccination must occur to eliminate the disease. Setting $\mathcal{R}_0=1$ yields the following expression for the herd immunity threshold vaccination rate:

$$p_{\rm HI} = -\frac{(k+\mu)(k_1k_2k_3 - \alpha\gamma\delta k_1 - (1-\alpha)\delta\gamma\epsilon)}{\epsilon\Lambda\beta k_3} + \frac{k+\mu}{\mu}.$$

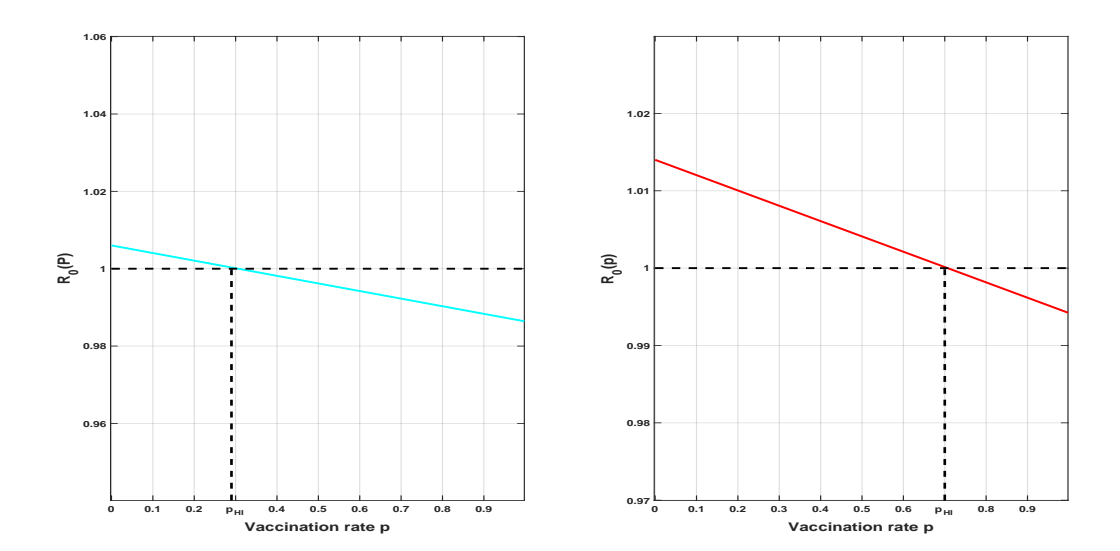


Figure 7.2: The fundamental reproduction rate varsus the vaccination rate p. The critical vaccination rate for achieving herd immunity is denoted by $p_{\rm HI}$.

Figure 7.2 shows the relationship between \mathcal{R}_0 and the vaccination rate p. When $p > p_{\rm HI}$, \mathcal{R}_0 drops below 1, resulting in the eradication of the disease. If $p < p_{\rm HI}$, \mathcal{R}_0 remains above 1, and the disease persists in the population.

7.5 Nash equilibrium vaccination strategy

In this section, a game-theoretic approach is used to determine optimal vaccination strategies within a tuberculosis epidemiological model. Parents must decide whether to vaccinate their child or not. The expected payoffs for both choices are computed based on a previously established framework (9):

$$E_{\rm v} = -C_{\rm v} - \pi_{\rm v} C_{\rm i},$$

$$E_{\rm nv} = -\pi_{\rm nv} C_{\rm i},$$

where $E_{\rm v}$ and $E_{\rm nv}$ represent the payoffs for choosing vaccination and no vaccination, respectively. Here, $\pi_{\rm v}$ and $\pi_{\rm nv}$ are the infection probabilities for vaccinated and non-vaccinated individuals, $C_{\rm i}$ is the cost of infection, and $C_{\rm v}$ is the cost of vaccination.

For simplicity, the payoffs are normalized by dividing both equations by C_i , which does not change the outcome of the game:

$$E_{\rm v} = -C - \pi_{\rm v},$$

$$E_{\rm pv} = -\pi_{\rm pv},$$

where $C = C_v/C_i$ is the relative cost of vaccination to infection.

To calculate the probabilities of infection for vaccinated and non-vaccinated individuals, we analyze the system compartments shown in Figure 5.1. A non-vaccinated individual starts in the S(t) compartment and can either become latently infected (move to L(t) at a rate of $\beta I(t)$) or die from natural causes at rate μ . The probability of transitioning from S(t) to L(t) is:

$$\frac{\beta \mathcal{I}(t)}{\beta \mathcal{I}(t) + \mu}.$$

Likewise, an individual in the $\mathcal{L}(t)$ compartment progresses to the $\mathcal{I}(t)$ compartment with a probability of $\frac{\epsilon}{\epsilon + \mu}$. Hence, the total infection probability for a non-vaccinated individual is:

$$\pi_{\rm nv} = \frac{\beta \mathcal{I}(t)}{\beta \mathcal{I}(t) + \mu} \cdot \frac{\epsilon}{\epsilon + \mu}.$$

For vaccinated individuals, immunity can diminish over time, leading to a return to susceptibility at a rate k. The probability of this event is $\frac{k}{k+\mu}$. From this susceptible state, the individual follows the same infection process as a non-vaccinated person. Therefore, the infection probability for a vaccinated individual is:

$$\pi_{v} = \frac{k}{k+\mu} \cdot \frac{\beta \mathcal{I}(t)}{\beta \mathcal{I}(t) + \mu} \cdot \frac{\epsilon}{\epsilon + \mu}.$$

Thus, the infection probabilities for both groups are:

$$\pi_{\rm nv} = \frac{\beta \mathcal{I}^*}{\beta \mathcal{I}^* + \mu} \cdot \frac{\epsilon}{\epsilon + \mu'}, \quad \pi_{\rm v} = \frac{k}{k + \mu} \cdot \frac{\beta \mathcal{I}^*}{\beta \mathcal{I}^* + \mu} \cdot \frac{\epsilon}{\epsilon + \mu}.$$

These probabilities are short-term estimates corresponding to an individual's vaccination decision within the context of a strategic game, not lifetime infection probabilities.

Next, the analysis determines the conditions under which an individual should choose vaccination and identifies the Nash equilibrium vaccination strategy for the population. Let p_{pop} represent the population's vaccination rate.

■ If $p_{\text{pop}} > p_{\text{HI}}$, then $\mathcal{R}_0 < 1$, leading to a disease-free equilibrium where $\beta \mathcal{I}^* = 0$. In this case, the infection probability is zero, and vaccination is unnecessary, as it incurs a cost without offering additional benefit: $E_{\text{v}} = -C < 0 = E_{\text{nv}}$.

■ If $p_{pop} < p_{HI}$, then $\mathcal{R}_0 > 1$, leading to an endemic equilibrium with:

$$\beta \mathcal{I}^* = \mu(\mathcal{R}_0 - 1).$$

To find the optimal strategy in endemic conditions, we calculate the difference in payoffs between vaccination and no vaccination:

$$\Delta E = E_{\rm v} - E_{\rm nv} = -C + \frac{\mu}{k+\mu} \cdot \frac{\beta \mathcal{I}^*}{\beta \mathcal{I}^* + \mu} \cdot \frac{\epsilon}{\epsilon + \mu}.$$

An individual should vaccinate if $\Delta E > 0$, implying that the payoff from vaccination is higher than from no vaccination. If $\Delta E < 0$, vaccination should not be chosen. The optimal strategy depends on the disease prevalence, which is influenced by the population's vaccination rate $p_{\rm pop}$, and the relative cost of vaccination to infection. Specifically, if:

$$C < \frac{\mu}{k+\mu} \cdot \frac{\beta \mathcal{I}^*}{\beta \mathcal{I}^* + \mu} \cdot \frac{\epsilon}{\epsilon + \mu},$$

then the risk of infection exceeds the cost of vaccination, and the individual should choose to vaccinate. If:

$$C > \frac{\mu}{k+u} \cdot \frac{\beta \mathcal{I}^*}{\beta \mathcal{I}^* + u} \cdot \frac{\epsilon}{\epsilon + u},$$

then the cost of vaccination is greater than the risk of infection, and the individual should not get vaccinated.

The Nash equilibrium strategy corresponds to the population vaccination rate $p_{\rm NE}$ at which no individual can improve their payoff by deviating. In the disease-free equilibrium ($p_{\rm pop} > p_{\rm HI}$), clearly $p_{\rm NE} = 0$. In the endemic state ($p_{\rm pop} < p_{\rm HI}$), the Nash equilibrium vaccination rate is found by solving $E_{\rm v} = E_{\rm nv}$, which yields:

$$C = \frac{\mu}{k+\mu} \cdot \frac{\beta \mathcal{I}^*}{\beta \mathcal{I}^* + \mu} \cdot \frac{\epsilon}{\epsilon + \mu}.$$

Thus, the Nash equilibrium vaccination rate, p_{NE} , is given by:

$$p_{NE} = -\frac{(k+\mu)\left(k_1k_2k_3 - \alpha\gamma\delta k_1 - (1-\alpha)\delta\gamma\epsilon\right)}{\left(-\frac{(k+\mu)}{\mu} \cdot \frac{(\epsilon+\mu)}{\epsilon}C - 1\right)\epsilon\Lambda\beta k_3} + \frac{k+\mu}{\mu}.$$

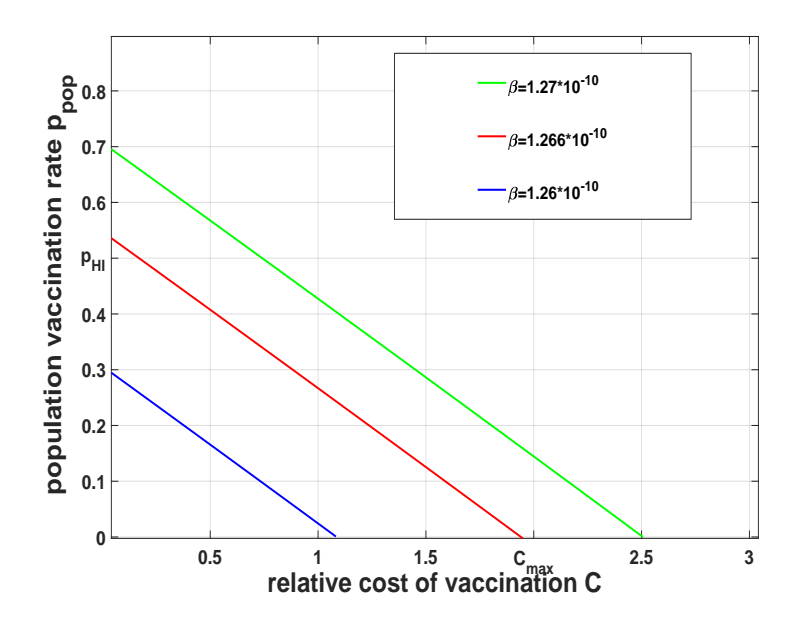


Figure 7.3: Optimal vaccination rate p_{NE} varsus the relative vaccination cost C for different values of β .

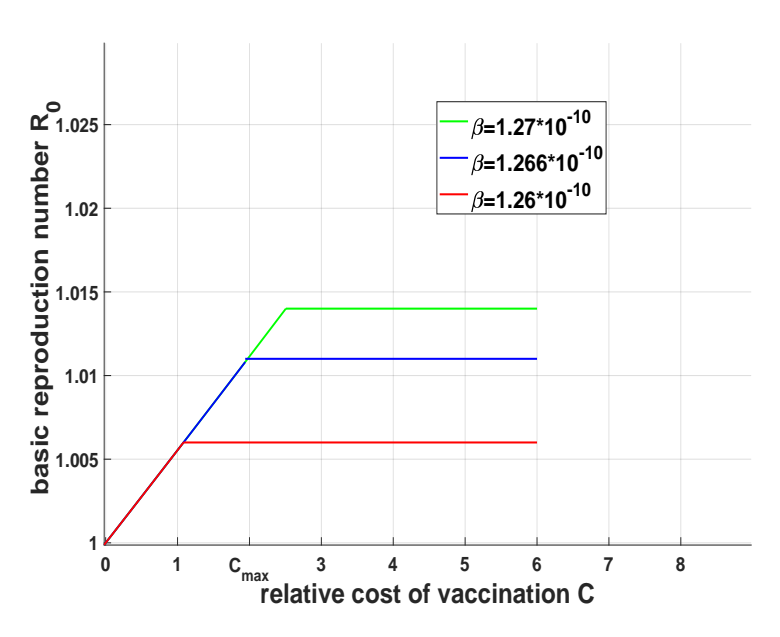


Figure 7.4: Basic reproduction number \mathcal{R}_0 Varsus the relative vaccination cost C, assuming the population follows the Nash equilibrium vaccination strategy.

The graphs of the optimal vaccination rate p_{NE} varsus the relative vaccination cost

C for three values of β are shown in Figure 7.3. The optimal vaccination rate does not exceed the herd immunity threshold vaccination rate $p_{\rm HI}$ and is equal to it only when vaccination cost is zero. For lower relative vaccination costs, the optimal vaccination rate stays close to the herd immunity threshold. Furthermore, there exists a critical relative vaccination cost, $C_{\rm max}$, above which vaccination will no longer be chosen.

The graphs in Figure 7.4 show the fundamental reproduction rate \mathcal{R}_0 varsus the relative vaccination cost C under the assumption that the population adopts the Nash equilibrium vaccination strategy. As the Nash equilibrium vaccination rate approaches the herd immunity threshold for small relative vaccination costs, \mathcal{R}_0 remains near 1 as long as the relative vaccination cost is sufficiently low.

7.6 | Uncertainty and sensitivity analysis

An uncertainty and sensitivity analysis (11; 54) was performed on both the epidemiological and game-theoretic models to assess the impact of parameter variations on the results. Table 7.1 presents the parameter values along with their respective ranges. The analysis concentrated on three main response functions: (i) the fundamental reproduction rate \mathcal{R}_0 derived from the epidemiological model, (ii) the optimal vaccination rate $p_{\rm NE}$ within the game-theoretic framework, and (iii) the relative difference between the herd immunity vaccination rate and the Nash equilibrium vaccination rate, formulated as $\left(\frac{p_{\rm HI}-p_{\rm NE}}{p_{\rm HI}}\right)$.

To account for parameter uncertainty, we applied the Latin hypercube sampling (LHS) method to generate 100 parameter sets based on the ranges specified in Table 7.1. The LHS approach provides an efficient way to produce near-random samples from a multidimensional parameter space, ensuring a comprehensive exploration of possible variations. The range of each parameter was segmented into 100 equal probability intervals, from which a value was randomly selected within each interval. These values were then paired randomly across all parameters to create 100 distinct samples. The resulting data is presented in Figures 7.5, 7.6, 7.7, 7.8, 7.9, and 7.10. Figures 7.5, 7.7, and 7.9 display the distribution of the response functions resulting from the uncertainty in the parameters, while Figures 7.6, 7.8, and 7.10 show the partial rank correlation coefficients (PRCCs), which indicate how sensitive each response function is to changes in the model parameters. The box plot in Figure 7.5 displays the variability of \mathcal{R}_0 across different parameter sets. \mathcal{R}_0 is most sensitive to changes in β , the transmission rate, as evidenced by its wider interquartile range compared to other parameters. Parameters such as γ and ε show moderate variability, while α , μ , and ρ exhibit less influence.

Parameters	Description	Algerian Value	Range
Λ	The recruitment rate	811,085	
μ	The natural death rate	0.00498	(0.00492,0.004985)
k	The rate of moving from $\mathcal V$ to $\mathcal S$	0.25	
β	The transmission rate	varies	$(1.28 \times 10^{-10}, 1.29 \times 10^{-10})$
γ	The recovery rate	0.0043	(0.0007,0.004)
ϵ	The progression rate	0.0656	(0.07,0.08)
α	Treatment failure rate	0.1095	(0,1)
δ	The rate at which the treated	0.1325	
	population leave the class T		
σ	The disease death rate in I	0.0136	
η	The disease death rate in T	4.2327×10^{-6}	
p	The vaccination rate	varies	(0,1)

Table 7.1: Model parameters for TB model (7.1).

These findings highlight the importance of targeting β through interventions like improved infection control measures to significantly reduce \mathcal{R}_0 .

The PRCC analysis for \mathcal{R}_0 , shown in Figure 7.6, further confirms the dominant role of β . Positive correlations suggest that increases in β and decreases in γ or ϵ drive \mathcal{R}_0 higher. This sensitivity analysis reinforces the need for strategies that increase recovery rates and reduce transmission rates.

The box plot in Figure 7.7 explores the distribution of p_{NE} , the optimal vaccination rate derived from the game-theoretic model. β again emerges as a key influencer with a relatively wider distribution, indicating its significant impact on vaccination dynamics. Other parameters like γ and ϵ show moderate effects, while α and μ are less impactful. These results underline the need for targeted vaccination campaigns focused on reducing β in high-transmission settings.

Figure 7.8 presents the PRCC for p_{NE} , revealing that parameters with strong positive correlations, such as γ , enhance optimal vaccination rates. Conversely, negative correlations with β suggest that higher transmission rates decrease the effectiveness of vaccination, emphasizing the importance of coupling vaccination with measures that reduce β .

The relative difference box plot, shown in Figure 7.9, illustrates the variability in $\frac{p_{\rm HI}-p_{\rm NE}}{p_{\rm HI}}$ across different parameters. This metric highlights the misalignment between the socially optimal and individually optimal vaccination rates. β , the transmission rate, exhibits the highest variability, indicating its substantial influence on the divergence between $p_{\rm HI}$ and $p_{\rm NE}$. Parameters γ and ϵ show moderate impacts, reflecting their roles in disease progression and recovery. Narrower spreads for α and μ suggest secondary roles in this context. A large spread in the relative difference underscores inefficiency in

individual decision-making, necessitating interventions like subsidies or mandates to align behaviors with herd immunity goals.

The PRCC analysis for the relative difference, depicted in Figure 7.10, identifies β as a dominant parameter with a strong negative correlation. This indicates that higher transmission rates align individual vaccination incentives closer to herd immunity goals, reducing the gap. Conversely, positive correlations with parameters like γ suggest that increased recovery rates can widen the gap, as individuals perceive less urgency to vaccinate. These findings emphasize the need for targeted interventions that reduce β while considering the interplay of other influential parameters.

The optimal vaccination rate, $p_{\rm NE}$, and the relative difference between the herd immunity vaccination rate and the Nash equilibrium vaccination rate, expressed as $\frac{p_{\rm HI}-p_{\rm NE}}{p_{\rm HI}}$, depend on the relative cost of vaccination, C. Given that an infected individual faces approximately a 50% risk of mortality, the cost of infection, $C_{\rm i}$, is significantly high. Consequently, the ratio of vaccination cost to infection cost, defined as $C = \frac{C_{\rm v}}{C_{\rm i}}$, remains relatively low. For this study, we selected a small value for the relative vaccination cost, setting C = 0.003.

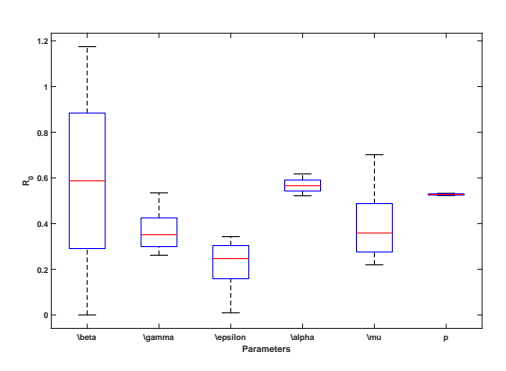


Figure 7.5: Distribution of the fundamental reproduction rate \mathcal{R}_0 across parameter sets.

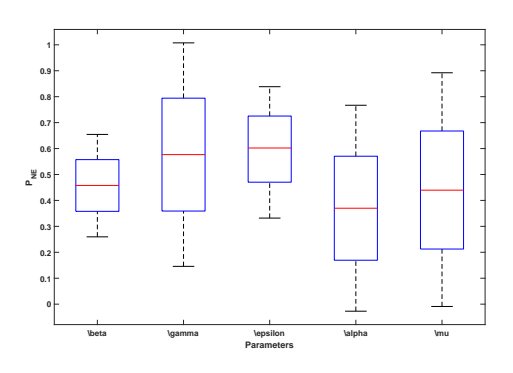


Figure 7.7: Distribution of the optimal vaccination rate p_{NE} across parameter sets.

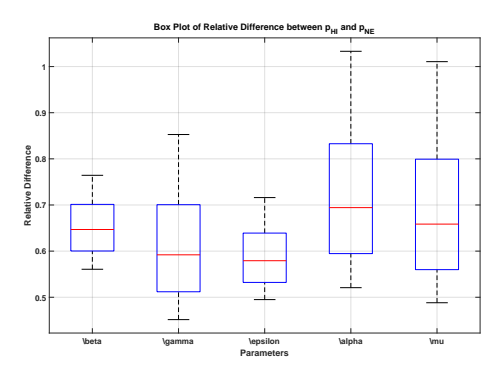


Figure 7.9: Distribution of the relative disparity between the Nash equilibrium vaccination rate and the herd immunity vaccination rate

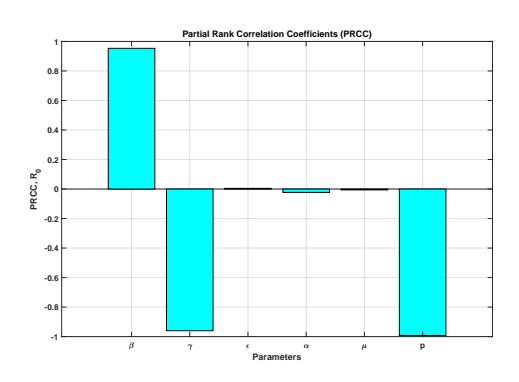


Figure 7.6: Partial Rank Correlation Coefficients (PRCCs) for \mathcal{R}_0 , showing the sensitivity to model parameters.

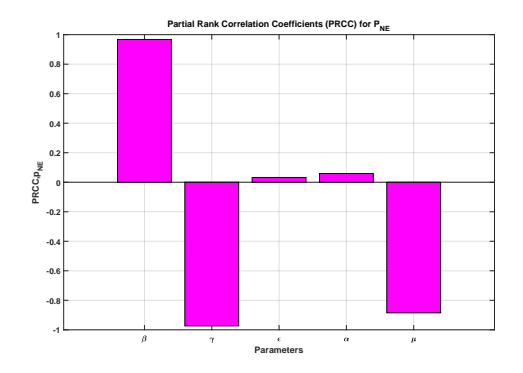


Figure 7.8: Partial Rank Correlation Coefficients (PRCCs) for p_{NE} , showing the sensitivity to model parameters.

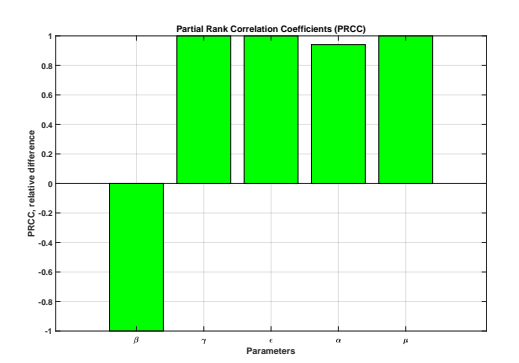


Figure 7.10: Partial Rank Correlation Coefficients (PRCCs) for the relative difference, showing the sensitivity to model parameters.

133

Conclusion

This study examined the impact of individual vaccination decisions through the application of a game-theoretic model to tuberculosis (TB) transmission, based on the work of (12). Model parameters were derived from data specific to the TB situation in Algeria. The results suggest that the optimal level of voluntary vaccination aligns closely with the threshold required for herd immunity. This outcome is consistent and stable, even when the model parameters are varied. Therefore, voluntary vaccination initiatives could play a crucial role in reducing TB prevalence and aiding in its eventual eradication in Algeria. For these programs to be effective, it is essential that the cost of the vaccine remains affordable, and public awareness about the disease is increased. Our sensitivity analysis showed that making vaccines both affordable and accessible is key to reducing the financial and logistical burdens on patients, including out-of-pocket costs, lost time, and travel expenses. National efforts are necessary for TB eradication, and rural areas should be a focus due to the higher TB burden in these regions. These efforts should involve improving vaccination access, providing adequate educational resources, and increasing general awareness of TB. Educational campaigns should highlight the availability and advantages of vaccination to encourage higher participation. Additionally, our analysis indicates that the high cost of TB treatment contributes to the alignment between optimal voluntary vaccination levels and those required for herd immunity. The high economic burden of TB infections makes the cost of vaccination relatively low, even if the vaccine is not provided for free. As a result, enhancing access to vaccines, rather than solely lowering their direct cost, is more critical to achieving sufficient coverage. Furthermore, the lack of awareness about TB remains a major obstacle to vaccination uptake, especially in rural parts of Algeria.

Conclusions and Outlook

"It is easy to miss the mark and difficult to hit it." – Aristotle

This thesis has delved into the application of mathematical modeling to understand and address complex epidemiological challenges, with a focus on infectious diseases like tuberculosis (TB). By leveraging continuous and discrete dynamical systems, including bifurcation theory, stability analysis, and game-theoretic approaches, this study has offered a significant understanding of TB transmission dynamics and its control measures. A significant contribution of this research is the development and analysis of the VSLIT model, which was applied to tuberculosis data from Algeria and Ukraine. These countries were chosen for their contrasting epidemiological contexts, allowing for a comprehensive evaluation of the model's robustness and applicability. The analysis highlighted the effectiveness of targeted interventions, such as vaccination and chemoprophylaxis, in reducing TB incidence and controlling the spread of multidrug-resistant and extensively drug-resistant tuberculosis. The results underscore the critical role of region-specific strategies in addressing unique epidemiological challenges. Additionally, discrete-time epidemic models with chemoprophylaxis further demonstrated the importance of timely interventions in mitigating TB transmission in high-burden regions like Russia and India. The incorporation of game-theoretic analysis provided a framework for understanding the impact of individual decision-making on vaccination uptake and achieving herd immunity. This approach was instrumental in identifying Nash equilibrium strategies that optimize public health outcomes while accounting for individual incentives. The findings from this study emphasize the value of mathematical models, such as the VSLIT model, as tools for guiding public health interventions. By tailoring strategies to specific regional contexts, such as those in Algeria and Ukraine, these models offer practical insights into controlling TB and other infectious diseases. Future research should continue refining these models, exploring additional datasets, and incorporating emerging challenges to enhance their utility in global health policymaking.

References

- [1] Ahmed, S., Malik, Z., et al. Game Theory Applications in Host-Microbe Interactions Toward Disease Manifestation: Mycobacterium tuberculosis Infection as an Example. *Frontiers in Microbiology*, 2022, **13**: 35096290.
- [2] Allen, L. J. Some Discrete-Time SI, SIR, and SIS Epidemic Models. *Mathematical Biosciences*, 1994, **124**(1): 83–105.
- [3] Allen, L. J. An Introduction to Mathematical Biology. *Pearson*, 2007.
- [4] Al-Tawfiq, J. A., and Zumla, A. The role of Bacillus Calmette–Guérin vaccination in preventing tuberculosis. *Journal of Infectious Diseases*, **210**(10):1578–1582, 2014.
- [5] Anagnost, J. J., and Desoer, C. A. An Elementary Proof of the Routh-Hurwitz Stability Criterion. *Circuits, Systems and Signal Processing*, 1991, **10**(1): 59–74.
- [6] Anderson, R. M., and May, R. M. Population Biology of Infectious Diseases. Report of the Dahlem Workshop on Population Biology of Infectious Disease Agents Berlin 1982. *Springer Science and Business Media*, 2012.
- [7] Anosov, D. V. Dynamical Systems I: Ordinary Differential Equations and Smooth Dynamical Systems. *Springer*, 1988, Berlin.
- [8] Arrowsmith, D. K., and Place, C. M. An Introduction to Dynamical Systems. *Cambridge University Press*, 1990.
- [9] Bauch, C., and Earn, D. (2004). Vaccination and the theory of games. *Proceedings of the National Academy of Sciences USA*, **101**(39): 13391—13394.

- [10] Bernoulli, D. Essai D'une Nouvelle Analyse De La Mortalité Causée Par La Petite Vérole Et Des Avantages De L'inoculation Pour La Prévenir. Mem. Math. Phys. Acad. Roy. Sci. Paris, 1760, 1–45.
- [11] Blower, S., and Dowlatabadi, H. (1994). Sensitivity and uncertainty analysis of complex models of disease. *Journal of Theoretical Biology*, **157**(3): 291–308.
- [12] Chennaf, B., Abdelouahab, M. S., and Lozi, R. Analysis of the Dynamics of Tuberculosis in Algeria Using a Compartmental VSEIT Model with Evaluation of the Vaccination and Treatment Effects. *Computation*, 2023, **11**(7): 146.
- [13] Chennaf, B., Abdelouahab, M. S., and Lozi, R. A Novel Compartmental VSLIT Model Used to Analyze the Dynamics of Tuberculosis in Algeria and Ukraine and the Assessment of Vaccination and Treatment Effects. *Ukrainian Mathematical Journal*, 2024, 75(12): 1932–1947.
- [14] Centers for Disease Control and Prevention (CDC). The Spanish Flu of 1918 and its Impact. *Emerging Infectious Diseases*, **24**(10):1772–1774, 2018.
- [15] Cole, S. R., Chu, H., and Greenland, S. Maximum Likelihood, Profile Likelihood, and Penalized Likelihood: A Primer. *American Journal of Epidemiology*, 2014, **179**(2): 145–153.
- [16] Cook, N. D. Born to Die: Disease and the Early Spanish Conquest of Mexico. *University of Oklahoma Press, Norman, OK*, 1998.
- [17] Cori, A., Ferguson, N.M., and Fraser, C. The global burden of tuberculosis: Estimating the incidence and mortality rate in different countries. *Lancet Infectious Diseases*, 2015, **15**(9): 1060-1069.
- [18] Dang-Vu, H., and Delcarte, C. Bifurcations et chaos: une introduction à la dynamique contemporaine avec des programmes en Pascal, Fortran et Mathematica. *Ellipses Ed. Marketing*, 2000.
- [19] Defoe, D. A Journal of the Plague Year. Edited by Louis Landa. Penguin Books, 1991. Originally published in 1722.
- [20] Derouich, M., Boutayeb, A., and Twizell, E. H. A Model of Dengue Fever. *BioMedical Engineering OnLine*, 2003, **2**(4): 1–10.
- [21] Derdei, B. Étude de Modèles Épidémiologiques: Stabilité, Observation et Estimation de Paramètres. *Université de Lorraine*, 2009.

- [22] Diekmann, O., Heesterbeek, J. A. P., and Metz, J. A. J. On the Definition and the Computation of the Basic Reproduction Ratio R0 in Models for Infectious Diseases in Heterogeneous Populations. *J. Math. Biol.*, 1990, **28**: 365.
- [23] European Centre for Disease Prevention and Control. COVID-19 Fact-sheet, 2024. https://www.ecdc.europa.eu/en/infectious-disease-topics/z-disease-list/covid-19/factsheet-covid-19, Accessed: 2025-03-01.
- [24] European Centre for Disease Prevention and Control. Middle East Respiratory Syndrome Coronavirus (MERS-CoV) Factsheet, 2024. https://www.ecdc.europa.eu/en/middle-east-respiratory-syndrome-coronavirus/factsheet, Accessed: 2025-03-01.
- [25] Elhadj, Z. Dynamical Systems: Theories and Applications. CRC Press, 2019.
- [26] Eldholm, V., Rieux, A., Monteserin, J., Lopez, J. M., Palmero, D., Lopez, B., Ritacco, V., Didelot, X., and Balloux, F. Impact of HIV co-infection on the evolution and transmission of multidrug-resistant tuberculosis. *eLife*, 2016, 5:e16644.
- [27] Evans, N. A. Population Biology of Infectious Diseases. In Anderson, R. M., and May, R. M. (Eds.), *Dahlem Research Workshops*, 1983, **25**: Springer-Verlag, Berlin.
- [28] Farr, W. Vital Statistics: A Memorial Volume of Selections from the Writings of William Farr. *Wiley*, 1840.
- [29] Ferrara, J. A Study of Nonlinear Dynamics in Mathematical Biology. *University of North Florida*, 2013.
- [30] Grigorieva, E. V., and Khailov, E. N. Optimal Intervention Strategies for a SEIR Control Model of Ebola Epidemics. *Mathematics*, 2017, 5(4): 1–19.
- [31] Guckenheimer, J., and Holmes, P. Nonlinear Oscillations, Dynamical Systems, and Bifurcations of Vector Fields. *Springer*, 2013, **42**. Applied Mathematical Sciences. New York, NY.
- [32] Gupta, V. K., Tiwari, S. K., Sharma, S., and Nagar, L. Mathematical Model of Tuber-culosis with Drug Resistance to the First and Second Line of Treatment. *Journal of New Theory*, 2018: 94–106.
- [33] Hale, J. K., and Koçak, H. Dynamics and Bifurcations. *Springer-Verlag*, 1991, New York, NY.

- [34] Hasanli, R. A Data-Driven Epidemic Model to Analyze and Forecast the Dynamics of COVID-19. *Middle East Technical University*, 2021.
- [35] Hassan, A., Akpan, A., Ogunlade, A. Optimal Control for a Tuberculosis Model with Reinfection and Post-Exposure Interventions. *Mathematical Methods in the Applied Sciences*, 2013, **36**: 2494-2507.
- [36] Herchline, T. E., and Bronze, M. S. Tuberculosis (TB). Medscape, 2019.
- [37] Hethcote, H. W. The Mathematics of Infectious Diseases. *SIAM Review*, 2000, **42**(4): 599–653.
- [38] Huremovic, D. Brief History of Pandemics (Pandemics Throughout History). *Psychiatry of Pandemics: A Mental Health Response to Infection Outbreak*, Springer, 2019, Chapter 1: 7–35.
- [39] Izzo, G., and Vecchio, A. A Discrete Time Version for Models of Population Dynamics in the Presence of an Infection. *Journal of Computational and Applied Mathematics*, 2007, **210**(1-2): 210–221.
- [40] Johnson, M. L., and Faunt, L. M. Parameter Estimation by Least-Squares Methods. *Methods in Enzymology*, 1992, **210**: 1–37.
- [41] Katleris, A. L., Jackson, C., Southern, J., Gupta, R. K., Drobniewski, F., Lalvani, A., Lipman, M., Mangtani, P., and Abubakar, I. Effectiveness of BCG Vaccination Against Mycobacterium tuberculosis Infection in Adults: A Cross-sectional Analysis of a UK-Based Cohort. *The Journal of Infectious Diseases*, 2020, 221: 146–155.
- [42] Kermack, W. O., and McKendrick, A. G. A Contribution to the Mathematical Theory of Epidemics. *Proc. R. Soc. Lond. A*, 1927, **115**: 700–721.
- [43] Kitaro, D. B., Bole, B. K., and Rao, K. P. Mathematical Analysis of Tuberculosis Transmission Model with Multidrug and Extensively Drug-Resistance Incorporating Chemoprophylaxis Treatment. *Jambura J. Math.*, 2024, **6**(1): 1–10.
- [44] Kuznetsov, Y. A. *Elements of Applied Bifurcation Theory*. Springer, 1998, **112**. Applied Mathematical Sciences. New York, NY.
- [45] LaSalle, J. P. Stability of Nonautonomous Systems. *Nonlinear Analysis: Theory, Methods Applications*, 1976, **1**(1): 83–91.
- [46] LaSalle, J. P. The Stability of Dynamical Systems. *Society for Industrial and Applied Mathematics (SIAM)*, 1976.

- [47] Layek, G. C. An Introduction to Dynamical Systems and Chaos. Vol. 449, *Springer*, New Delhi, 2015.
- [48] Levenberg, K. A Method for the Solution of Certain Non-Linear Problems in Least Squares. *Quarterly of Applied Mathematics*, 1944, **2**(2): 164–168.
- [49] Li, X., and Wang, W. A Discrete Epidemic Model with Stage Structure. *Chaos, Solitons and Fractals*, 2005, **26**(3): 947–958.
- [50] Li, M. Y. Predicting Epidemic Dynamics and Control Strategies. *Journal of Epidemiology and Public Health*, 2018, **2**: 1-8.
- [51] Ma, Z., and Li, J. Dynamical Modeling and Analysis of Epidemics. *World Scientific*, 2009.
- [52] Martcheva, M. Mathematical Models in Epidemiology. Springer, 2015.
- [53] Martelli, M. Introduction to Discrete Dynamical Systems and Chaos. *John Wiley and Sons*, 2000.
- [54] Marino, S., Hogue, I., Ray, C., and Kirschner, D. (2008). A methodology for performing global uncertainty and sensitivity analysis in systems biology. *Journal of Theoretical Biology*, **254**(2), 178–196.
- [55] Marquardt, D. W. An Algorithm for Least-Squares Estimation of Nonlinear Parameters. *Journal of the Society for Industrial and Applied Mathematics*, 1963, **11**(2): 431–441.
- [56] Mickens, R. E. Discretizations of Nonlinear Differential Equations Using Explicit Nonstandard Methods. *Journal of Computational and Applied Mathematics*, 1999, **110**(1): 181–185.
- [57] Nocedal, J., and Wright, S. J. Numerical Optimization. Springer, 2006.
- [58] Oliveira, S., Silva, M., Rocha, C. Optimal Control Strategies for Tuberculosis Treatment: A Case Study in Angola. *Mathematical Problems in Engineering*, 2012: 1-12.
- [59] Ouannas, A. Sur la Synchronisation des Systèmes Chaotiques Discrets. *Constantine* 1 *University*, 2015.
- [60] Perko, L. Nonlinear Systems: Global Theory. *Differential Equations and Dynamical Systems*, Springer, 2001, Chapter 2, 181–314.

- [61] Perko, L. Differential Equations and Dynamical Systems. Volume 7, Springer Science and Business Media, 2013.
- [62] Poincaré, H. Les méthodes nouvelles de la mécanique céleste, Volume 2. *Gauthier-Villars et fils*, imprimeurs-libraires, 1893. (French)
- [63] Population Growth in Algeria, 2024. https://www.donneesmondiales.com/afrique/algerie/croissance-population.php, Accessed: November 2024.
- [64] Population Growth in Ukraine, 2024. https://www.donneesmondiales.com/europe/ukraine/croissance-population.php, Accessed: November 2024.
- [65] Population Growth in India, 2024. https://www.donneesmondiales.com/asie/inde/croissance-population.php, Accessed: November 2024.
- [66] Population Growth in Russia, 2024. https://www.donneesmondiales.com/europe/russie/croissance-population.php, Accessed: November 2024.
- [67] Porwal, C., Kaushik, A., Makkar, N., Banavaliker, J. N., Hanif, M., Singla, R., and Singh, U. B. Incidence and Risk Factors for Extensively Drug-Resistant Tuberculosis in Delhi Region. *PLoS One*, 2013, **8**(2): e55299.
- [68] Raghavan, R., Sharma, V., Reddy, G. Optimal Control of Tuberculosis: A Review. *Mathematical Methods in the Applied Sciences*, 2014, **37**: 2954-2970.
- [69] Rodrigues, H. S. F. Optimal Control and Numerical Optimization Applied to Epidemiological Models. *Universidade de Aveiro*, 2012.
- [70] Ronoh, M., Jaroudi, R., Fotso, P., Kamdoum, V., Matendechere, N., Wairimu, J., and Lugoye, J. A Mathematical Model of Tuberculosis with Drug Resistance Effects. *Applied Mathematics*, 2016, 7(12): 1303–1316.
- [71] Ross, R. The Prevention of Malaria. 2nd ed., Murray, London, 1911.
- [72] Sallet, G. INRIA and IRD EPICASA. Technical Report, 2010.
- [73] Scheinerman, E. R. Invitation to Dynamical Systems. Courier Corporation, 2013.
- [74] Smith, D. L., and Brauer, F. (2007). Game-theoretic approaches to vaccination strategies in populations with heterogeneous risk of infection. *Journal of Theoretical Biology*, **246**(3), 487–495.

- [75] Song, T., Shan, J. The impact of climate temperature on the birth rate and biting rate of mosquitoes in relation to Dengue virus incidence. *Environmental Studies*, 2020, June.
- [76] WHO. Global Tuberculosis Report, 2024. https://extranet.who.int/tme/generateCSV.asp?ds=notifications, Accessed: November 2024.
- [77] Thompson, J. M. T., and Stewart, H. B. *Nonlinear Dynamics and Chaos*. John Wiley and Sons, 2002.
- [78] The World Bank Group. Tuberculosis Treatment Success Rate (% of New Cases) Algeria, 2024. https://data.worldbank.org/indicator/SH.TBS.CURE. ZS?locations=DZ, Accessed: November 2024.
- [79] The World Bank Group. Tuberculosis Treatment Success Rate (% of New Cases) Ukraine, 2024. https://data.worldbank.org/indicator/SH.TBS.CURE. ZS?locations=UA, Accessed: November 2024.
- [80] Trading Economics. Immunization, BCG (% of One-Year-Old Children) Algeria, 2024. https://www.tradingeconomics.com/algeria/immunization-bcg-percent-of-one-year-old-children-wb-data.html/, Accessed: November 2024.
- [81] Trading Economics. Immunization, BCG (% of One-Year-Old Children) Ukraine, 2024. https://www.tradingeconomics.com/ukraine/immunization-bcg-percent-of-one-year-old-children-wb-data.html/, Accessed: November 2024.
- [82] Trading Economics. Immunization, BCG (% of One-Year-Old Children) India, 2024. https://tradingeconomics.com/india/immunization-bcg-percent-of-one-year-old-children-wb-data.html, Accessed: November 2024.
- [83] Van den Driessche, P., and Watmough, J. Reproduction Numbers and Subthreshold Endemic Equilibria for Compartmental Models of Disease Transmission. *Math. Biosci.*, 2002, 180: 29–48.
- [84] Vynnycky, E., Fine, P. E. M. The role of the latent infection period in the long-term trends in tuberculosis incidence and mortality. *International Journal of Epidemiology*, 1997, **26**(2): 238–245.

- [85] Waaler, H., Geser, A., and Andersen, S. The Use of Mathematical Models in the Study of the Epidemiology of Tuberculosis. *American Journal of Public Health and the Nations Health*, 1962, **52**(6): 1002–1013.
- [86] Wang, Y., Zhang, X., Liu, T. Treatment Seeking Dilemma for Tuberculosis as Timed Strategic Interaction. *Physica A: Statistical Mechanics and its Applications*, 2023, **632**: 1–9.
- [87] Wang, Y., and Cao, J. Global Stability of General Cholera Models with Nonlinear Incidence and Removal Rates. *Journal of the Franklin Institute*, 2015, **352**(6): 2464–2485.
- [88] Wells, C. D., and others. HIV Infection and Multidrug-Resistant Tuberculosis—The Perfect Storm. *The Journal of Infectious Diseases*, 2007, **196**: 86–107.
- [89] World Health Organization. *Tuberculosis*, 2024. https://www.who.int/news-room/fact-sheets/detail/tuberculosis
- [90] World Health Organization. Extensively Drug-Resistant Tuberculosis (XDR-TB): Recommendations for Prevention and Control. Weekly Epidemiological Record, 2006, 81(45): 430–432.
- [91] World Health Organization. (2022). *Global tuberculosis report* 2022. Retrieved from https://www.who.int/publications/i/item/9789240064896 (Accessed: December 30, 2024).
- [92] World Health Organization. (2023). *Tuberculosis*. Retrieved from https://www.who.int/news-room/fact-sheets/detail/tuberculosis (Accessed: December 30, 2024).
- [93] World Health Organization. Immunization, BCG (% of One-Year-Old Children) Russia, 2024. https://apps.who.int/gho/data/view.main.80500?lang=en, Accessed: November 2024.
- [94] Wiggins, S. Introduction to Applied Nonlinear Dynamical Systems and Chaos. *Springer*, 2003, **2**. Texts in Applied Mathematics.
- [95] Yeni, G., Akın, E., and Vaidya, N. K. Time scale theory on stability of explicit and implicit discrete epidemic models: applications to Swine flu outbreak. *Journal of Mathematical Biology*, **88**(1):6, 2024.

[96] Ziegler, P. The Black Death: The World's Most Devastating Plague. *Harper and Row*, 1969.